Functional role of N-cadherin and neuroligin-1 at glutamatergic synapses

Inaugural-Dissertation

zur Erlangung des Doktorgrades

der Mathematisch-Naturwissenschaftlichen Fakultät

der Heinrich-Heine-Universität Düsseldorf

vorgelegt von

Bernd van Stegen

aus Wesel

Düsseldorf, Februar 2015

aus dem Institut für Neuro- und Sinnesphysiologie
der Heinrich-Heine-Universität Düsseldorf

Gedruckt mit der Genehmigung der
Mathematisch-Naturwissenschaftlichen Fakultät der
Heinrich-Heine-Universität Düsseldorf

Referent: Prof. Dr. K. Gottmann

Korreferent: Prof. Dr. H. Aberle

Tag der mündlichen Prüfung: 22.04.2015

Abstract

Neurotransmission at chemical synapses is initiated by presynaptic exocytosis of transmitter-filled vesicles followed by subsequent vesicle endocytosis. The coupling of exocytosis and compensating endocytosis is essential to maintain proper transmission upon prolonged synaptic activity. In this work, the influence of the cell adhesion molecules (CAMs) N-cadherin and neuroligin-1 on presynaptic function was addressed with a particular interest in the coupling of vesicular exo- and endocytosis. Activity-dependent FM4-64 stainings revealed enhanced cycling of presynaptic vesicles in post-synaptogenic neurons overexpressing N-cadherin or neuroligin-1. Moreover, FM4-64 experiments in N-cadherin knockout neurons showed a cooperation of both CAMs in the transsynaptic regulation of presynaptic vesicle cycling. In this context, N-cadherin was also shown to control synaptic localization of neuroligin-1. A differential analysis of vesicular exo- and endocytosis with synaptophysin-pHluorin (SypHy) in neurons expressing N-cadherin or neuroligin-1 revealed an exocytotic effect of both CAMs and an endocytotic effect exclusively for N-cadherin. Double-stimulation SypHy experiments demonstrated that the effect of N-cadherin on endocytosis depends on the release activity level of the vesicle cluster and indicated an important role of N-cadherin in the coupling of presynaptic vesicle exo- and endocytosis. Further experiments revealed changes in localization of N-cadherin and neuroligin-1 upon intense synaptic activity from a strongly clustered to a more diffuse pattern. In summary, the present study strongly supports a model of the regulation of vesicle exo- and endocytosis coupling that is based on activity-dependent changes of the spatial localization of N-cadherin and neuroligin-1. Upon strong synaptic activity, this structural relocalization regulates presynaptic vesicle exo- and endocytosis, thus enabling the maintenance of proper synaptic function in highly active synapses. In addition to the roles of CAMs in vesicle cycling, the pathophysiological effect of amyloid-β (Aβ) peptides was examined in hiPSC derived neurons. Intriguingly, FM4-64 experiments indicated an Aβ-induced defect in the axonal transport of vesicle cluster, but no effect of Aβ peptides on vesicle cycling at bona-fide synapses.

Zusammenfassung

Die Signalübertragung an chemischen Synapsen wird initiiert durch die präsynaptische Exozytose von transmittergefüllten Vesikeln gefolgt von Vesikelendozytose. Die Kopplung von Exozytose und kompensierender Endozytose ist essentiell für die Aufrechterhaltung synaptischer Transmission bei anhaltender neuronaler Aktivität. In der vorliegenden Arbeit wurde der Einfluss der Zelladhäsionsmoleküle (CAMs) N-cadherin und Neuroligin-1 auf die Funktionalität der Präsynapse untersucht, mit besonderem Augenmerk hinsichtlich der Kopplung vesikulärer Exo- und Endozytose. Aktivitätsabhängige Färbungen mit dem Farbstoff FM4-64 offenbarten ein gesteigertes „cycling“ präsynaptischer Vesikel in post-synaptogenen Neuronen durch Überexpression von N-cadherin oder Neuroligin-1. Des Weiteren zeigten FM4-64 Experimente in N-cadherin knockout Neuronen eine Kooperation der CAMs in der transsynaptischen Regulation des „cycling“ präsynaptischer Vesikel. In diesem Zusammenhang bestätigte sich auch ein Einfluss von N-cadherin auf die Lokalisation von Neuroligin-1. Eine differenziertere Analyse vesikulärer Exo- und Endozytose mit Synaptophysin-pHluorin (SypHy) in N-cadherin- oder Neuroligin-1-exprimierenden Neuronen zeigte einen exozytotischen Effekt beider CAMs sowie einen endozytotischen Effekt ausschließlich für N-cadherin. Durch Doppelstimulationsexperimente mit SypHy konnte verdeutlicht werden, dass dieser Endozytoseeffekt von der Freisetzungsaktivität des Vesikelklusters abhängt, was auf eine wichtige Rolle von N-cadherin in der präsynaptischen Kopplung hindeutet. Weitere Untersuchungen zeigten Veränderungen in der Lokalisation von N-cadherin und Neuroligin-1 von stark geklusterten Strukturen hin zu einer eher diffusen Verteilung bei starker synaptischer Aktivität. Zusammenfassend unterstützen die Ergebnisse ein Modell der Regulation präsynaptischer Kopplung, welches auf der aktivitätsabhängigen Veränderung der Lokalisation von N-cadherin und Neuroligin-1 basiert und die Aufrechterhaltung der Synapsenfunktion während starker Aktivität gewährleistet. Zusätzlich wurden pathophysiologische Effekte des Amyloid-β (Aβ) Peptides in hiPSC abgeleiteten Neuronen untersucht. Dabei zeigten FM4-64 Experimente einen Aβ-induzierten Defekt im axonalen Vesikeltransport ohne Beeinträchtigung des „cycling“ präsynaptischer Vesikel in „bona-fide“ Synapsen.

Table of contents

1 Introduction

The central nervous system (CNS) is performing the storage and processing of information that enters from diverse areas of the body. Within the CNS the brain represents the central converting unit. In higher vertebrates, this complex but highly organized structure consists of up to 100 billion specialized cells (neurons) that transfer and store information via electric signals. Neuronal function is supported by different types of glial cells. This second type of cells within the nervous system has a variety of functions that enable proper neuronal network activity. For instance, astrocytes take up presynaptically released glutamate to prevent continuous postsynaptic activity. Neurons usually consist of a single axon a soma and several dendrites. The dendrites receive information at their postsynaptic sites and conduct them to the cell soma. At the initial segment of the axon, the electrical information is transformed into action potentials and guided along the axon to connected neurons within the neuronal network. Mostly, axons and dendrites branch out to build up extensive connections. These neuronal networks are not fixed structures but are characterized by dynamic alterations that strengthen and weaken connections. Crucial for these dynamic processes are electrical and chemical synapses. These specialized contacts transmit electrical signals from one neuron to another with one neuron assembling up to 10000 synapses. Two classes of synapses can be distinguished. Electrical synapses can transmit information bidirectional between neurons by gap junctions. In contrast, chemical synapses consist of two morphologically distinct structures. At the presynaptic terminal, the action potential is transformed into a chemical signal by the release of neurotransmitter. The transmitter are binding to specific receptors that are localized within the postsynaptic membrane. The binding of neurotransmitter molecules opens ion channels and the inward flow of e.g. cations depolarizes the postsynaptic membrane, hence transferring the chemical signal back to an electrical signal. Finally, these currents are guided along the dendrite to the soma. It is thought that transsynaptic cell adhesion molecules (CAMs) play a major role in the formation of synaptic contacts in immature neurons. Recent studies also suggest that CAMs are important for proper synaptic function in more mature neurons after synaptogenesis.

1.1 Transmission at the chemical synapse

A chemical synapse consists of three structural and functional diverse parts, the presynapse, the synaptic cleft and the postsynaptic structure. The presynaptic terminal represents the endpoint of an axon. At this side of the synapse the electrical information is transformed to a chemical signal in terms of neurotransmitter-release. These small molecules are released from synaptic vesicles and cross the synaptic cleft (20-40 nm) to activate specific receptors on the postsynaptic side. The influx of ions through these receptors generates their postsynaptic electrical signals. Dependent on the postsynaptic receptors, chemical synapses can be excitatory or inhibitory. Compared to electrical synapses, synaptic transmission at chemical synapses is slow but can be modulated at the pre- and postsynaptic side. Thus these synapses are essential for adaptive dynamic processes within neuronal networks. Besides the usual axo-dendritic synapse, there are a variety of different possible combinations like axo-axonic, axo-somatic or even dendro-dendritic synaptic contacts. Also autaptic contacts, where the axon contacts its own dendrites, are described but only in very few cases.

1.1.1 Presynaptic transmitter release

Presynaptic terminals are specialized structures of the axon and represent the starting point of synaptic transmission. An incoming action potential depolarizes the presynaptic terminal and opens voltage-gated Ca^{2+}-channels. The Ca^{2+}-influx increases the Ca^{2+}-concentration within the presynaptic terminal (Augustine et al., 1987; Lisman et al., 2007; Südhof, 2013). Particular in local Ca^{2+}-microdomains near the presynaptic membrane the Ca^{2+}-concentration increases from basic values within the range of nM up to µM levels (Bollmann et al., 2000; Schneggenburger and Neher, 2000; Jahn and Fasshauer, 2012). The increase in Ca^{2+}-concentration induces the exocytosis of transmitter-filled vesicles and the subsequent release of neurotransmitter within the synaptic cleft (Heuser et al., 1979). The exocytosis of presynaptic vesicles occurs 100 to 200 µs after the inward flow of Ca^{2+}-ions and depends on the binding of Ca^{2+} to the vesicular protein synaptotagmin (Augustine et

al., 1994; Llinas et al., 1982; review in Pang and Südhof, 2010; Südhof, 2013). The presynaptically released neurotransmitter diffuse across the synaptic cleft to bind postsynaptic receptors. Dependent on the released transmitter, the binding can induce excitatory (EPSC: excitatory postsynaptic current) or inhibitory (IPSC: inhibitory postsynaptic current) effects. The most common excitatory neurotransmitter in the mammalian CNS is L-glutamate. Binding of glutamate to postsynaptic receptors activates unspecific cation channels and the influx of cations depolarizes the postsynaptic terminal thereby inducing an EPSP (Dingledine et al., 1999; Hollmann and Heinemann, 1994; Traynelis et al., 2010; Mayer 2011). The most prominent inhibitory neurotransmitter in the brain is GABA (gamma-aminobutyric acid). The binding of an inhibitory neurotransmitter induces the inward flow of Cl^- thus hyperpolarizing the postsynapse (IPSP).

1.1.2 Postsynaptic glutamate receptors

The primary function of the postsynapse is to receive information (in terms of neurotransmitter) and to retransform them into electrical signals. The postsynapse is functionally characterized by different types of receptors that are selective for the presynaptically released neurotransmitter. Hence, the interaction of released neurotransmitter and postsynaptic receptors determines whether a synapse operates excitatory or inhibitory. In the following, we want to focus on the main characteristics of the postsynapse of excitatory synapses. After release of glutamate from the presynapse, it binds to postsynaptic glutamate receptors and induces EPSPs. Two major types of ionotropic glutamate receptors have been described. Glutamate binding to ionotropic AMPA (α-amino-3-hydroxy-5-methylisoxazol-4-propionacid), NMDA (N-methyl-D-aspartate) and kainate receptors causes opening of an ion pore selective for cations (Traynelis et al., 2010; Mayer 2011). By contrast, glutamate binding to metabotropic glutamate receptors (mGluRs) affects G protein signal cascades and thus indirectly induces modulation of ion channels (Nakanishi, 1994). Ionotropic and metabotropic glutamate receptors feature diverse structural characteristics. Metabotropic glutamate receptors consist of seven transmembrane domains that cross the postsynaptic membrane (Nakanishi, 1994). Ionotropic

glutamate receptors consist of four homologous subunits enclosing the ion pore. Each subunit has three transmembrane and one hydrophobic domain (Traynelis et al., 2010; Mayer 2011). In contrast to most AMPA and kainate receptors (permeable for Na^+ and K^+), NMDA receptors are also permeable for Ca^{2+}-ions. This characteristic enables the key function of NMDA receptors in synaptic plasticity where Ca^{2+}-influx initiates signaling cascades that potentiate synapses (Kerchner and Nicoll, 2008; Traynelis et al., 2010; Mayer 2011; Bliss and Collingridge, 2013).

1.1.3 Postsynaptic density of excitatory synapses

The postsynaptic density (PSD) comprises an electron dense structure near the postsynaptic membrane (Siekevitz, 1985; Sheng and Kim, 2011). It is composed of different types of scaffolding proteins, regulatory enzymes and cytoskeletal structures. The PSD ensures proper apposition of pre- and postsynaptic sites during brain development and improves the localization of receptors in close proximity to presynaptic vesicle cluster. Furthermore, proteins of the PSD perform catalytic functions. The size of the PSD correlates with the number of glutamate receptors and the extent of spines (Kasai et al., 2003), with the total number of protein within the PSD still in discussion. Based on localization and function, several groups of PSD proteins can be distinguished. For instance, the membrane associated molecules like glutamate receptors or cell adhesion molecules. The most abundant proteins within the PSD are catalytic enzymes of the CaMKII family (Peng et al., 2004). CaMIIα catalyses the recruitment of additional AMPA receptors to the postsynaptic membrane after Ca^{2+}-influx through NMDA receptors, hence facilitating long-term potentiation (LTP) (Hayashi et al., 2000). In glutamatergic synapses, the second most abundant molecules belong to the group of scaffolding proteins. The postsynaptic density protein 95 (PSD95) plays a major role within the postsynaptic density. It binds to NMDA receptors, AMPA receptors (via TARPs), cell adhesion molecules and other ion channels and is crucial for the proper localization of these proteins within the PSD (Kim and Sheng, 2004; Sheng and Kim, 2011). It is essential for the functionality of the whole PSD as revealed by RNAi knockdown experiments (Chen et al., 2011). PSD95 is a member of the membrane-associated guanylate

kinase (MAGUK) superfamily. Proteins of this group contain three PDZ domains, one SH3 domain and a guanylate kinase part. The PDZ domains are crucial for protein-protein interaction and can bind various molecules within the PSD (Peng et al., 2004; Funke et al., 2005; Kim and Sheng, 2004). For instance, PSD95 interacts with NMDA receptors through binding of its first two PDZ domains to the GluN2 subunit of the receptor (Kornau et al., 1995; Niethammer et al., 1996). Furthermore, it enhances postsynaptic receptor clustering by stabilizing NMDA receptors at the cell surface (Prybylowski et al., 2005) or by targeting of NMDA receptors to the PSD (Sprengel et al., 1998). Moreover, PSD95 couples NMDA receptors to signaling pathways like nitric oxide synthase (Aarts et al., 2002) or SynGAP (synaptic GTPase activating protein) (Kim et al., 2005). PSD95 also affects AMPA receptors and thereby modulates synaptic function as revealed by changes in EPSCs upon overexpression (El-Husseini et al., 2000) and RNAi knockdown experiments (Futai et al., 2007). Additionally, PSD95 is involved in the modulation of synaptic function and transsynaptic signaling by binding of cell adhesion molecules like neuroligin (Irie et al., 1997) that binds presynaptically localized neurexins (Ichtchenko et al., 1995; Comoletti et al., 2007; Südhof, 2008). Also other scaffolding molecules of the PSD support the functional interaction of CAMs within the postsynapse and hence enable transsynaptic signaling. For instance, it has been shown that neuroligin is linked with N-cadherin via the PDZ domain containing molecule S-SCAM. This transsynaptic pathway induces presynaptic vesicle clustering in immature cortical neurons (Stan et al., 2010).

1.2 Presynaptic vesicle exo- and endocytosis

One crucial feature of the development and the proper function of dynamic networks within the CNS is the ability of synaptic contacts to adapt to changes in neuronal activity. In this context, a main characteristic of chemical synapses is their capability to react to activity changes hence enabling dynamic processes. Modifications of synaptic signal transmission can occur pre- and postsynaptically. Presynaptically, the strength of synaptic transmission is basically determined by the release of neurotransmitter via exocytosis and compensatory endocytosis of transmitter-filled vesicles. On the postsynaptic site, ionotropic and metabotropic receptors are targets for synaptic modulation. The main topic of this work was the analysis of presynaptic functionality and its modulation by cell adhesion molecules with a particular focus on vesicular exo- and endocytosis.

1.2.1 The presynaptic vesicle cluster

Neurotransmission by chemical synapses depends on the release of neurotransmitter from vesicles of the presynaptic vesicle cluster. The presynaptic vesicles can be classified into three different groups with diverse spatial locations and release kinetics (Fig. 1.1; for review see Rizzoli and Betz, 2005). The smallest group of vesicles comprises the readily releasable pool (RRP). Vesicles of the RRP are docked at the presynaptic membrane and primed for fast exocytosis upon stimulation (Südhof, 2004). This pool contains only 5-20 vesicles and needs to be refilled by the recycling pool. The recycling pool contains up to 20 % of the whole vesicle cluster and refills the RRP upon prolonged stimulation (Schikorski and Stevens, 1997; for review see Harata et al., 2001). The largest pool of synaptic vesicles represents the reserve pool (≙ resting pool). The function of these vesicles has not been clarified yet, especially in hippocampal neurons where these vesicles are very difficult to release under physiological conditions (Harata et al., 2001). It has been shown that also the endocytosis of these vesicles is slower compared with RRP and recycling pool vesicles indicating endosomal intermediates of reserve pool vesicles (Takei et al., 1996; for review see Aravanis et al., 2003). Based on these

observations, it is obvious that RRP and recycling pool vesicles are working together to enable prolonged synaptic transmission under physiological conditions. The specific function of the reserve pool is not clear, but a key role upon very strong synaptic activity can at least be predicted.

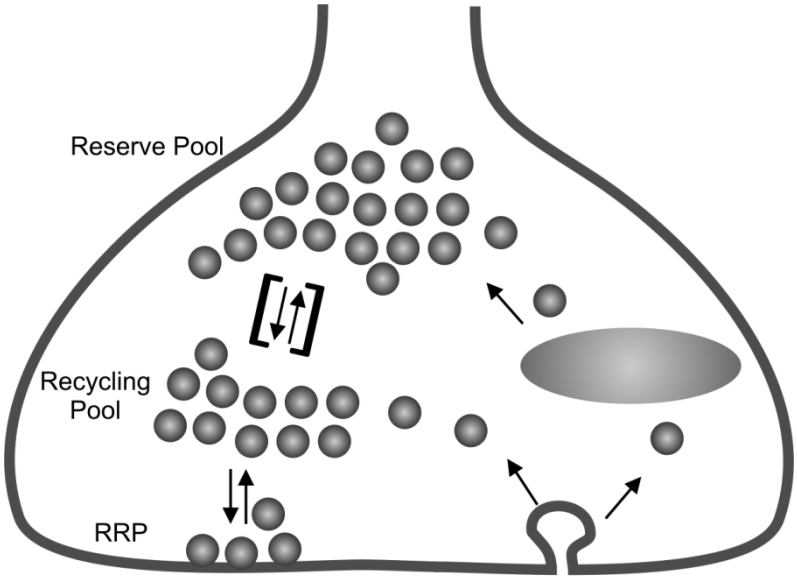

Figure 1.1 The presynaptic vesicle cluster
The presynaptic vesicle cluster can be divided into three groups. Primed vesicles are docked at the presynaptic membrane and comprise the readily releasable pool (RRP). Fused vesicles of the RRP get refilled by the recycling pool. The largest pool is the reserve pool that shows little interaction with the RRP and the recycling pool.

1.2.2 The presynaptic vesicle cycle

Proper function of chemical synapses depends on the availability of transmitter-filled and release-competent vesicles. This in turn relies on a precise interplay of neurotransmitter release by vesicle exocytosis and vesicle recycling via endocytosis. To enable repeated rounds of release during strong synaptic activity, synaptic vesicles run through a controlled trafficking cycle called the synaptic vesicle cycle (Südhof, 2004; Jahn and Fasshauer, 2012). The vesicle cycle can be subdivided into six basic steps (Fig. 1.2).

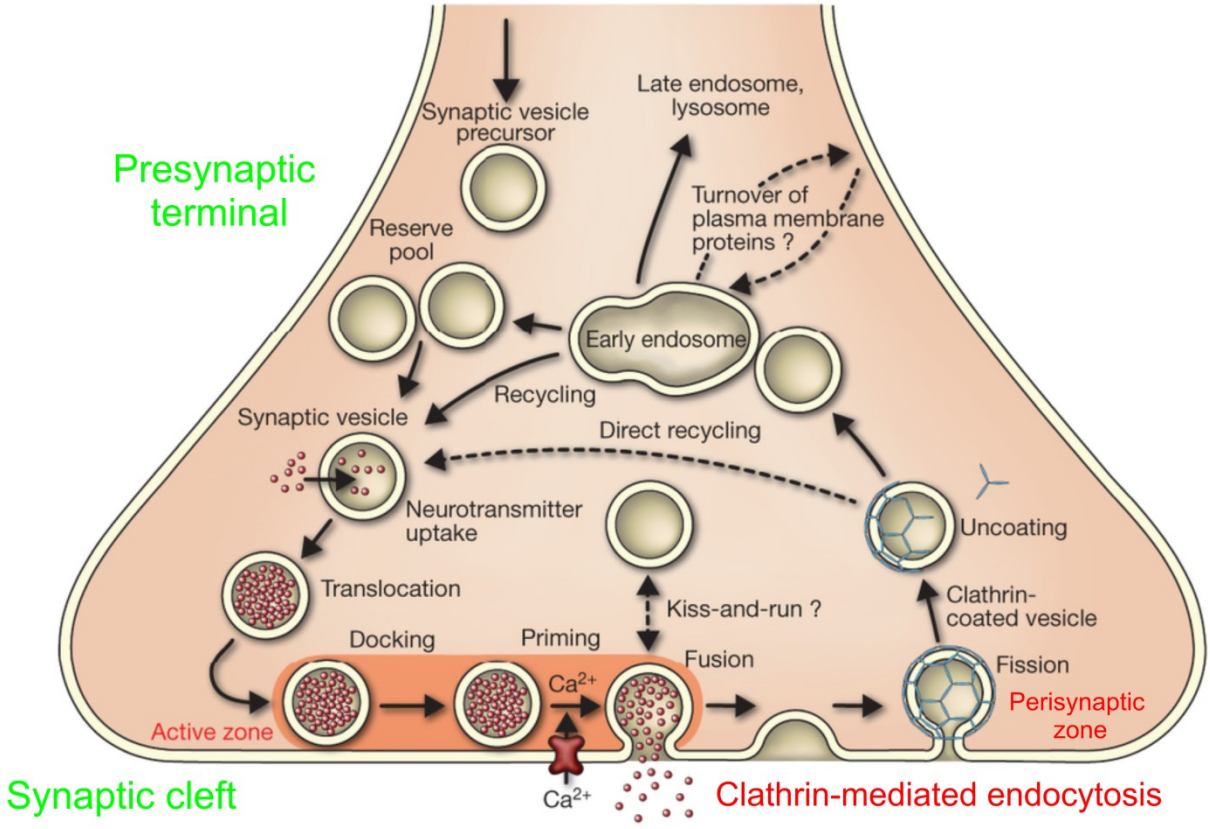

Figure 1.2 The synaptic vesicle cycle
(modified after Jahn and Fasshauer, 2012)
Synaptic vesicles get loaded with neurotransmitter within the presynaptic terminal. Filled vesicles get translocated to the plasma membrane where they dock and prime to be ready for fast exocytosis. Depolarization of the plasma membrane causes Ca^{2+}-influx through voltage-gated Ca^{2+}-channels and triggers vesicle fusion and neurotransmitter release. After exocytosis, small parts of the plasma membrane get endocytosed generally by clathrin-mediated endocytosis (CME). Under particular conditions, vesicles can also fuse by a fast kiss-and-run mechanism. After CME, vesicles get uncoated and refill the vesicle pool probably by passing an endosomal intermediate.

1) First, transmitter-filled vesicles cluster in front of the active zone. This process is activity-dependent and supported by the vesicle- and actin-binding protein synapsin (Llinas et al., 1991). At resting conditions, synapsin connects actin to the vesicles hence fixing them within the vesicle cluster. The intracellular Ca^{2+}-concentration regulates the uncoupling of synaptic vesicles from the cytoskeleton by activating a myosin light chain kinase (Chi et al., 2001; Jordan et al., 2005; Shtrahman et al., 2005). Thus the movement of synaptic vesicles to the active zone is the initial activity-dependent step of the vesicle cycle. 2) After vesicle movement, vesicles dock at the presynaptic membrane. 3) In a further step, vesicles get primed and go into a ready-to-fuse state. In this stage, a so called SNARE-complex (soluble NSF

attachment protein receptor complex) develops to enable a fast and direct fusion pore opening upon Ca^{2+}-influx. This complex is a bundle of two presynaptic membrane-associated proteins SNAP-25 and syntaxin and synaptobrevin2 (VAMP2), a protein that is anchored within the vesicle membrane (Mochida, 2000; Brunger, 2000; Rizo and Rosenmund, 2008; Südhof 2013). The formation of this complex is initiated by Munc18, a protein that binds syntaxin (Deàk et al., 2009). 4) Upon depolarization, Ca^{2+}-ions bind to synaptotagmin and induce conformational changes of the SNARE-complex hence decreasing the distance from vesicle- to presynaptic membrane (Chapman, 2002; Rizo and Südhof, 2002; Rizo and Rosenmund, 2008; Südhof 2013). Finally, a fusion pore opens and neurotransmitter molecules leave the vesicle and diffuse across the synaptic cleft to postsynaptic receptors. After transmitter release, the SNARE-complex gets disassembled by the ATPase NSF (N-ethylmaleimide Sensitive Factor) which is mobilized by α-SNAP (Whiteheart et al., 1994; Clary et al., 1990). 5) Following exocytosis of synaptic vesicles, parts of the presynaptic membrane get endocytosed again. This process occurs much slower than vesicle fusion and in different ways such as clathrin-mediated endocytosis (CME) or the more disputed “kiss-and-run”-mechanism (for review see Südhof, 2004). 6) Finally, vesicles get re-acidified by a V-type ATPase and refilled with neurotransmitter through H^+/neurotransmitter antiport and translocated to the recycling vesicle pool for a new round of fusion (Inoue et al., 2003).

1.2.2.1 Synaptic vesicle exocytosis

Synaptic transmission relies on the release of neurotransmitter from presynaptic terminals. The exocytosis of transmitter-filled vesicles occurs at the presynaptic active zone, a well characterized area including the presynaptic membrane and a cluster of proteins called the cytomatrix of the active zone (CAZ). The initiating step prior to exocytosis is docking and priming of synaptic vesicles, an ATP-dependent process that enables fast responds of the vesicles to Ca^{2+}-influx. This process is generally induced by two protein complexes, the SNARE (soluble NSF attachment protein receptor) proteins and the SM (Sec1/Munc18-like) proteins. Three SNARE proteins form the SNARE-complex, a four helix bundle essential for Ca^{2+}-triggered

synaptic transmission (Söllner et al., 1993; Poirier et al., 1998; Sutton et al., 1998). The vesicular anchored VAMP2 contributes, similar to the membrane-associated syntaxin, one SNARE motif. The membrane-associated protein SNAP-25 provides two SNARE motifs to interact with other proteins. Their role in vesicle fusion was basically established by the characterization of neurotoxins like tetanus or botulinum neurotoxin. These substrate specific proteases were shown to block presynaptic vesicle fusion by cleaving synaptobrevin (Link et al., 1992; Schiavo et al., 1992), SNAP-25 (Blasi et al., 1993(a)) or syntaxin (Blasi et al., 1993(b)). Synaptic vesicle exocytosis starts with the formation of a tight protein bundle called the SNARE-complex that runs through an assembly-disassembly cycle. The SNARE proteins form a trans-SNARE-complex by hydrophobic, α-helical interaction of synaptobrevin, synataxin and SNAP-25. This complex connects vesicular and presynaptic membrane and enables fusion pore opening upon Ca^{2+}-influx. The fusion and following complete merge of both membranes is initiated by Ca^{2+}-binding to the synaptic vesicle associated protein synaptotagmin. Synaptotagmin has two Ca^{2+}-binding sites and is anchored to the vesicular membrane via a transmembrane-domain. The C2A binding site can bind two Ca^{2+}-ions and the C2B domain binds three 3 Ca^{2+}-ions (Ubach et al., 1998; Geppert et al., 1994; reviewed in Südhof, 2013). Furthermore, synaptotagmin binds to syntaxin via its C2 domain (Lai et al., 2011). Ca^{2+}-binding to synaptotagmin leads to conformational changes of the SNARE-complex from a trans-interaction to a cis-conformation (Pang and Südhof, 2010). Furthermore, the action of synaptotagmin is promoted by complexins; small molecules that bind to SNARE complexes (McMahon et al., 1995; Südhof, 2004). Membrane fusion is catalyzed by several SM proteins like Munc-18 or Munc-13 (Verhage et al., 2000; Varoqueaux et al., 2002). For instance, it has been shown that Munc18 and Munc-13 interact to control the priming of synaptic vesicles. At rest, Munc-18 interacts with syntaxin through high affinity binding, thereby blocking the assembly of the SNARE-complex. Munc-13 on his part activates a proteinkinase (PKC) that interferes with the Munc-18/syntaxin-complex so syntaxin-1 gets in an open configuration and ready for SNARE assembly (Betz et al., 1997; Brose et al., 2000; Fujita et al., 1996; Burkhardt et al., 2008; Südhof and Rothman, 2009; Hu et al., 2011). In addition to SM proteins, SNARE-complex assembly is also supported

by two chaperone systems. A trimeric complex composed of CSPα (cysteine string protein α), the heat shock protein Hsc 70 and SGT (glutamate and threonine-rich protein) has been identified to be essential for proper synaptic function (Tobaben et al., 2001; Sharma et al., 2012). Furthermore, Burré et al. characterized the role of synucleins as presynaptic chaperons that can even compensate CSPα-knockout induced neurodegeneration in vertebrates (Burré et al., 2010; Chandra et al., 2005). Besides SM proteins and chaperons, SNARE-complex formation and fusion pore opening is also catalyzed and regulated by several other proteins within the active zone. For example, RIM (Rab3-interacting molecules) proteins are important for vesicle docking and priming and in the recruitment of Ca^{2+}-channels (VDCCs) to the active zone (Koushika et al., 2001; Deng et al., 2011; Kaeser et al., 2012; Han et al., 2011). It has also been shown that RIM proteins can modulate Ca^{2+}-channels and affect short-term plasticity (Uriu et al., 2010; Kaeser et al., 2012; Schoch et al., 2002; Castillo et al., 2002). RIM-BP (RIM-binding proteins) bind RIM proteins and hence are also essential for Ca^{2+}-channel recruitment (Kaeser et al., 2012). Munc-13 is an active zone protein involved in vesicle priming (Brose et al., 1995; Augustine et al., 1999). Several other proteins like α-Liprins, piccolo and bassoon are essential for vesicle clustering and thereby also crucial for proper synaptic vesicle exocytosis (Dai et al, 2006; Mukherjee et al., 2010). Presynaptic adaptor proteins like CASK, Velis or Mints also act on synaptic vesicle exocytosis (for review see Südhof, 2012). After exocytosis and transmitter release, synaptic vesicles and proteins involved in SNARE-complex formation have to be recycled to enable continuous signal transmission. This is ensured by compensatory endocytosis of small parts of the presynaptic membrane that contain all vesicle membrane associated molecules.

1.2.2.2 Synaptic vesicle endocytosis

Synaptic endocytosis is essential to maintain the availability of vesicles during high rates of synaptic transmission and perpetual exocytosis. The initial upstream step of endocytosis is the disassembly of the SNARE-complex. This is initiated by the ATPase NSF under ATP consumption and controlled by α-SNAP (Whiteheart et al., 1994; Clary et al., 1990). Subsequently, parts of the lipid bilayer and specific

vesicular molecules get endocytosed to maintain synaptic transmission. In general, three different forms of synaptic endocytosis have been discovered. The most disputed mechanism is called “kiss-and-run”-endocytosis (Stevens and Williams, 2000). “Kiss-and-run”-endocytosis shows no full fusion of the vesicle membrane with the presynaptic plasma membrane. Only a small (~ 5 nm) fusion pore develops so that neurotransmitter can enter the synaptic cleft (Rizzoli and Jahn, 2007). It has been shown that “kiss-and-run”-endocytosis is characterized by low release probability and preferentially occurs during high frequency stimulation (Gandhi and Stevens, 2003; Harata et al., 2006). A more common form of endocytosis comprises activity-dependent bulk endocytosis. Here a relatively large part of the presynaptic membrane gets endocytosed and is stored as an endosome within the presynaptic terminal. In a subsequent step, synaptic vesicles are formed out of the endosomes and refill the vesicle cluster after neurotransmitter uptake. Bulk endocytosis can be specifically induced by high frequency stimulation in vitro (Clayton et al., 2008). The most prevalent and best characterized mechanism is clathrin-mediated endocytosis. CME is characterized by clathrin-coats that enwrap the membrane invaginations that are formed out of the plasma membrane. First observations of clathrin-coated pits were made in the frog neuromuscular junction (NMJ) by electron microscopy (Heuser et al., 1974). The clathrin-coat is recruited under assistance of several clathrin-adaptor proteins like AP-2, AP-180 or stonin2 (for review see Saheki and De Camilli, 2012). Thereby the adaptor proteins ensure the recycling of former vesicular membrane and their components like SNARE proteins. For instance, AP-2 and stonin2 bind the Ca^{2+}-sensor synaptotagmin (Haucke and De Camilli, 1999; Diril et al., 2006). AP-2 also binds vesicular neurotransmitter transporter hence recognizing vesicular components (Fei et al., 2008). Furthermore Koo et al. described the specific binding of AP-180 to synaptobrevin as “SNARE-motif-mediated sorting” of vesicular membrane parts (Koo et al., 2011). Thus AP-2 and AP-180 initiate the attachment of clathrin and dynamin to the endocytotic zone (Wakeham et al., 2000). Finally, the clathrin-coated pits get pinched-off by the GTPase dynamin under GTP hydrolysis (Hinshaw and Schmid, 1995; Ferguson and De Camilli, 2012). The essential role of dynamin was demonstrated by experiments using the temperature-sensitive shibire mutation in Drosophila that shows a strong phenotype caused by the blockade of

endocytosis and depletion of synaptic vesicles (Koenig and Ikeda, 1989). These first observations were confirmed in several studies, for instance in synapses lacking dynamin (Raimondi et al., 2011). In physiological experiments, the small molecule dynasore can be used to specifically block synaptic endocytosis as it interferes with GTPase activity thus demonstrating the importance of dynamin for the fission of synaptic vesicles (Macia et al., 2006; Hua et al., 2013). Several studies revealed endosomal structures within the presynaptic terminal during CME (Harata et al., 2006; Saheki and De Camilli, 2012).

1.3 Synaptic cell adhesion molecules

Neuronal cell adhesion molecules are transmembrane proteins that connect the pre- and postsynapse by homophilic binding to each other or by heterophilic interaction with other proteins. CAMs provide mechanical stability and can induce synaptic modulation via transsynaptic signaling. In particular, the roles of CAMs in the development of immature neurons are well characterized and range from stability and initial target recognition to synaptic differentiation and the regulation of synaptic structures during synaptogenesis (Fig. 1.3; for review see Yamagata et al., 2003; Siddiqui and Craig, 2011).

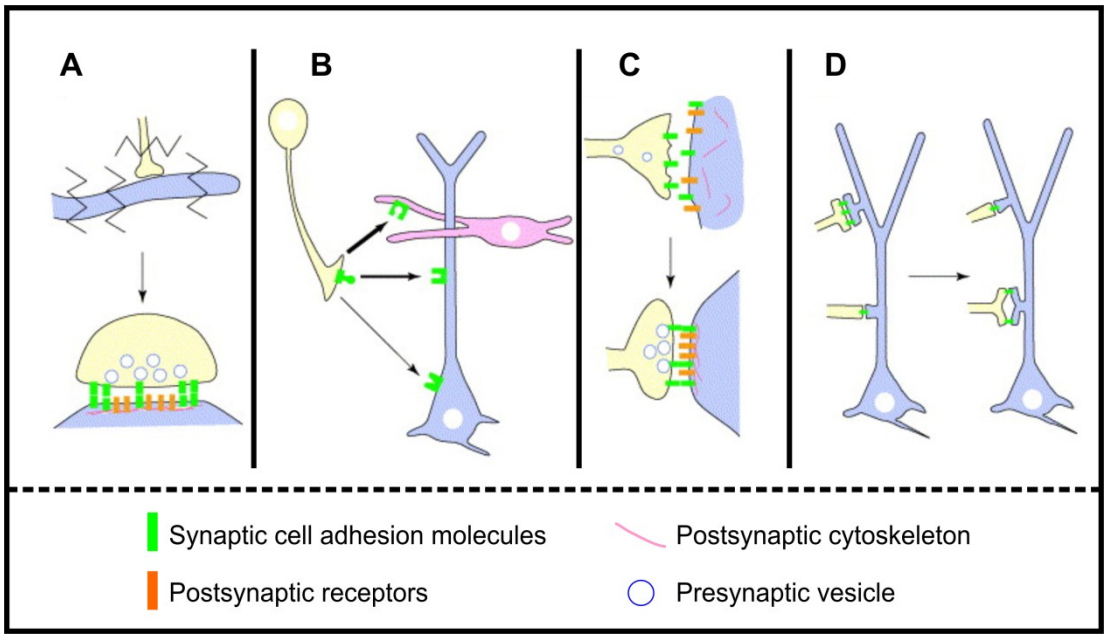

Figure 1.3 The roles of synaptic cell adhesion molecules in synapse formation and function
(modified after Yamagata et al., 2003)
Illustration of potential roles of different CAMs in synapse formation and function. (**A**) Mechanical stability mediates a solid coherence of pre- and postsynaptic components. (**B**) Recognition of appropriate partners or regions for synaptogenesis. (**C**) Synaptic differentiation by recruitment of synapse specific molecules to the pre- and postsynaptic terminal. (**D**) Modulation of synaptic size and shape subsequently affects synaptic efficiency.

Extracellular, neuronal adhesion molecules can bind to each other within the synaptic cleft or bind to proteins of the extracellular matrix. Intracellular, CAMs are generally

connected to signaling molecules or cytoskeletal proteins within the presynaptic active zone or the PSD. Besides integrins and proteins of the immunoglobulin superfamily (Ig), cadherins and the neuroligin/neurexin complex represent the most prominent synaptic cell adhesion molecules of the CNS. A large group within the CNS are the cadherins (Ca^{2+}-dependent adhesion molecules). This superfamily of adhesion molecules consists of three different groups: classic cadherins (e.g. N-, R- and E-cadherin), protocadherins and the cadherin-related neuronal receptors (CNR). The most common cadherin in the mammalian CNS is neuronal (N)-cadherin. N-cadherin proteins are present at both, the pre- and postsynaptic site and bind homophilically to each other within the synaptic cleft in a Ca^{2+}-dependent manner (for review see Pokutta and Weis, 2007; Brigidi and Bamji., 2011). Another well characterized complex is the neuroligin/neurexin cell adhesion system. Neuroligin is present at the postsynaptic site and binds to neurexins that are anchored in the presynaptic plasma membrane hence representing a heterophilic interaction of two divergent CAMs (Krueger et al., 2012).

1.3.1 The homophilic N-cadherin adhesion complex

N-cadherin mediates adhesion, signaling, synapse formation and synaptic plasticity by homophilic interactions within the synaptic cleft and intracellular binding to catenins. N-cadherin is synthesized from a precursor polypeptide by proteolytic elimination of the N-terminal propeptide and a short signaling sequence. N-cadherin belongs to the type I classical cadherins and consists of five extracellular domains (ECDs), one transmembrane domain and a cytoplasmatic tail that enables interactions with signaling molecules and cytoskeletal structures. The ECDs are enclosed by four Ca^{2+}-binding sites that enable homophilic interactions in trans and cis (Fig. 1.4; Pokutta and Weis, 2007; Brasch et al., 2012). The extracellular part contains a specialized sequence of the amino acids histamine, alanine and valine (HAV motif) that is important for the homophilic interaction (Yap et al., 1997; Williams et al., 2000; Pokutta and Weis, 2007; Brasch et al., 2012). Trans-interaction of N-cadherin creates weakly connected cadherin monomers whereas the cis-interaction is much stronger resulting in the formation of cis-dimers with strong trans-interaction

(Shapiro et al., 1995; Brasch et al., 2012). Homophilic interaction between N-cadherin in trans is mediated through binding of the ECD1 of both N-cadherin molecules, whereas cis interaction is made by binding of the ECD1 of one N-cadherin molecule to the ECD2 of another N-cadherin molecule (Pokutta and Weis, 2007). Within the pre- and postsynaptic structures, N-cadherin interacts via its C-terminal end with catenins that in turn regulate actin (Yamada et al., 2005).

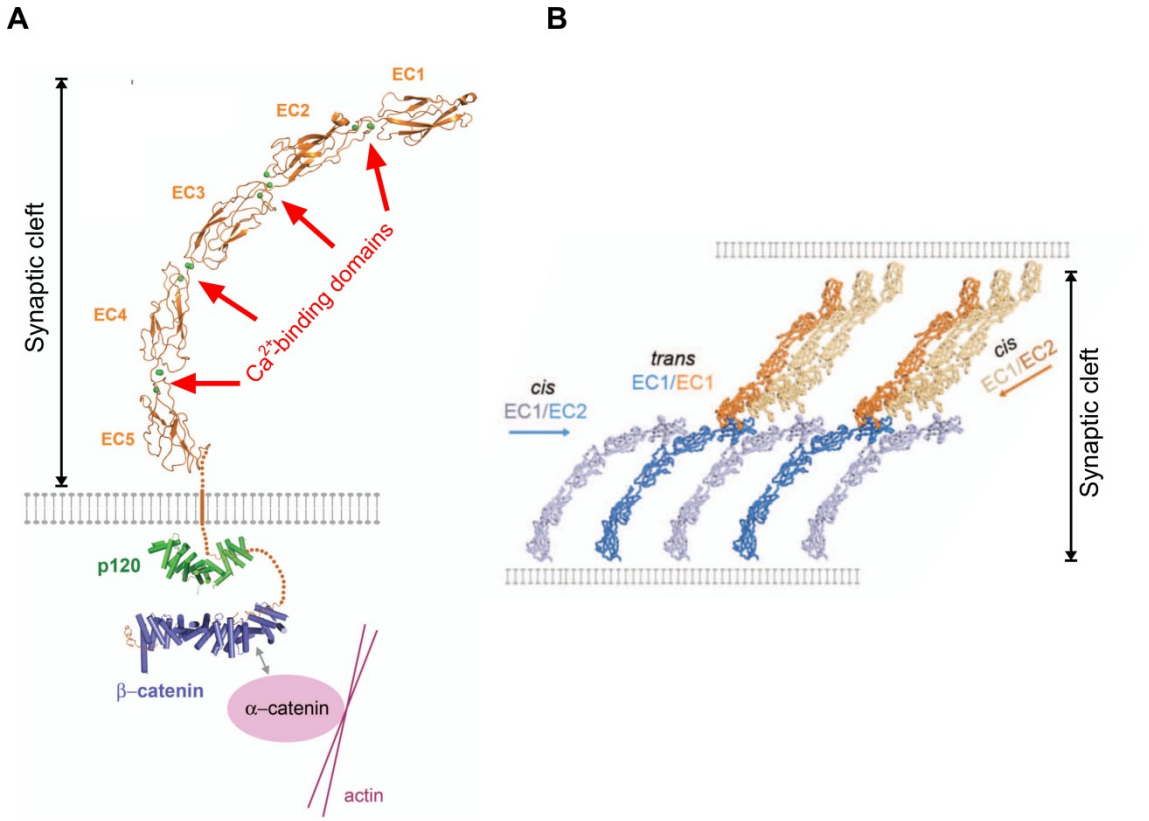

Figure 1.4 Homophilic adhesion of cadherins
(modified after Brasch et al., 2012)
(**A**) Overall structure of classical cadherins. The extracellular domain consists of 5 domains (EC1-EC5). The cytoplasmic domain binds to p120 and β-catenin. C-terminal interaction of β-catenin with α-catenin links cadherins to the actin-cytoskeleton. (**B**) Extracellular adherens of cadherins by cis- and trans-interaction. Trans-interaction is mediated by EC1/EC1 binding. Cis-interaction is made by EC1/EC2 binding.

The expression of N-cadherin in the CNS changes during development and maturation. In immature neurons, N-cadherin is expressed in nascent excitatory and inhibitory synapses, whereas it disappears in mature inhibitory synapses during brain development. Additionally, the synaptic localization of N-cadherin within excitatory synapses changes upon development. More precisely, N-cadherin moves from the

center of the active zone to the perisynaptic zone during synapse maturation (Benson and Tanaka, 1998; Elste and Benson, 2006). N-cadherin adhesion is well known to regulate synapse formation and synaptic maturation of immature neurons. Effects of interfering with N-cadherin function were found both, pre- and postsynaptically. On the presynapse it has been shown that inhibiting N-cadherin adhesion decreased the recruitment of synaptic vesicles in immature hippocampal neurons (Togashi et al., 2002; Stan et al., 2010). On the postsynaptic site, N-cadherin affects the formation and maturation of spines by indirect interaction with the actin-cytoskeleton via α- and β-catenins (Togashi et al., 2002). It has been shown, that manipulating N-cadherin signaling leads to increased development of immature filopodia-like processes by altered interaction with catenins (Bozdagi et al., 2010; Abe et al., 2004). Furthermore, activity-dependent spine morphogenesis and long-term potentiation (LTP) are controlled by N-cadherin (Mendez et al., 2010; Bozdagi et al., 2010). N-cadherin has been proposed to directly influence spine functionality by interaction with the AMPA receptor subunit GluR2 irrespective of signaling via catenins or actin. It has been described that N-cadherin interacts with the extracellular domain of GluR2 to increase mEPSC frequency and spine formation (Saglietti et al., 2007). N-cadherin attendance also reflects the activity of neuronal networks on the synapse level. Upon high synaptic activity, endocytosis of N-cadherin is reduced and results in elevated membrane-associated N-cadherin levels (Tai et al., 2007). However, another study describes an activity-driven decline of N-cadherin adhesion. Here it was shown that NMDA receptor activity increased the activity of presenilin-1 that cleaves N-cadherin within its transmembrane domain (Marambaud et al., 2003). Besides the impact of N-cadherin on structure and morphology of dendritic spines and synapses in general, several studies describe a crucial role in the functionality of synaptic contacts. N-cadherin knockout lead to increased synaptic depression (Jüngling et al., 2006) and strongly reduced long-term potentiation (Bozdagi et al., 2010). In addition, a transsynaptic function of N-cadherin was described with postsynaptic N-cadherin regulating presynaptic function (Jüngling et al., 2006). Furthermore it was shown in hippocampal slices that the induction and stability of LTP is controlled by N-cadherin adhesion (Bozdagi et al., 2004; Bozdagi et al., 2010). More recent studies also predict a functional cooperation of N-cadherin

with other cell adhesion molecules to affect synapse maturation and functionality. It has been shown that N-cadherin cooperates with the cell adhesion system neuroligin/neurexin to induce vesicle clustering at the presynaptic site. The transsynaptic signaling was mediated by the scaffold molecule S-SCAM that connects N-cadherin and neuroligin within the postsynaptic terminal hence enabling transsynaptic signaling (Stan et al., 2010; Aiga et al., 2011). Interestingly, N-cadherin can also regulate synaptic formation and function in a negative fashion. A mismatch situation with N-cadherin selectively expressed at the postsynaptic site leads to impaired synaptic function revealed by reduced AMPA receptor mediated EPSCs. A long-term mismatch expression finally results in synapse elimination and axon retraction (Pielarski et al., 2013). In vivo, the expression pattern of homophilic cell adhesion molecules might create a code to stabilize synaptic contacts and to reorganize network structures. A crucial role of N-cadherin expression in axon outgrowth and formation of functional circuits was already predicted in previous studies (Redies et al., 1993; Obst-Pernberg et al., 2001). However, the functional roles of N-cadherin are not restricted to vesicle clustering or spine formation in immature neurons. Furthermore a crucial role of N-cadherin on the functionality of mature synapses has been proposed. Examining synaptic functionality by electrophysiology and optical methods revealed that interfering with postsynaptic N-cadherin reduces presynaptic release (Jüngling et al., 2006; Vitureira et al., 2011).

1.3.2 The heterophilic neuroligin/neurexin interaction

Another well characterized transsynaptic cell adhesion system is the neuroligin-1/neurexin interaction. In this heterophilic cell adhesion system, the postsynaptic CAM neuroligin-1 binds to neurexins that are anchored within the presynaptic membrane (Fig. 1.5). Neuroligins compose of a single extracellular domain, a transmembrane domain and a cytoplasmatic tail that binds to PDZ domain containing molecules within the postsynaptic terminal via a PDZ-domain recognition motif. In mammals, neuroligins are encoded by at least four genes (NLG1-4) (Ichtchenko et al., 1996). Localization studies indicated neuroligin-1 expression exclusively in excitatory synapses (Song et al., 1999) and neuroligin-2 located to inhibitory

synapses (Varoqueaux et al., 2004). In contrast, neuroligin-3 expression has been detected in both, inhibitory GABAergic and excitatory glutamatergic synapses (Budreck and Scheiffele, 2007).

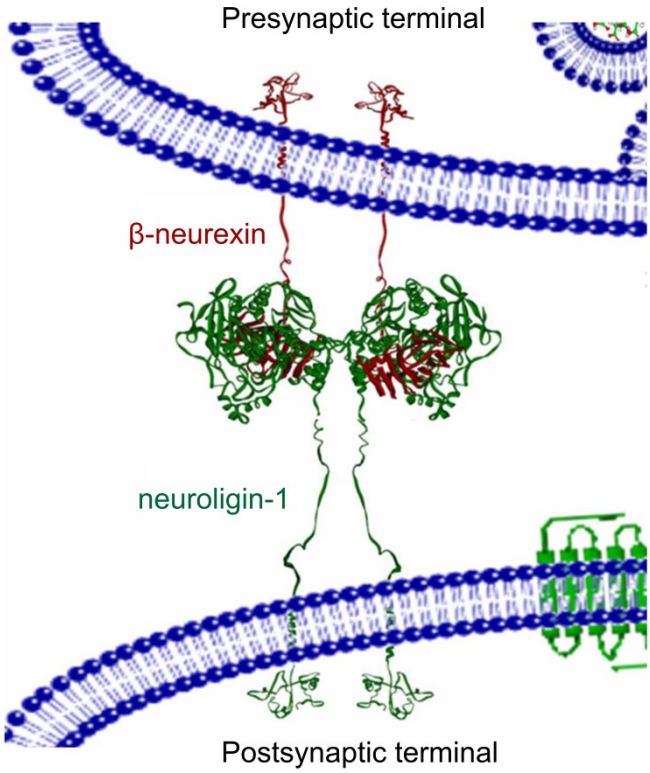

Figure 1.5 The transsynaptic neuroligin/neurexin interaction
(modified after Comoletti et al., 2008)
Illustration of the transsynaptic neuroligin-1/β-neurexin interaction. Neuroligin-1 (green ribbon) is anchored to the postsynaptic membrane and binds to β-neurexin within the synaptic cleft. β-neurexin (red ribbon) is tethered at the presynaptic terminal.

Postsynaptic neuroligins bind to presynaptic neurexins (Ichtchenko et al., 1995). Neurexins were first discovered as receptors for the black-widow spider neurotoxin α-latrotoxin, a toxin that causes massive release of neurotransmitter in vertebrates (Ushkaryov et al., 1992). Neurexins can be grouped into two classes: α-neurexins and β-neurexins, each encoded by three genes (Missler and Südhof, 1998). α- and β-neurexins differ in the number of extracellular domains. α-neurexins contain six LNS (laminin, nectin, sex-hormone binding globulin) domains and β-neurexins are smaller proteins with just one LNS domain. Neuroligin-1 can bind numerous isoforms of all three neurexins and became the best characterized neuroligin/neurexin

adhesion system in subsequent studies (Ichtchenko et al., 1995; Südhof, 2008). The binding of neuroligin-1 to neurexins via their N-terminal extracellular domains within the synaptic cleft is controlled by alternative splicing of both genes (Boucard et al., 2005). The C-terminal domain of neuroligins and neurexins each contain a PDZ-domain recognition motif that binds PDZ domains that are characteristic elements of pre- and postsynaptic scaffolding molecules (Missler and Südhof, 1998). The most common C-terminal binding partners of β-neurexins within the presynaptic terminal are CASK and Mints that also bind to each other thus forming a large tripartite protein complex (Butz et al., 1998). Within the postsynaptic terminal neuroligins can bind to several proteins of the postsynaptic density like PSD95 or S-SCAM (Irie et al., 1997; Chen et al., 2000). Similar to N-cadherin, neuroligin-1/β-neurexin adhesion is Ca^{2+}-dependent and requires preceding clustering of neuroligins as revealed by neuroligin oligomerization mutants that fail to bind β-neurexin (Nguyen and Südhof, 1997; Dean et al., 2003). Neuroligin-1/β-neurexin adhesion is thought to control key steps of initial synapse formation and synapse maturation within the CNS. The role of neuroligins in the formation of synaptic contacts was impressively demonstrated by an artificial experimental approach with non-neural cells contacting neurons. In this approach, the postsynaptic expression of neuroligins (Nlg-1 and Nlg-2) in fibroblast cells induced synaptogenesis in contacting axons. On the other site, blocking endogenous neuroligin/neurexin interaction with soluble neurexin decreased presynaptic synapse formation (Scheiffele et al., 2000). The artificially generated hemi-synapses are physiologically and structurally analogs of normal synapses (Scheiffele et al., 2000; Fu et al., 2003; Sara et al., 2005). Subsequent studies further demonstrated the roles of neuroligins and neurexins in synapse formation and function. For example, the overexpression of HA-Nlg-1 increases levels of presynaptic and postsynaptic proteins like synaptophysin or PSD95. In parallel, the overexpression of Nlg-1 increases mEPSC and mIPSC frequency indicating an increased number of functional presynaptic sites (Prange et al., 2004). A series of subsequent studies confirmed and extended these observations in less artificial culture systems for diverse neuroligin isoforms (Varoqueaux et al., 2006; Wittenmayer et al., 2009; Chih et al., 2005; Levinson and El-Husseini, 2005). Identically to mammals, four neuroligin genes (dnlg1-4) were identified in Drosophila. It has been shown that neuroligin-1

affects synaptic differentiation and function in Drosophila neuromuscular junctions (NMJs) at the pre- and postsynaptic site via transsynaptic interaction with neurexin-1 and the presynaptic active zone protein Syd-1 (Banovic et al., 2010; Owald et al., 2012). Furthermore, studies on Drosophila dnl2 null mutants revealed a crucial role of neuroligin-2 in synapse maturation and function (Sun et al., 2011). More recent studies showed the requirement of neuroligin-3 for the development and differentiation in NMJs (Xing et al., 2014) and the essential role of neuroligin-4 in sleep regulation (Li et al., 2013).

1.4 Aims of the study

Major goal of this work was the examination of the roles of N-cadherin and neuroligin-1 in presynaptic function. Furthermore, a potential cooperation between these two CAMs in the regulation of presynaptic vesicle cycling was addressed. These questions were instigated by previous studies that described a functional cooperation of N-cadherin and neuroligin-1 in presynaptic vesicle clustering in immature synapses (Stan et al., 2010; Aiga et al., 2011). Furthermore, a series of previous studies indicated functional effects of N-cadherin and neuroligin-1 on presynaptic vesicle cycling as revealed by fluorescence microscopy or electrophysiology. However, a differential analysis of potential exo- and endocytotic effects of these CAMs in mature, postsynaptogenic neurons still has to be done. Immunocytochemical stainings for the vesicle membrane associated protein VAMP2 were performed to verify the maturity of the cell culture system as indicated by the lack of synaptogenesis by overexpression of N-cadherin and neuroligin-1 protein. Activity-dependent methods were used for the subsequent study of potential effects of these CAMs on presynaptic function. FM4-64 staining and destaining experiments were performed to study basic characteristics of presynaptic functionality. FM dye is taken up exclusively by active cycling vesicles, hence providing functional information in contrast to immunostainings that are restricted to structural observations. Furthermore, FM experiments enable the distinct analysis of presynaptic function in contrast to electrophysiological approaches that mainly reveal postsynaptic properties. In this context, the use of pHluorin-based imaging was of particular interest to further improve the significance of analysis of presynaptic functions. Therefore, experiments with the genetically encoded probe synaptophysin-pHluorin (SypHy) were performed in an autaptic glial microisland cell culture system. SypHy enables the differential analysis of presynaptic vesicle exo- and endocytosis within one experiment based on sensitive recordings of changes of intravesicular pH values. The autaptic culture system allows the simultaneous analysis of several presynaptic SypHy puncta within one experiment. Furthermore, it enables the concurrent overexpression of homophilic N-cadherin at the pre- and postsynaptic site. SypHy protein was expressed in individual neurons together with DsRed2 as a marker for transfected cells because of the quenched SypHy fluorescence signal in

the resting state of the synapse. The action of N-cadherin and neuroligin-1 was examined in “gain-of-function” and “loss-of-function”-experiments by overexpression or knockout of these molecules.

In the second part of this study, the roles of N-cadherin and neuroligin-1 were deepened with a special focus on the coupling of presynaptic vesicle exo- and endocytosis. Although the compensation of vesicular exocytosis by subsequent endocytosis appears to be indispensable for the maintenance of proper synaptic function, little is known about the mechanisms and molecules that are involved in the coupling of presynaptic vesicle cycling. In an elaborated experimental approach, N-cadherin was further analyzed with special regard to its behavior upon increased synaptic activity. Therefore, double-stimulation SypHy experiments were performed in N-cadherin knockout neurons to compare compensatory vesicle endocytosis upon weak and strong exocytosis. Finally, immunocytochemical stainings were performed to analyze structural changes of pre- and postsynaptic molecules upon intense synaptic activity and altered coupling of presynaptic vesicle exo- and endocytosis.

2 Materials and methods

2.1 Culture media and chemicals

2.1.1 Cell culture media

Neurobasal medium (NB medium)

NB medium	500 ml	Gibco; Cat. No. 21103-049
+ B27- Supplement 50x	10 ml	Gibco; Cat. No. 17504-036
+ Glutamax-I-Supplement	2,5 ml	Gibco; Cat. No. 35050-038
+ Penicillin-Streptomycin solution 100x	5 ml	Gibco; Cat. No. 15140-122

Basal medium (BME medium)

Basal Medium Eagle 1x	500 ml	Gibco; Cat. No. 41010-026
+ FBS	50 ml	Gibco; Cat. No. 10500-064
+ L-Glutamin (200 mM)	5 ml	Gibco; Cat. No. 25030-024
+ Glucose (40 %)	3 ml	J.T.Baker; Cat. No. 0114
+ Insulin-Transferrin-Selenium solution	5 ml	Gibco; Cat. No. 51300-044
+ Penicillin-Streptomycin solution 100x	5 ml	Gibco; Cat. No. 15140-122

Solutions used for primary culture and glia preparation

PBS Dulbecco`s phosphate-buffered saline ($PBS^{+/+}$)	Gibco; Cat. No. 14040-091
PBS Dulbecco`s phosphate-buffered saline without Ca^{2+}, Mg^{2+}	Gibco; Cat. No. 14190-094

1x Trypsin-EDTA (0,05 %)		Gibco; Cat. No. 25300-054
Trypsin (0,25 %)		Gibco; Cat. No. 25050-014
ARA-C (Cytosin-β-D-Arabinofuranosid hydrochloride)	10µM	Sigma-Aldrich; Cat. No. C-6645
Poly-L-Ornithine	1 mg/ml	Sigma-Aldrich; Cat. No. P-3655
Boric acid	0,15 M	Sigma-Aldrich; Cat. No. 083K0055

Solutions used for transfection

NeuroMag Beads	OZ Biosciences Cat. No. NM51000
Endotoxin-free H_2O	Quiagen; Cat. No. 1018458

Solutions used for determination of cell viability

calcein-AM	1/2000	Molecular Probes Cat. No. C1430

2.1.2 Buffer for immunocytochemical stainings

Blocking buffer I

FBS	10 %	Gibco; Cat. No. 10500-064
Sucrose	5 %	Merck; Cat. No. 1076871000
BSA	2 %	Sigma-Aldrich; Cat. No. A4919
TritonX100	0,3 %	Sigma-Aldrich; Cat. No. X100

...in PBS Dulbecco`s phosphate- buffered saline ($PBS^{+/+}$)

	82,7 %	Gibco; Cat. No. 14040-091

Blocking buffer II

equivalent to blocking buffer I but without FBS. Equal replacement of FBS with $PBS^{+/+}$.

2.1.3 Extracellular solutions

Solutions for FM experiments (high [K^+] stainings)

FM4-64-Extra I

NaCl	130 mM	J.T.Baker; Cat. No. 0278
KCl	5 mM	Sigma-Aldrich; Cat. No. 31248
$CaCl_2$	2,5 mM	Sigma-Aldrich; Cat. No. 12074
$MgCl_2$	1 mM	Sigma-Aldrich; Cat. No. 63068
HEPES	20 mM	AppliChem; Cat. No. A 1069,0100
Glucose	0 mM	Merck; Cat. No. 1083370250

FM4-64-Extra I (90 mM K^+ depolarization solution)

NaCl	45 mM	J.T.Baker; Cat. No. 0278
KCl	90 mM	Sigma-Aldrich; Cat. No. 31248
$CaCl_2$	2,5 mM	Sigma-Aldrich; Cat. No. 12074
$MgCl_2$	1 mM	Sigma-Aldrich; Cat. No. 63068
HEPES	20 mM	AppliChem; Cat. No. A 1069,0100
Glucose	0 mM	Merck; Cat. No. 1083370250
FM4-64	20 µM	Molecular Probes; Cat. No. T-13320

FM4-64-Extra I (wash solution)

NaCl	130 mM	J.T.Baker; Cat. No. 0278
KCl	5 mM	Sigma-Aldrich; Cat. No. 31248
$CaCl_2$	1 mM	Sigma-Aldrich; Cat. No. 12074
$MgCl_2$	10 mM	Sigma-Aldrich; Cat. No. 63068
HEPES	20 mM	AppliChem; Cat. No. A 1069,0100
Glucose	0 mM	Merck; Cat. No. 1083370250
ADVASEP-7	1 mM	Sigma-Aldrich; Cat. No. A3723

adjusted to pH 7,3 with NaOH

Solutions for FM4-64 experiments (electrical stimulations)

Extracellular solution II

NaCl	119 mM	J.T.Baker; Cat. No. 0278
KCl	2,5 mM	Sigma-Aldrich; Cat. No. 31248
$CaCl_2$	2 mM	Sigma-Aldrich; Cat. No. 12074
$MgCl_2$	2 mM	Sigma-Aldrich; Cat. No. 63068
HEPES	25 mM	AppliChem; Cat. No. A 1069,0100
Glucose	30 mM	Merck; Cat. No. 1083370250
DL-AP5	50 µM	Tocris; Cat. No. 0105
DNQX	10 µM	Tocris; Cat. No. 0189
FM4-64	10 µM	Molecular Probes; Cat. No. T-13320

Extracellular wash solution II

NaCl	119 mM	J.T.Baker; Cat. No. 0278
KCl	2,5 mM	Sigma-Aldrich; Cat. No. 31248
$CaCl_2$	0 mM	Sigma-Aldrich; Cat. No. 12074
$MgCl_2$	2 mM	Sigma-Aldrich; Cat. No. 63068
HEPES	25 mM	AppliChem; Cat. No. A 1069,0100
Glucose	30 mM	Merck; Cat. No. 1083370250
DL-AP5	50 µM	Tocris; Cat. No. 0105
DNQX	10 µM	Tocris; Cat. No. 0189
ADVASEP-7	1 mM	Sigma-Aldrich; Cat. No. A3723

Extracellular solution II (5 mM Ca^{2+})

NaCl	119 mM	J.T.Baker; Cat. No. 0278
KCl	2,5 mM	Sigma-Aldrich; Cat. No. 31248
$CaCl_2$	5 mM	Sigma-Aldrich; Cat. No. 12074
$MgCl_2$	2 mM	Sigma-Aldrich; Cat. No. 63068
HEPES	25 mM	AppliChem; Cat. No. A 1069,0100

Glucose	30 mM	Merck; Cat. No. 1083370250
DL-AP5	50 µM	Tocris; Cat. No. 0105
DNQX	10 µM	Tocris; Cat. No. 0189
FM4-64	10 µM	Molecular Probes; Cat. No. T-13320

adjusted to pH 7,4 with NaOH

Solutions for Synaptophysin-pHluorin experiments

Extracellular solution III (SypHy)

NaCl	136 mM	J.T.Baker; Cat. No. 0278
KCl	2,5 mM	Sigma-Aldrich; Cat. No. 31248
$CaCl_2$	2 mM	Sigma-Aldrich; Cat. No. 12074
$MgCl_2$	1,3 mM	Sigma-Aldrich; Cat. No. 63068
HEPES	10 mM	AppliChem; Cat. No. A 1069,0100
Glucose	10 mM	Merck; Cat. No. 1083370250
DL-AP5	50 µM	Tocris; Cat. No. 0105
DNQX	10 µM	Tocris; Cat. No. 0189

NH_4Cl solution (SypHy)

NaCl	36 mM	J.T.Baker; Cat. No. 0278
KCl	2,5 mM	Sigma-Aldrich; Cat. No. 31248
$CaCl_2$	2 mM	Sigma-Aldrich; Cat. No. 12074
$MgCl_2$	1,3 mM	Sigma-Aldrich; Cat. No. 63068
HEPES	10 mM	AppliChem; Cat. No. A 1069,0100
Glucose	10 mM	Merck; Cat. No. 1083370250
NH_4Cl	100 mM	Sigma-Aldrich; Cat. No. A0171-100G

Extracellular solution III (SypHy- 0 mM Ca^{2+})

NaCl	136 mM	J.T.Baker; Cat. No. 0278

KCl	2,5 mM	Sigma-Aldrich; Cat. No. 31248
$CaCl_2$	0 mM	Sigma-Aldrich; Cat. No. 12074
$MgCl_2$	1,3 mM	Sigma-Aldrich; Cat. No. 63068
HEPES	10 mM	AppliChem; Cat. No. A 1069,0100
Glucose	10 mM	Merck; Cat. No. 1083370250
DL-AP5	50 µM	Tocris; Cat. No. 0105
DNQX	10 µM	Tocris; Cat. No. 0189

Extracellular solution III (SypHy- 5 mM Ca^{2+})

NaCl	136 mM	J.T.Baker; Cat. No. 0278
KCl	2,5 mM	Sigma-Aldrich; Cat. No. 31248
$CaCl_2$	5 mM	Sigma-Aldrich; Cat. No. 12074
$MgCl_2$	1,3 mM	Sigma-Aldrich; Cat. No. 63068
HEPES	10 mM	AppliChem; Cat. No. A 1069,0100
Glucose	10 mM	Merck; Cat. No. 1083370250
DL-AP5	50 µM	Tocris; Cat. No. 0105
DNQX	10 µM	Tocris; Cat. No. 0189

Extracellular solution III (SypHy- 50 mM K^+)

NaCl	88,5 mM	J.T.Baker; Cat. No. 0278
KCl	50 mM	Sigma-Aldrich; Cat. No. 31248
$CaCl_2$	2 mM	Sigma-Aldrich; Cat. No. 12074
$MgCl_2$	1,3 mM	Sigma-Aldrich; Cat. No. 63068
HEPES	10 mM	AppliChem; Cat. No. A 1069,0100
Glucose	10 mM	Merck; Cat. No. 1083370250
DL-AP5	50 µM	Tocris; Cat. No. 0105
DNQX	10 µM	Tocris; Cat. No. 0189

adjusted to pH 7,3 with NaOH

Supplements for SypHy experiments

Bafilomycin A1	1 µM	Sigma-Aldrich; Cat. No. B1793-10UG
Dynasore hydrate	80 µM	Sigma-Aldrich; Cat. No. D7693
Neurexin 1β/Fc Chimera	2 µg/ml	R&D Systems; Cat. No. 5268-NX-050

2.2 Cell culture

Experiments were performed on primary neurons that were dissociated from cortices of E18 or E19 mouse fetuses from two mouse lines (C57/BL6 and $Ncad^{flox}$). In autaptic cultures, the growth of processes (especially of the axon) was constricted by previous seeding of glial cells forming microislands that function as a natural border of neurite outgrowth. Neuronal mass cultures forming almost exclusively synapses were cultured on Poly-L-Ornithine (PO) coated coverslips.

2.2.1 Cleaning and coating of coverslips

Neuronal mass cultures were seeded on PO-coated coverslips. Before coating, the coverslips had to be cleaned for a better attachment of the PO-coating onto the glass surface. About 500 coverslips (15 mm; Assistant) were placed in a big glass petri dish containing freshly prepared 1M HCl and shaken for 2h at 200 rpm. Subsequently, the coverslips were rinsed 3x and shaken for 2 min in demineralized water. After checking the pH, the coverslips were rinsed and shaken 2x in Millipore water. Remaining water was removed by several washing steps in 100% ethanol. Finally, the coverslips were dried for 2h at 180°C in a heat sterilizer. The baked coverslips were filled into a red-capped glass bottle and sterilized for 3h at 180°C. For PO-coating, the coverslips were placed into 6 well plates and incubated with 80 µl PO (1 mg/ml in 150 mM borate buffer (pH 8,35)). On the next day the coverslips were washed 3x with sterile aqua dest. Finally, the coverslips were dried for at least 24h before adding neurons.

2.2.2 Preparation of primary dissociated cortical neurons

Primary neocortical neurons were dissociated from fetuses from E18 or E19 mice. Depending on the experimental approach, fetuses from wild type C57/BL6 or from floxed N-cadherin mice ($Ncad^{flox}$) were used.
First, mice were killed with CO_2 and decapitated. Then the fetuses were taken out of the uteri and kept in a 100x20 mm tissue culture dish (Sarstedt) on ice. All following

steps were done under a clean bench to prevent contamination. First, the scalp and the skullcap were opened with two forceps (Dumont 4-5) and the brain was removed using a micro-scoop. The brain was transferred to a culture dish (Falcon; 35x10 mm) with ice cold $DPBS^{+/+}$ to prevent drying out and contamination of the tissue. Under a binocular (20x magnification) the two hemispheres were separated using a scalpel (Feather No. 11). After removing the meninges, the cortices were minced into smaller pieces and collected in 1 ml $DPBS^{+/+}$. The dissociation was induced by adding 200 µl 0,25% Trypsin and incubation at 37° for 5 min. The digestion was stopped by adding FBS containing BME medium. Finally, the tissue was mechanically dissociated in BME using a 200 µl pipette tip. The cell suspension was diluted in 3 ml BME medium and two centrifugation steps were done to remove non-dissociated tissue pieces and rests of meninges. First the cell suspension was centrifuged for 1 min at 400 rpm. The supernatant was collected and centrifuged for 5 min at 900 rpm. The pellet was dissolved in BME medium and the cell concentration was determined with a counting chamber (Neubauer). For non-autaptic mass cultures 30-40.000 cells were placed in the middle of PO-coated coverslips and incubated for 1h at 37°C. The cultures were grown in 2 ml NB medium + B27 supplement for up to 15 days.

2.2.3 Cultivation of neuronal networks on glial microislands

For a better performance of synaptophysin-pHluorin experiments, I established a culture system of small neuronal networks (10-20 neurons) on glial microislands (Fig. 2.1). In this autaptic system it is possible to analyze postsynaptic overexpression of adhesion molecules with presynaptically expressed SypHy. This culture system makes it possible to manipulate molecules at the pre- and postsynaptic site at the same time with just one transfection, which is particularly interesting for studying homophilic cell adhesion molecules like N-cadherin. To cultivate confluent monolayers of astrocytes, cortical tissue from E18-E19 or from P0-P3 mice (C57/BL6) was dissociated analogous to 2.2.1. The cell suspension of 2 hemispheres was cultivated in 25 cm^2 cell culture flasks (Nunc) for 1-3 months in BME medium until all neurons had died off and the astrocytes had grown to a confluent layer. The BME medium was exchanged every week to support growing of glial cells. To make

glial microislands, astrocytes were detached from the flask and seeded out again at a lower concentration on glass coverslips. Therefore the culture was washed with preheated DPBS$^{-/-}$ and incubated in 3 ml Trypsin-EDTA (0,05 %) for 5 min at 37°C. The proteolytic reaction was stopped with 5 ml FBS containing BME medium. The suspension was centrifuged for 1 min at 2000 rpm and the pellet was resuspended in 1 ml BME medium.

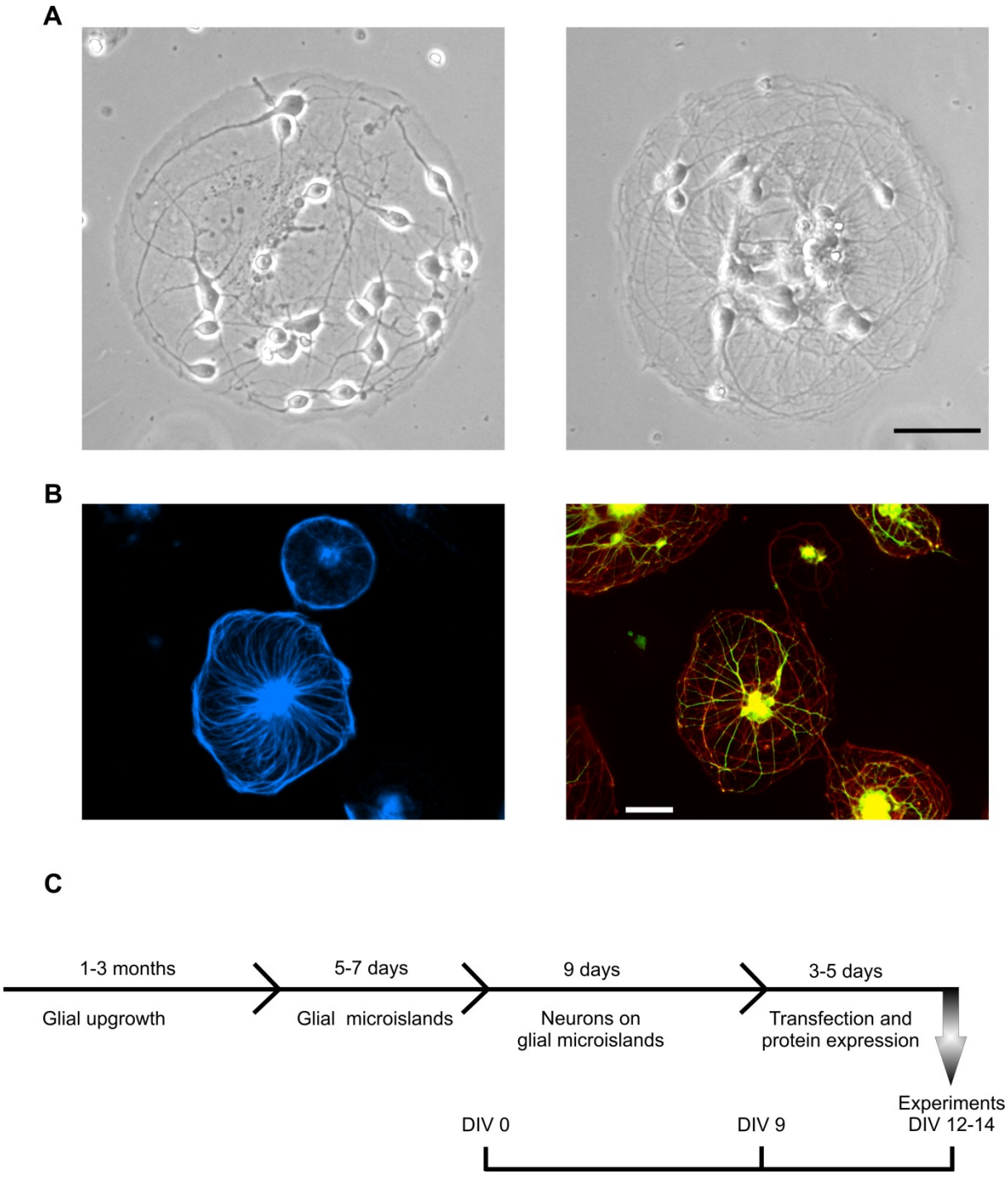

Figure 2.1 Formation of autaptic neuronal networks in glial microisland cultures
(**A**) Phase contrast images of primary dissociated neurons on astrocytes on DIV1 (left) and DIV 4 (right). (**B**) ICC images of a glial microisland culture. Astrocytes were labelled with an antibody for GFAP (Glial fibrillary acidic protein) (left). Dendrites were stained with an antibody for MAP2 (green) and axons with an antibody for tau protein (red). Scale bars in (**A**) and (**B**): 50 µm. (**C**) Timeline of glial microisland preparation. Glial microislands were plated 5-7 days before neurons. Usually, transfections were performed at DIV 9 and experiments were done at DIV 12-14.

To create single cell microislands, 40-60 µl of the suspension were applied onto each glass coverslip. The cells were incubated in 2 ml BME medium for 4-7 days. At DIV 0 (days in vitro), 40-80.000 cortical neurons from 2.2.2 were added to each coverslip and incubated in glia conditioned BME medium. 6 h later, the BME medium was replaced by 3 ml NB medium + B27 supplement. Afterwards, the NB medium was exchanged on DIV 3, 6 and 9 by fresh pre-incubated NB medium.

2.3 Transfection of primary dissociated cortical neurons

Transfections were performed to examine protein function in “gain-of-function”-experiments (e.g. N-cadherin or neuroligin-1 overexpression) or to knock out proteins in a “loss-of-function”-approach (e.g. conditional N-cadherin knockout). Furthermore, plasmids were used to express fluorescent molecules (e.g. PSD95-DsRed2), to express genetically encoded probes (e.g. Synaptophysin-pHluorin) or to express a marker for transfected cells (e.g. DsRed2).

2.3.1 List of plasmids

The following plasmids were used in this study:

pEGFP-N1
Enhanced Green Fluorescent Protein; Kanamycin resistance; Clontech.

pDsRed2-N1
Discosoma sp. Red Fluorescent Protein 2; Kanamycin resistance; Clontech.

Neuroligin-1-EGFP

Neuroligin-1 (Rattus norvegicus) fused to multiple cloning site of pEGFP-N1; Kanamycin resistance; (gift from Dr. T. Dresbach, University of Göttingen, Germany).

N-cadherin-EGFP

N-cadherin (murine) fused to pEGFP-N1; Kanamycin resistance; (gift from Dr. C. Gauthier-Rouviere, University of Montpellier, France).

pBS598EF1alpha-EGFPcre

Cre recombinase fused to EGFP inserted into pBS598 vector (addgene); Ampicillin resistance.

pCMV-Neuroligin-1

Neuroligin-1 (Rattus norvegicus) fused to multiple cloning site of pCMV-Myc-C vector; Ampicillin resistance; (gift from Dr. N. Brose, University of Göttingen, Germany).

pMS149.1-N-cadherin

N-cadherin (murine) inserted into pMS149.1 vector; Ampicillin resistance; (gift from Dr. R. Kemler, MPI Freiburg, Germany)

SypHy-A4 (Rat Synaptophysin-pHluorin)

pH sensitive pHluorin fused to rat synaptophysin inserted into pEGFP-C1; Kanamycin resistance; (gift from Dr. L. Lagnado, Cambridge, UK; available at addgene (plasmid 24478))

pDsRed2-N1-PSD95

PSD95 fused to multiple cloning site of pDsRed2-N1 (Clontech); Kanamycin resistance; (gift from Dr. V. Lessmann, University of Magdeburg, Germany).

2.3.2 Magnetofection™ as a tool for cell transfection

Single cortical neurons were transfected by Magnetofection™. In this mechanic way of cell transfection, DNA is introduced through magnetic nanoparticles (Plank et al., 2003). Plasmid DNA and cationic magnetic nanoparticles form a complex which is taken up by primary neurons upon propulsion by a magnetic field. Plasmid DNA/nanoparticle-complexes on the cell surface are taken up by endocytosis so that the DNA can induce protein expression within the cells. For neuronal transfection, the plasmid DNA was mixed with nanoparticles (NeuroMag; OZ Biosciences) in NB medium without supplements and incubated for 15 min at RT. Then the DNA/NeuroMag-complexes were added to the neuronal cell culture in 6 well plates. Transfection efficiency was enhanced by Magnetofection™ on an oscillating magnetic plate (magnefect LT; nanoTherics) for 30 min at 37°C. After transfection, the cell culture medium was replaced with fresh medium and the culture was incubated at 37°C (2-5 days) for protein expression.

2.3.3 Conditional N-cadherin knockout

In this study I focused on the role of N-cadherin in synaptic function in mature neurons. For functional experiments, N-cadherin knockout neurons were used. Besides its function in brain tissue, N-cadherin also has a key role in embryonic heart development. Absence of N-cadherin leads to a lethal phenotype (e.g. heart defects) in early embryonic stages around E10 (Radice et al., 1997). Therefore, it is impossible to prepare primary dissociated neurons from conventional N-cadherin knockout mice. To circumvent this issue I made use of a conditional N-cadherin knockout mouse developed by Dr. Glenn Radice (Jefferson Medical College, Philadelphia, USA) which is available from Jackson Labs (Kostetskii et al., 2005). The $Ncad^{flox}$ mouse genome contains loxP sites flanking exon1 of the N-cadherin (Cdh2) gene. The homozygous mice are viable, fertile and show normal physical and behavioral characteristics. In this study, I used E18 $Ncad^{flox}$ mice fetuses to prepare primary dissociated cortical neurons identical to 2.2.2 and 2.2.3. To delete the N-cadherin gene, I transfected individual cells in neuronal cultures with a CreEGFP

plasmid. The subsequent CreEGFP expression in transfected neurons induced the deletion of exon1 of N-cadherin which contains translational start sites and transcriptional regulatory sequences (Radice et al., 1997). Hence, the expression of the CreEGFP plasmid in these neurons deleted the N-cadherin alleles. These neurons were used to analyze the role of N-cadherin in synaptic function in several "loss-of-function"-approaches.

2.4 Fluorescence microscopy

2.4.1 Imaging Setup Axiovert 200M for live cell imaging and immunocytochemical stainings

To examine the roles of N-cadherin and neuroligin-1 on presynaptic vesicle exo- and endocytosis, diverse experimental approaches and different methods were used. Except for superresolution microscopy (SIM) all experiments were done on an inverted Axiovert 200M microscope (Zeiss). Images were acquired with a 63x objective (Plan-Apochromat 63x/1,4 oil; Zeiss), a 40x objective (EC Plan-Neofluor 40x/1,3 oil; Zeiss) or a 20x objective (A Plan 20x/0,30 Ph1; Zeiss). Images were recorded with a 12 bit CoolSnap ES2- charged coupled device camera and exposure was controlled by two external shutters (Vincent Associates, Uniblitz VMM-D1). Following filter sets from Zeiss were used in this study to control dye excitation and light emission.

Filter set No.	Excitation [nm]	Beam splitter [nm]	Emission [nm]
49 (DAPI)	365	395	445/50
17 (FITC)	485/20	510	515/565
43 (CY3)	545/25	570	605/70

Table 2.1 Filter sets for fluorescence microscopy

In immunocytochemical stainings and for neuroligin-1 localization experiments, z-stack images (depth: 0,3-0,5 µm) were acquired controlled by MetaVue software. 3D

deconvolution operations were performed offline using AutoDeblur software (Visitron Systems) to reduce background fluorescence and to increase signal to noise ratio. Maximum projection images were done using MetaMorph software. Depending on the experimental approach, images were thresholded via the autothreshold operation in MetaMorph or manually using the intensity profiles of the individual images in MetaVue. Finally, in some experiments a low-pass filter was used to exclude single pixel noise in MetaVue or MetaMorph software.

2.4.2 Immunocytochemical stainings of pre- and postsynaptic molecules

Immunocytochemical stainings were performed to examine basic structural properties of pre- and postsynaptic components. The stainings gave information about the maturity of cortical cultures (VAMP2 stainings) or about structural changes associated with high synaptic activity (VAMP2, PSD95 or N-cadherin stainings).
All following steps, except overnight incubation of primary antibody, were done on a shaker (< 50 rpm). First, coverslips with cortical neurons were transferred to a new chamber (6-, 12-, 24-well) and washed 3x with $DPBS^{+/+}$. Fixation was induced by incubation in 4% paraformaldehyde (PFA) for 20 min under a laboratory hood. Cultures were washed 3x with $DPBS^{+/+}$ to completely remove PFA. Then neurons were permeabilized with TritonX100 containing blocking buffer I for 30 min to enable staining of intracellular components. Subsequently, the primary antibody was added to blocking buffer I and incubated either 1 h at room temperature or overnight at 4°C. Cultures were washed 3x10 min with $DPBS^{+/+}$ before incubating with secondary antibody in blocking buffer II for 1h at room temperature. From now on all steps were done in the dark to prevent photobleaching of the fluorophore-tagged secondary antibody. Prior to microscopic analysis, cultures were washed 3x10 min to reduce unspecific staining. Imaging was performed on Axiovert-200M microscope or on ELYRA-PS (Zeiss). Images with the Axiovert-200M setup were captured as z-stacks by MetaVue software and subsequently deconvolved offline with AutoDeblur software to reduce out-of-focus fluorescence. Following, primary antibodies were used in this study:

Primary antibody	Dilution	Company; Cat. No
VAMP2 (rabbit polyclonal)	1/2000	Abcam; Cat. No. 3347
VAMP2 (mouse monoclonal)	1/1000	Synaptic Systems; Cat. No. 104211
VAMP2 (guinea pig polyclonal)	1/500	Synaptic Systems; Cat. No. 104204
Tau (mouse monoclonal)	1/500	Synaptic Systems; Cat. No. 314011
N-cadherin (rabbit polyclonal)	1/500 - 1/2000	Abcam; Cat. No. 18203
PSD95 (mouse monoclonal)	1/400 - 1/1000	Abcam; Cat. No. 2723
GFAP (rabbit polyclonal)	1/1000	DAKO; Cat. No. Z0334
MAP2 (chicken polyclonal)	1/1000	Abcam; Cat. No. 92434
N-cadherin (mouse)	1/400	BD Biosciences; Cat. No. 610920

Table 2.2 Utilized primary antibodies for immunocytochemistry

The primary antibodies were marked by the following fluorophore-conjugated secondary antibodies:

Secondary antibody	Dilution	Company; Cat. No.
Alexa 555 goat anti rabbit	1/1000	Molecular Probes; Cat. No. A21428
Alexa 555 goat anti mouse	1/500	Molecular Probes; Cat. No. A21147
Alexa 488 goat anti chicken	1/1000	Molecular Probes; Cat. No. A11039
Alexa 488 goat anti mouse	1/1000	Molecular Probes; Cat. No. A21151
Alexa 488 goat anti guinea pig	1/1000	Molecular Probes; Cat. No. A11073
Alexa 647 goat anti mouse	1/1000	Molecular Probes; Cat. No. A21241
AMCA anti rabbit	1/1000	Jackson; Cat. No. 111-155-144
AMCA anti chicken	1/1000	Jackson; Cat. No. 103-155-155

Table 2.3 Secondary antibodies used for immunocytochemistry

2.4.3 Monitoring localization changes of synaptic molecules upon strong synaptic activity

To examine potential structural changes caused by high synaptic activity, cultures were stimulated and immediately fixed prior to immunocytochemical staining for N-cadherin, VAMP2 or PSD95. To examine the localization of neuroligin-1 in this approach, neurons were transfected with neuroligin-1-EGFP. To check the role of PSD95 on neuroligin-1 localization, cultures were cotransfected with DsRed2-PSD95 and neuroligin-1-EGFP. For structural analysis, cultures (DIV 12-14) were stimulated 5 min in 50 mM K^+ containing extracellular solution and directly fixed with paraformaldehyde. For control experiments cells were incubated in normal extracellular solution (5 min in 2,5 mM K^+). To analyze reversibility, cultures were recovered in normal extracellular solution (30 min in 2,5 mM K^+) after stimulation and subsequently fixed with PFA. The experiment was also performed with stimulation in the presence of dynasore (80 µM) to block vesicular endocytosis. Hence, immunocytochemical stainings were done for several pre- and postsynaptic molecules and for the cell adhesion molecule N-cadherin. Finally, fluorescence images were acquired on Axiovert 200M microscope or on ELYRA-PS (Zeiss) to perform high resolution images.

2.4.4 Analysis of synaptic function with FM4-64

To analyze the functionality of synapses, it is necessary to use methods that result in activity-dependent signals to characterize pre- and postsynaptic function. In this context, immunocytochemical stainings on fixed cells are restricted to give structural information and cannot be used for detailed analysis of synaptic function. To study the cycling of presynaptic vesicles, I therefore made use of the two activity-dependent fluorescence indicators FM4-64 and Synaptophysin-pHluorin. The styryl dye FM4-64 is a well established probe to measure exo- and endocytotic processes in a variety of systems and is commonly used to analyze synaptic vesicle turnover. For a short overview of the staining method see also Fig. 2.2. To label active synaptic vesicles, FM4-64 (10-20 µM) was added to the extracellular solution of cortical

neurons (usually between DIV 12-15) and it was dissolved in the hydrophobic membrane. Then vesicle cycling was induced by stimulating the nerve terminal (90 mM K^+ for 2min or 400 stimulations at 20 Hz) leading to FM4-64 uptake by vesicle endocytosis of dye-containing membrane (Newton and Murthy, 2006). In a longer washing step (10 min) FM4-64 remaining in the surface membrane was washed away to reduce the background staining and to increase the signal to noise ratio. To increase the washing efficiency, 1 mM ADVASEP-7 was added, a quenching substance with a higher affinity to FM4-64 than the cell membrane. The washing step was done in Ca^{2+}-free extracellular solution to inhibit the release of FM dye by spontaneous activity. After the washing step, clear distinct puncta representing the active vesicle cluster labeled with FM4-64 dye were present. These puncta can be used to quantify synaptic vesicle cycling, i.e. the interplay of exo- and endocytosis. To measure the speed of exocytosis in more detail, destaining experiments were performed to measure the kinetics of FM4-64 dye loss upon stimulation as an approximation of vesicular exocytosis. FM4-64 destaining was induced by electrical field stimulation (1200 stimulations at 20 Hz) in extracellular solution, which in the absence of FM dye leads to a decrease in fluorescence due to exocytosis of FM labeled vesicles with the presynaptic membrane. At the end of the experiment, a second electrical stimulation (2000 stimulations at 20 Hz) induced the exocytosis of remaining intravesicular FM4-64 and thus provided the unspecific background level of fluorescence.

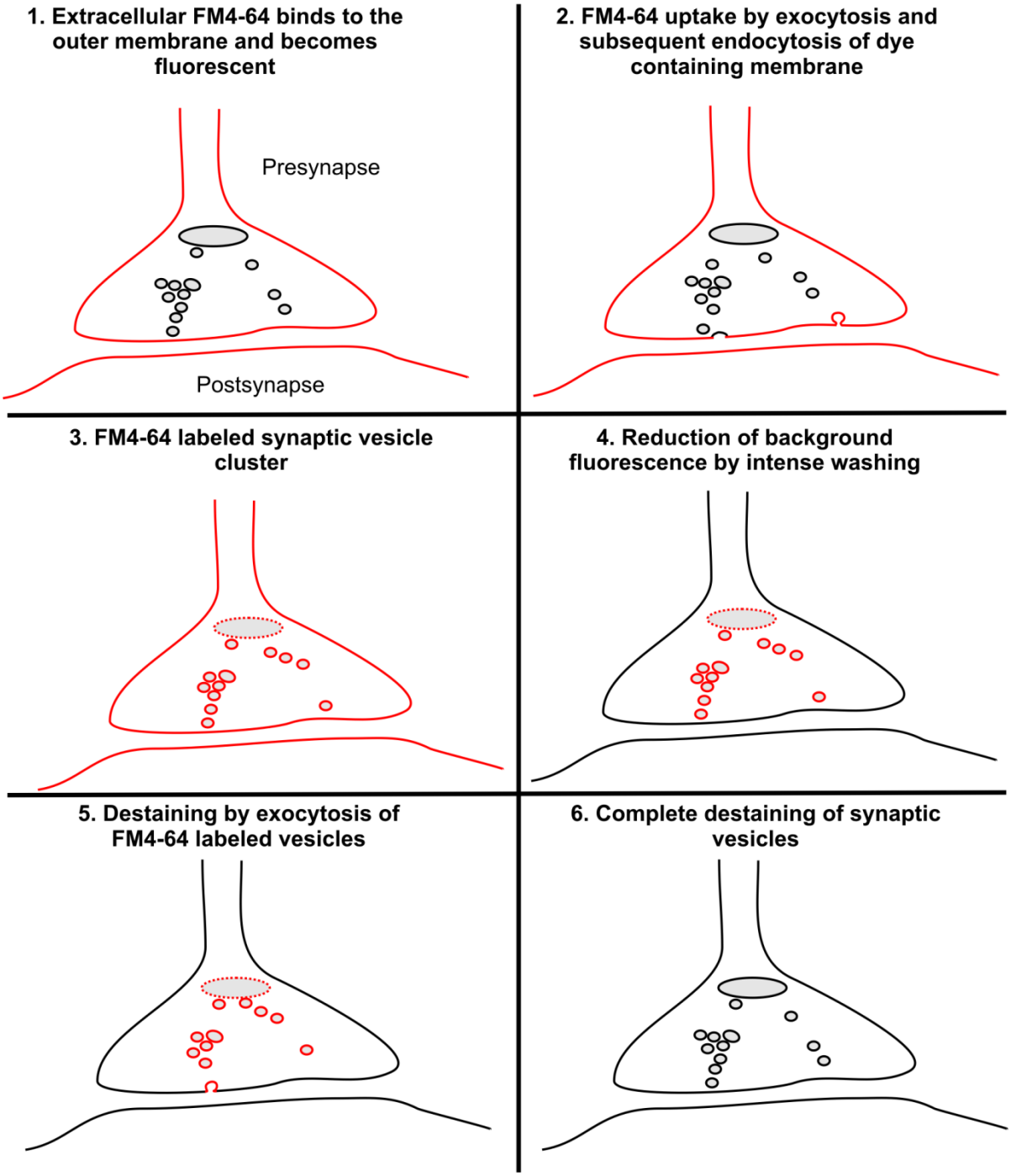

Figure 2.2 Staining and destaining of synaptic vesicle cluster with FM4-64
Illustration of FM4-64 staining and destaining procedure. FM4-64 is highlighted in red. (**1.**) FM4-64 dye binds to the pre- and postsynaptic membrane and becomes fluorescent in the hydrophobic environment. (**2.**) Upon stimulation, uptake of FM4-64-bounded membranes by endocytosis establishes FM4-64 labelled vesicle cluster (**3.**). (**4.**) After washing in Ca^{2+}-free extracellular solution, active vesicle cluster get visible as distinct fluorescent puncta. (**5.**) A second stimulation in absence of dye results in a loss of fluorescence by exocytosis and vesicle destaining (**6.**)

2.4.5 Analysis of vesicular exo- and endocytosis using Synaptophysin-pHluorin

Experiments with the genetically encoded probe Synaptophysin-pHluorin (SypHy) were performed to get detailed information about the roles of N-cadherin and neuroligin-1 in the cycling of synaptic vesicles. SypHy experiments reveal differential measurements of vesicular exo- and endocytosis simultaneously with just one experiment. The combination of SypHy imaging with manipulations of synaptic adhesion molecules (e.g. overexpression of N-cadherin or neuroligin-1) enables the study of the roles of these molecules in vesicle cycling. SypHy is a fusion protein of a pH sensitive variant of EGFP named pHluorin (Miesenböck et al., 1998) with the synaptic vesicle protein synaptophysin invented and provided by Dr. L. Lagnado (Granseth et al., 2006). The basic mechanism of SypHy imaging is the pH dependent fluorescence of pHluorin (Fig. 2.3).

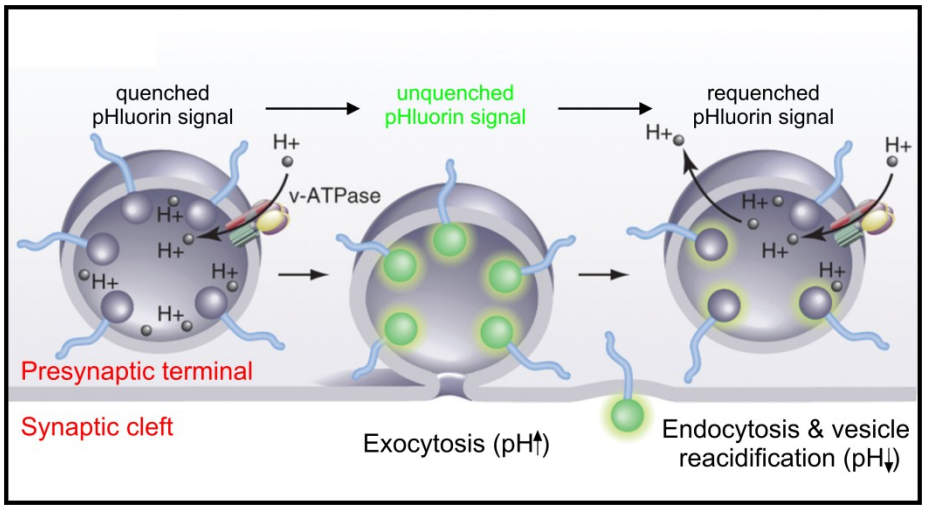

Figure 2.3 pHluorin-based measurement of vesicle turnover at the presynapse
(modified after Kavalali and Jorgensen, 2014)
Illustration of pHluorin-based imaging of synaptic exo- and endocytosis. The pH-sensitive EGFP construct pHluorin can be fused to proteins of the vesicle membrane for the defined measurement of vesicular turnover. The three most commonly tagged molecules are synaptobrevin (SynaptopHluorin), synaptophysin (SypHy) or the vesicular glutamate transporter (vGlut1-pHluorin). (**Left**) At the resting state, pHluorin-fluorescence is quenched because of the low pH within the vesicles (~ pH 5.5). (**Middle**) Upon stimulation, synaptic vesicles fuse and pHluorin gets exposed to the extracellular pH (~ pH 7,3) and fluorescence gets unquenched. The increase in fluorescence represents the kinetics of exocytosis. (**Right**) After exocytosis, vesicles get endocytosed and the requenching of the fluorescence is mediated by reacidification through vesicular ATPases.

Intravesicular pHluorin is quenched because of the low pH within vesicles in the resting state of the presynaptic terminal. Upon electrical stimulation, vesicles fuse with the presynaptic membrane and the pH increases up to the extracellular level. Hereby the pHluorin gets unquenched and fluorescent puncta can be observed by fluorescence microscopy. The detectable increase in fluorescence describes kinetics and amount of vesicle exocytosis. After exocytosis, vesicles get endocytosed and reacidified while pHluorin gets quenched again. The observed decline in fluorescence represents the kinetics of endocytosis and can clearly be distinguished from exocytosis (Royle et al., 2008; Sankaranarayanan et al., 2000). In this work, experiments with SypHy were performed on autaptic cultures to analyze the roles of N-cadherin and neuroligin-1 in synaptic vesicle cycling. For this, cortical neurons (DIV 9-10) were transfected with the SypHy-A4 plasmid (gift from Dr. L. Lagnado). DsRed2 was cotransfected as a marker for a better visualization of transfected neurons and detection of autaptic contacts. I also overexpressed N-cadherin or neuroligin-1 in the same neurons and compared vesicle turnover with control neurons expressing only SypHy and DsRed2. Further, SypHy experiments in conditional N-cadherin knockout neurons were performed by co-transfecting Cre recombinase in neurons from floxed N-cadherin mice ($Ncad^{flox}$). SypHy experiments were performed 3 to 5 days after transfection. To induce vesicle cycling, neurons were transferred to a stimulation chamber (Live Cell Instrument) in extracellular solution containing AP-5 (50 µM) and DNQX (10 µM) to prevent recurrent network activity. Neurons were stimulated with 1 ms pulses (biphasic) of 100 mA at room temperature. Based on the experimental approach, between 200 and 800 stimulations with a frequency of 20 Hz were applied. At the end of each experiment, vesicles were alkalized using an extracellular solution containing 100 mM NH_4Cl to stimulate the maximal SypHy fluorescence reflecting the expression level. This signal was used for normalization of SypHy fluorescence data. During the whole experiment, fluorescence images were acquired with time intervals of 2-5 seconds and fluorescence intensities over time were analyzed offline using MetaVue software. For further details regarding SypHy imaging (experimental setup and analysis) see also **2.5.2** and **3.2**.

2.4.6 Superresolution analysis using structured illumination microscopy

Spatial resolution is one of the most limiting parameters to analyze biological structures within cells. Therefore it is of particular interest to optimize imaging techniques to improve the resolution for the observation of small cell components. In wide-field microscopy, the optical resolution underlies the diffraction limit (described by Ernst Abbe). During the last decades, several techniques were developed to overcome the diffraction limit and thus improve spatial resolution. One of these methods is Structured Illumination Microscopy (SIM) developed by John W. Sedat and colleagues (Gustafsson et al., 2008; Schermelleh et al., 2008). This technology provides several advantages over other superresolution methods. Since it is based on conventional wide-field microscopy, it can be used for multicolor imaging. It is possible to observe several molecules and their interaction within one specimen in contrast to electron microscopy. Furthermore, SIM can be performed with common fluorescence dyes and without specialized sample preparation.

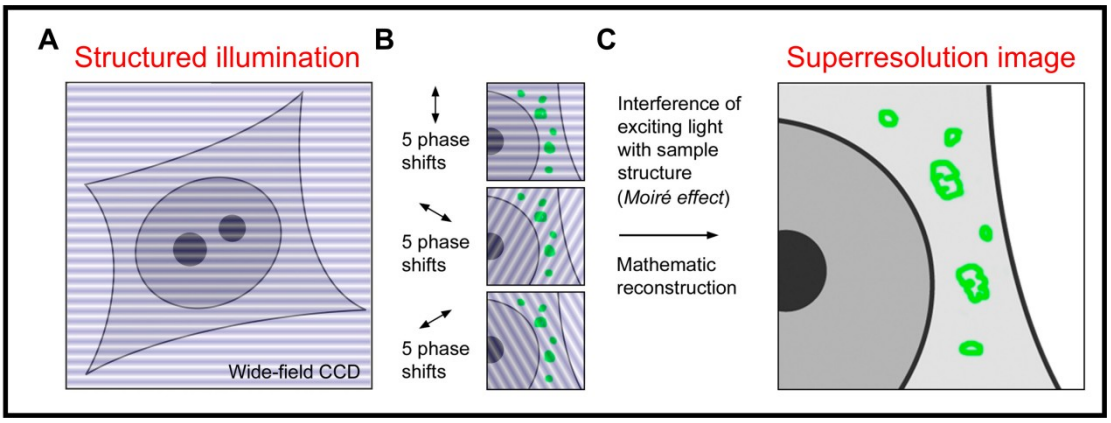

Figure 2.4 Overcoming the diffraction limit by structured illumination
(modified after Schermelleh et al., 2010)
(**A**) Samples are excited with a grid-like illumination. (**B**) Interference of the structured illumination with the sample structure generates the Moiré fringes. (**C**) Offline backprocessing of the Moiré fringes generates the superresolution image.

SIM is based on conventional wide-field microscopy but with doubled resolution in the x/y and z-direction. Crucial characteristics of SIM are the unequal illumination of the sample combined with an offline reconstruction to get superresolution images (Fig. 2.4). Therefore, laser light is passing an optical grating that additionally slides in

the x/y-direction resulting in a defined structured illumination of the sample. The interference of this grid-like illumination with known pattern and the structure of the excited sample generates Moiré fringes. Thus these images transform the high spatial frequency sample information down to lower frequencies, so that the information can bypass the diffraction limit and be taken up by the optical system. To get high resolution images, this information is processed back to the high frequency level in an offline software-controlled process (Schermelleh et al., 2010).

2.5 Image processing and statistical analysis

Image processing and analysis was performed with MetaMorph and MetaVue software (Visitron Systems). Deconvolution of 3D z-stack images was done via AutoDeblur software (Visitron Systems). Statistical evaluation and creation of graphs were performed with Sigmaplot 11.0. Microsoft Excel was used for data exchange between MetaMorph and MetaVue, respectively and Sigmaplot. For statistical evaluation, data were represented as mean values with standard error. Significance was tested using Student`s t-test for two groups and using one way ANOVA for three or more groups. Data groups were regarded as statistically significant for $P<0,05$ (* $P<0,05$; ** $P<0,01$ and *** $P<0,001$). Figure arrangement was performed in CorelDRAW 12.

2.5.1 Analysis of FM experiments

To analyze images of FM stainings (high $[K^+]$-stainings), fluorescence images were imported in MetaMorph and smaller sections were thresholded with the autothreshold function. FM puncta on dendrites were determined by overlay images of the EGFP signal (dendrites) and the FM4-64 staining. Finally, regions of interest (ROIs) were created around the thresholded FM puncta that overlapped with the dendrites. Puncta area and the lengths of the dendrites (for calculation of puncta density) were measured automatically by MetaMorph and exported to an Excel file. All statistics were done in Sigmaplot 11.0 by loading the Excel file into a Sigmaplot sheet. FM

stainings were represented in terms of FM puncta density (FM puncta on 10 µm dendrite) and mean puncta area (μm^2).

To analyze FM stainings induced by electrical stimulation, fluorescence images were imported in MetaVue. Thresholding was based on the intensity profile of the respective FM signal of each staining. In some experiments, a low-pass filter was applied to remove single pixel noise. The further analysis and statistical evaluation was similar to FM stainings induced by high [K^+].

For FM destaining experiments, cultures were stained via electrical stimulation in the presence of FM4-64 in the extracellular solution. To determine the kinetics of vesicular exocytosis, cultures were stimulated a second time but in the absence of FM dye. Finally, a second strong stimulus was applied to ensure complete destaining and to determine the background fluorescence level. Images were taken in intervals of five seconds to record the loss in fluorescence of FM puncta over time and thus the kinetics of exocytosis. Time-lapse sequences were subsequently processed and analyzed offline in MetaVue and Sigmaplot. First, puncta on dendrites were defined analogous to FM stainings. After thresholding and creation of overlay images (with EGFP signal to determine dendritic puncta), regions of interest were drawn around FM puncta. Subsequently, average pixel intensities of each region over time were determined automatically by MetaVue and exported to an Excel file. The local fluorescence intensities in individual synaptic vesicle cluster over time were background subtracted to exclude unspecific fluorescence. For this the fluorescence intensities at the end of the destaining experiment (after two electrical stimulations) of individual puncta were subtracted from the corresponding time-lapse sequence. Intensity values of each individual punctum were normalized to its baseline level prior to stimulation to enable the pooling of different experiments. Exocytosis was quantified by the percentage decrease of the fluorescence intensity of each punctum at the end of the first stimulation (60 s). Puncta without destaining were excluded from averaging to avoid inclusion of unspecific staining. In a few cases, moderate movements in the x/y-direction over time were corrected with the StackReg plug-in in ImageJ and subsequently processed in MetaVue. Experiments with strong shifts in the x/y- or the z-direction that could not be corrected by ImageJ were excluded.

2.5.2 Analysis of Synaptophysin-pHluorin experiments

Each SypHy experiment generated a time-lapse sequence of the pHluorin-signal over time that included the baseline-signal before stimulation, the increase in fluorescence upon stimulation and the decay in fluorescence after stimulation. In addition, an image of the DsRed2-signal of the transfected neuron was acquired to show neuronal structures and to detect autapses. At the end of each experiment, an equal amount of extracellular solution that contained 100 mM NH_4Cl was applied to the normal extracellular solution within the stimulation chamber (50 mM NH_4Cl final concentration). The extracellularly applied ammonium rapidly entered all synaptic vesicles and dequenched all expressed SypHy molecules. Images of this NH_4Cl-induced total SypHy signal were used for normalization and to compensate for variations in the expression level of SypHy. Analysis and quantification was performed in MetaVue and Sigmaplot software. The initial step to analyze SypHy experiments was the determination of ROIs around autaptic contacts. For this, the fluorescence image of the NH_4Cl induced total signal was thresholded on the basis of its intensity profile and merged with the corresponding DsRed2 image. In some experiments, a low-pass filter was used to remove single pixel noise. SypHy puncta on dendrites were regarded as autapses and ROIs were drawn around the thresholded puncta. Additionally, one ROI was created in the background to record fluctuations in background fluorescence over time. ROIs were loaded into the time-lapse sequences and average pixel intensity values over time were determined for each punctum. Furthermore, average pixel intensities of the NH_4Cl induced maximal signals of each ROIs were determined. All data were exported and further processed with Sigmaplot. First, the average pixel intensities of the background were subtracted from every single ROI. Afterwards, the baseline fluorescence (0 s) was subtracted to correct for differences in spontaneous activity. Average pixel intensities of each punctum were then normalized to the background subtracted NH_4Cl induced signal of the appropriate ROI. Individual puncta not showing fluorescence increase upon stimulation (non-releasing sites) were excluded from analysis to avoid an influence on the decay kinetics. Small shifts in the x/y-direction of the time sequences were corrected in ImageJ. Experiments with larger shifts in the x/y- or in the z-direction had

to be excluded from analysis. In double-pulse experiments with two successive stimulations (1. stimulus: 200 stimuli at 20 Hz; 2. stimulus: 800 stimuli at 20 Hz) individual puncta without an increase in exocytotic signal amplitude in response to the first stimulus versus the second stimulus were rejected due to disturbed vesicle cycling during the course of the experiment.
Some basic control experiments without overexpression of adhesion molecules like Ca^{2+}-dependence of exocytosis signals or addition of dynasore and bafilomycin A1 were done on all puncta without selecting autapses. In these experiments all active SypHy puncta above threshold (NH_4Cl image) were analyzed. Furthermore, in the analysis of Ca^{2+}-dependence experiments SypHy signals were not normalized to the NH_4Cl induced signal, because the same cultures were stimulated repeatedly in different extracellular solutions.

2.5.3 Analysis of immunocytochemical stainings

Fluorescence images of immunocytochemical stainings were acquired using the motor-driven deconvolution microscope Axiovert 200M (Zeiss). Additionally, SIM was carried out to perform a more detailed imaging of structural relations within synapses.

2.5.3.1 Axiovert 200M setup

To obtain stacks of images along the z-axis perpendicular to the object, 3D z-stack images with 0,3 to 0,5 µm depth (in different experiments) were made using the motor-driven microscope Axiovert 200M. The number of planes was individually adapted to the thickness of the respective culture. Bottom and top levels were manually defined by focusing through the z-axis and 3D z-stacks were acquired in MetaVue automatically by running through the focal planes. Generated z-stack images were further processed and analyzed in AutoDeblur and MetaMorph. Quantification and statistical evaluation were performed in Sigmaplot. For image processing, z-stack images were first deconvolved with AutoDeblur. Deconvolution of the 3D z-stacks was done to increase the signal-to-noise ratio and to obtain more

focused images. The deconvolution operation corrects for optical distortions that occur as the microscope generates and processes 3D images. The reason for the distortion is that point light sources cannot be collected by an optical system as a clear dot but instead appear like a double cone with its tips centered within the point light source. The deconvolution method estimates the out-of-focus fluorescence that is characterized by the so called point-spread function (PSF) and depends on diverse features of the optical system. The PSF can be approximately calculated for every individual optical system and is used to calculate back the out-of-focus light to its place of origin, hence increasing the signal-to-noise ratio. In this study, 3D z-stack images were processed in AutoDeblur via blind deconvolution. In this specific algorithm, the PSF is unknown. The software assumes different PSF and selects the procedure with the best improvement. To estimate the PSF, the software integrates diverse information like the used objective, the wavelength of the emitted light or the depth of the image planes. The deconvolved z-stack images were further processed in MetaMorph. First, a maximum projection image was created out of the stack by determining the maximum intensity of each pixel from all image planes in the z-direction and calculating one maximum intensity image. Subsequently, the maximum projection was thresholded by the autothreshold function or manually depending on the experimental approach and the properties of the image. In some cases, parts of the image were cut out prior to thresholding to exclude unspecific staining (especially around cell somata) and to improve thresholding accuracy. In some experiments, thresholded images were further processed with a low-pass filter. The low-pass filter operation in MetaMorph or MetaVue corrects for single pixel noise and creates a smoothened image. This filter modifies the value of a single pixel by offsetting the values of the surrounding pixels to create an average value. The low-pass filter determines this average value of each individual pixel and creates a smoothened image with reduced single pixel noise. After thresholding and optional low-pass filter operation, ROIs were created and average pixel intensity, puncta area or puncta density were determined with MetaMorph and quantified in Sigmaplot.

2.5.3.2 ELYRA-PS setup

Superresolution microscopy (SIM) was performed with the Zeiss Elyra PS setup in cooperation with the group of Prof. Dr. Hermann Aberle (Funktionelle Zellmorphologie; University of Düsseldorf) with kind assistance of Rebekka Ochs at the Center for Advanced Imaging (CAI Düsseldorf). Immunocytochemical stainings were exposed to laser light at four different wavelengths (405nm, 488nm, 561nm, 642nm) to create multicolor images with a high resolution in the x/y-direction for a more detailed analysis of the spatial organization of different pre- and postsynaptic molecules like VAMP2, PSD95 or the cell adhesion molecule N-cadherin. Images were captured with an alpha Plan-Apochromat 63x/1,46 oil objective (Zeiss).

3 Results

3.1 Effects of N-cadherin and neuroligin-1 expression on synaptic vesicle cycling

The two cell adhesion molecules N-cadherin and neuroligin-1 are well characterized to affect diverse synaptic processes like initial recognition and maturation of synaptic contacts. Furthermore, it has been shown that the cell adhesion systems N-cadherin/catenin and neuroligin-1/neurexin also cooperate to induce presynaptic maturation (Stan et al., 2010). Generally, previous studies were done on immature neurons and focused on the roles of cell adhesion molecules in not fully maturated synapses. However, much less is known about the influence of these molecules on the functionality of mature neurons. This work examined the roles of N-cadherin and neuroligin-1 in the functionality of mature synapses, particularly with regard to presynaptic vesicle exo- and endocytosis. In first experiments, the postsynaptic expression of N-cadherin and neuroligin-1 was manipulated by overexpression or knockout approaches and vesicle cycling was studied with the activity-dependent dye FM4-64.

3.1.1 Influence of N-cadherin and neuroligin-1 expression on presynaptic vesicle cluster

Initial experiments were done in immature neurons (DIV 7) to test the plasmids used. Primary cortical neurons were cultured on PO for at least 4 days and were transfected with N-cadherin-EGFP or neuroligin-1-EGFP and compared to control neurons expressing EGFP.

3.1.1.1 Synaptogenic effect of N-cadherin and neuroligin-1 expression in immature neurons

First, cortical neurons were transfected at DIV 4 with N-cadherin-EGFP, neuroligin-1-EGFP and EGFP, respectively. Three days after transfection, cultures were fixed in

4% PFA and immunostained with an antibody against synaptobrevin-2 (VAMP2). As a presynaptic vesicle membrane associated molecule, immunocytochemical stainings for VAMP2 can be used to detect changes in presynaptic vesicle clustering.

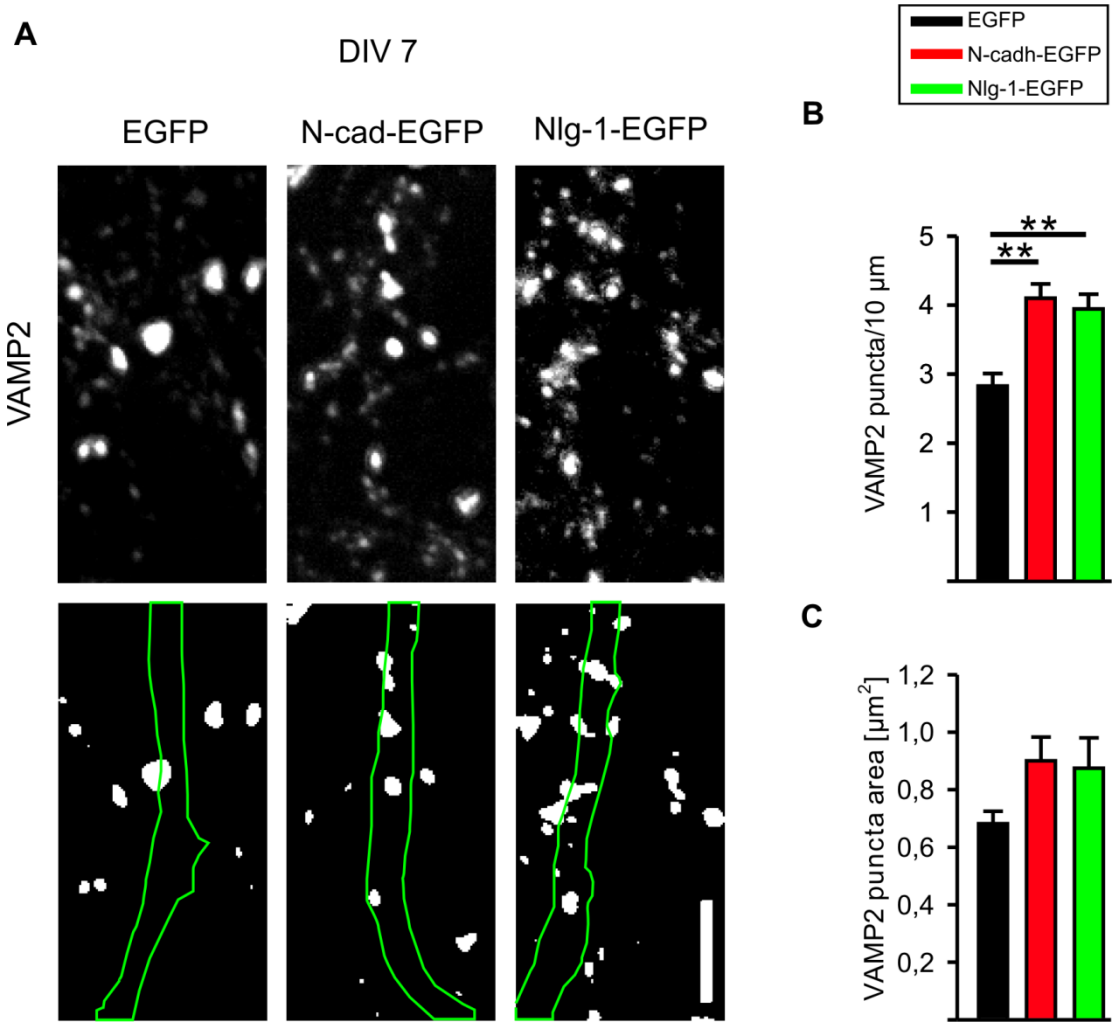

Figure 3.1 N-cadherin and neuroligin-1 expression induce synaptic vesicle clustering in immature neurons
Postsynaptic overexpression of N-cadherin-EGFP and neuroligin-1-EGFP, respectively, induces additional presynaptic vesicle cluster in immature (DIV 7) cortical neurons. (**A**) Fluorescence images of immunostainings for the synaptic vesicle protein VAMP2. Grey-scale (upper panel) and thresholded (lower panel) images of the VAMP2 signal. Left: VAMP2 signal of control cells expressing EGFP. Middle: VAMP2 signal of N-cadherin-EGFP expressing cells. Right: VAMP2 signal of neuroligin-1-EGFP expressing cells. Dendrites are outlined in thresholded images. Scale bar: 5 µm. (**B**) Quantification of VAMP2 puncta density on dendrites. (**C**) Quantification of VAMP2 puncta size. EGFP: n= 29; N-cadherin-EGFP: n= 29; neuroligin-1-EGFP: n= 25 (n represents number of cells). Error bars represent S.E.M. ** P< 0,01 (One Way Anova with Holm-Sidak Post Hoc Test).

To increase the signal-to-noise ratio and to remove background fluorescence, z-stack images were acquired with MetaVue and processed offline with AutoDeblur software. After deconvolution, maximum projection images were created and further processed with a low-pass filter in MetaMorph software. To analyze the VAMP2 signal, the EGFP signal of dendrites was merged with the corresponding VAMP2 signal. Next, regions of interest were determined around thresholded VAMP2 puncta that contacted dendrites. The overexpression of N-cadherin-EGFP as well as the overexpression of neuroligin-1-EGFP increased the density of VAMP2 puncta on dendrites in immature neurons (Fig. 3.1A). Postsynaptic overexpression resulted in a significantly ($P< 0,01$) increased VAMP2 puncta density in N-cadherin-EGFP expressing neurons (4,10 ± 0,21 puncta/10 µm dendrite, n= 29 cells) as well as in neuroligin-1-EGFP expressing neurons (3,94 ± 0,22 puncta/10 µm dendrite, n= 25 cells) as compared to control (2,83 ± 0,18 puncta/10 µm dendrite, n= 29 cells; Fig. 3.1B). The VAMP2 puncta area was not significantly altered, neither in N-cadherin-EGFP expressing neurons (0,90 ± 0,08 μm^2, n= 29 cells), nor in neuroligin-1-EGFP expressing neurons (0,87 ± 0,11 μm^2, n= 25 cells) as compared to EGFP expressing controls (0,68 ± 0,04 μm^2, n= 29 cells; Fig. 3.1C).

These data confirm synaptogenic effects of N-cadherin and neuroligin-1 in immature neurons and indicate the proper expression and functionality of the plasmid-encoded proteins (N-cadherin-EGFP and neuroligin-1-EGFP) in primary dissociated cortical neurons.

3.1.1.2 Effect of N-cadherin and neuroligin-1 expression on vesicle cycling in immature neurons

To examine whether the overexpression of N-cadherin-EGFP or neuroligin-1-EGFP results in new functional synapses, vesicle cluster were labeled with the activity-dependent dye FM4-64. In contrast to immunostainings, only actively cycling vesicles get labeled by endocytotic dye uptake upon synaptic stimulation. Analogously to the previous experiment, immature (DIV 5) cortical neurons were transfected with N-cadherin-EGFP, neuroligin-1-EGFP or EGFP. Two days later, cultures were stimulated for 2 min with a modified extracellular solution containing 90 mM KCl in

the presence of FM4-64 (20 µM). After intense washing, distinct FM4-64 puncta representing presynaptic vesicle cluster were observed on postsynaptic dendrites. For analysis, overlay images of FM4-64 stainings and the corresponding EGFP signal were created and smaller parts were thresholded with the autothreshold function in MetaMorph. The postsynaptic overexpression of N-cadherin-EGFP or neuroligin-1-EGFP clearly increased the FM4-64 puncta density (Fig. 3.2A).

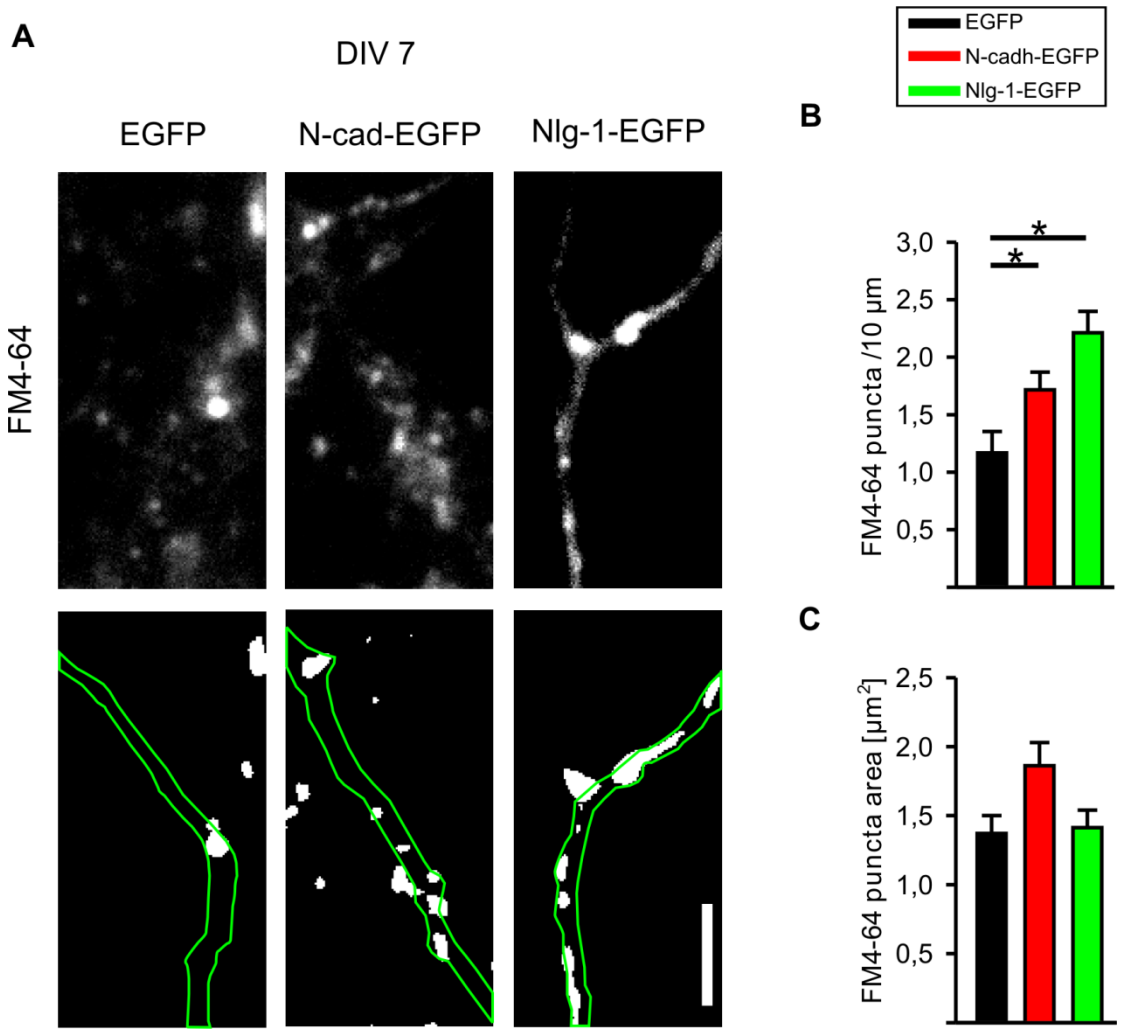

Figure 3.2 Induction of synaptic vesicle cycling by N-cadherin and neuroligin-1 expression
Vesicle cycling was stimulated by extracellular application of 90 mM K^+ for 2 min. (**A**) Grey-scale (upper panel) and thresholded (lower panel) fluorescence images of FM4-64 labelled vesicle cluster. Left: FM4-64 signal of EGFP expressing control cells. Middle: FM4-64 signal of N-cadherin-EGFP expressing cells. Right: FM4-64 signal of neuroligin-1-EGFP expressing cells. Dendrites are outlined in thresholded images. Scale bar: 5 µm. (**B**) Quantification of FM4-64 puncta density. (**C**) Quantification of FM4-64 puncta size. EGFP: n= 22; N-cadherin-EGFP: n= 16; neuroligin-1-EGFP: n= 17 (n represents number

of cells). Error bars represent S.E.M. * P< 0,05 (Kruskal-Wallis One Way Analysis of Variance on Ranks with Dunn`s Post Hoc Test).

Overexpression increased the density of active vesicle cluster in N-cadherin-EGFP expressing neurons (1,72 ± 0,15 puncta/10 µm dendrite, n= 16 cells) and in neuroligin-1-EGFP expressing neurons (2,21 ± 0,19 puncta/10 µm dendrite, n= 17 cells) significantly (P< 0,05) compared to control EGFP expressing neurons (1,17 ± 0,19 puncta/10 µm dendrite, n= 22 cells; Fig. 3.2B). The FM4-64 puncta area was not changed (EGFP: 1,37 ± 0,13 μm^2, n= 22 cells; N-cadherin-EGFP: 1,86 ± 0,17 μm^2, n= 16 cells; neuroligin-1-EGFP: 1,41 ± 0,13 μm^2, n= 17 cells; Fig. 3.2C).
These observations demonstrate that the expression of N-cadherin-EGFP or neuroligin-1-EGFP induces additional synaptic vesicle cluster with FM4-64. This can be explained if the overexpression of N-cadherin-EGFP or neuroligin-1-EGFP induces synaptogenic clustering of cycling vesicles. On the other site, a direct effect of the two cell adhesion molecules on the cycling efficiency can be predicted.

3.1.2 Influence of N-cadherin and neuroligin-1 expression on vesicle cycling in mature neurons

The aim of this study was to investigate the roles of the cell adhesion molecules N-cadherin and neuroligin-1 in the regulation of synaptic vesicle cycling. Vesicle cycling is mainly characterized by exocytosis of synaptic vesicles from the presynaptic terminal and the compensating endocytosis of parts of the plasma membrane. In the following, analysis of the functionality of the presynaptic vesicle cycle was done in mature neurons to minimize potential synaptogenic effects of the investigated cell adhesion molecules. To do so, cortical cell cultures were transfected with N-cadherin-EGFP or neuroligin-1-EGFP at DIV 11, a point in time at which the main part of synaptogenesis has happened. To test this issue, synaptogenesis was checked by immunostainings for VAMP2 similar to Fig. 3.1 but in more mature neurons (DIV 15). To examine the roles of N-cadherin and neuroligin-1 in vesicle cycling, FM4-64 stainings were performed in mature neurons overexpressing N-cadherin-EGFP or neuroligin-1-EGFP.

3.1.2.1 Vesicle clustering in mature N-cadherin and neuroligin-1 overexpressing neurons

VAMP2 immunostainings were performed to test the maturity of the culture system in regard to synaptogenesis. Cortical neurons were transfected with EGFP, N-cadherin-EGFP or neuroligin-1-EGFP analogously to the previous experiments but at DIV 11. Immunostainings for VAMP2 were performed at DIV 15.

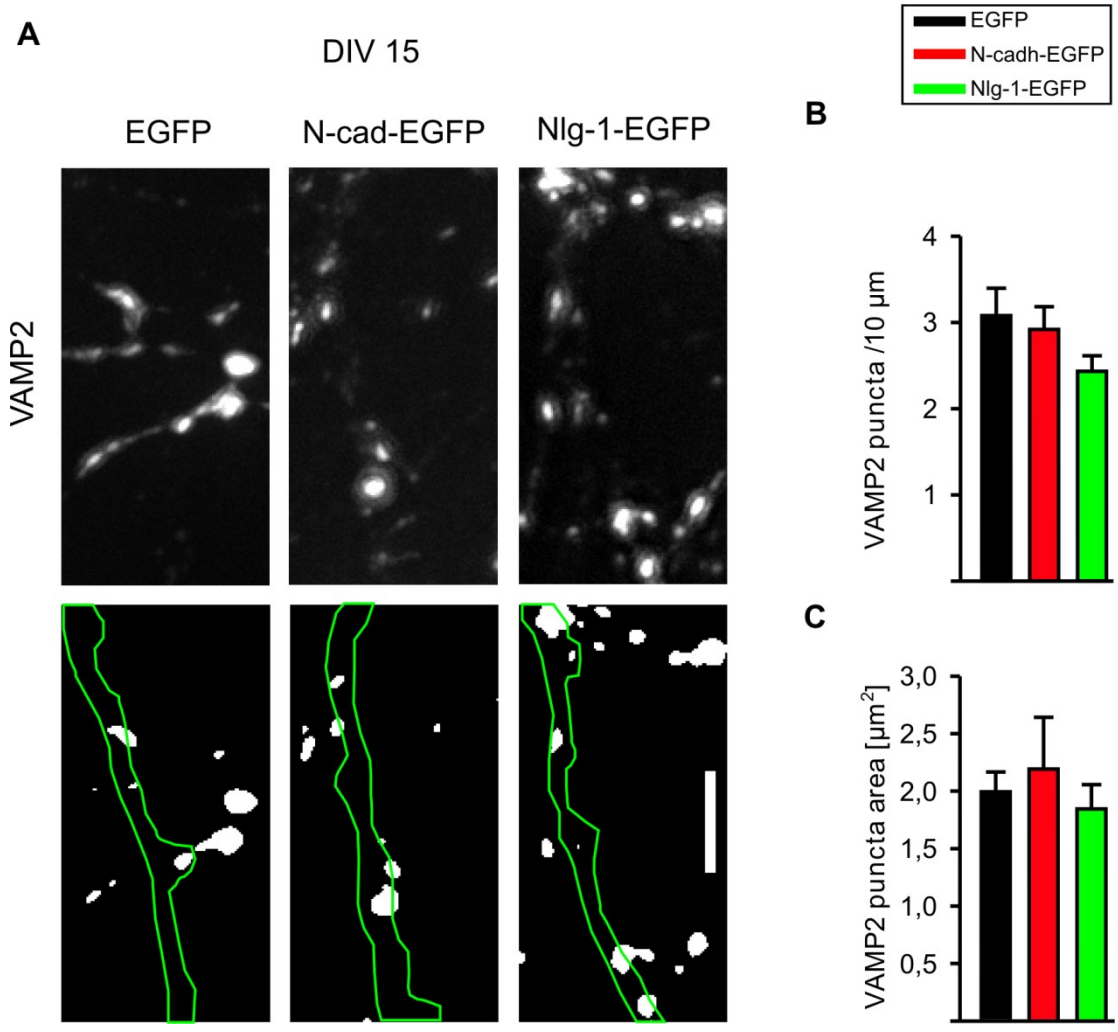

Figure 3.3 Absence of additional synaptogenesis upon overexpression of N-cadherin or neuroligin-1 in neurons at DIV 15
Postsynaptic overexpression of N-cadherin-EGFP and neuroligin-1-EGFP had no effect on presynaptic vesicle cluster in mature (DIV 15) cortical neurons. (**A**) Fluorescence images of immunostainings for VAMP2. Grey-scale (upper panel) and thresholded (lower panel) images of the VAMP2 signal. Left: VAMP2 signal of control cells expressing EGFP. Middle: VAMP2 signal of N-cadherin-EGFP expressing cells. Right: VAMP2 signal of neuroligin-1-EGFP expressing cells. Dendrites are outlined in thresholded images. Scale bar: 5 µm. (**B**) Quantification of VAMP2 puncta density on dendrites. (**C**)

Quantification of average VAMP2 puncta size. EGFP: n= 16; N-cadherin-EGFP: n= 15; neuroligin-1-EGFP: n= 15 (n represents number of cells). Error bars represent S.E.M.

Postsynaptic overexpression of N-cadherin-EGFP or neuroligin-1-EGFP showed no synaptogenic effect, neither on the density nor on the area of presynaptic VAMP2 puncta (Fig. 3.3A). The puncta density in N-cadherin-EGFP transfected neurons (2,92 ± 0,26 puncta/10 µm dendrite, n= 15 cells) as well as in neuroligin-1-EGFP expressing neurons (2,43 ± 0,18 puncta/10 µm dendrite, n= 15 cells) was unaltered compared to control cells expressing EGFP (3,08 ± 0,32 puncta/10 µm dendrite, n= 16 cells; Fig. 3.3B). Also the VAMP2 puncta area showed no differences between the three groups (EGFP: 1,99 ± 0,17 μm^2, n= 16 cells; N-cadherin-EGFP: 2,19 ± 0,45 μm^2, n= 15 cells; neuroligin-1-EGFP: 1,84 ± 0,21 μm^2, n= 15 cells; Fig. 3.3C).
Based on these observations it can be postulated that the cortical neurons in this cell culture system have reached a more mature state at DIV 15, because unlike in immature cells (DIV 7, Fig. 3.1), the overexpression of N-cadherin-EGFP and neuroligin-1-EGFP caused no further synaptogenesis in transfected neurons.

3.1.2.2 Effects of N-cadherin and neuroligin-1 expression on cycling of presynaptic vesicles

The next step was to test N-cadherin and neuroligin-1 for potential effects on the cycling of presynaptic vesicles in mature neurons. Analogously to the previous experiments in immature neurons (Fig. 3.2), cortical cultures were stained with the activity-dependent dye FM4-64. In Fig. 3.4, FM4-64 uptake was induced by high extracellular potassium ion concentration treatment. In Fig. 3.5, cultures were stimulated by electrical field stimulation in the presence of FM4-64. N-cadherin as well as neuroligin-1 overexpression induced vesicle cycling in mature neurons at DIV 14 (Fig. 3.4A). The overexpression of N-cadherin-EGFP (2,24 ± 0,25 puncta/10 µm dendrite, n= 15 cells) as well as the overexpression of neuroligin-1-EGFP (2,84 ± 0,40 puncta/10 µm dendrite, n= 18 cells) significantly ($P< 0,05$) increased the density of FM4-64 puncta compared to EGFP expressing control neurons (1,47 ± 0,11 puncta/10 µm dendrite, n= 26 cells; Fig. 3.4B). The FM4-64 puncta size was not

affected (EGFP: 1,18 ± 0,10 µm^2, n= 26 cells; N-cadherin-EGFP: 1,33 ± 0,09 µm^2, n= 15 cells; neuroligin-1-EGFP: 1,38 ± 0,13 µm^2, n= 18 cells; Fig. 3.4C).

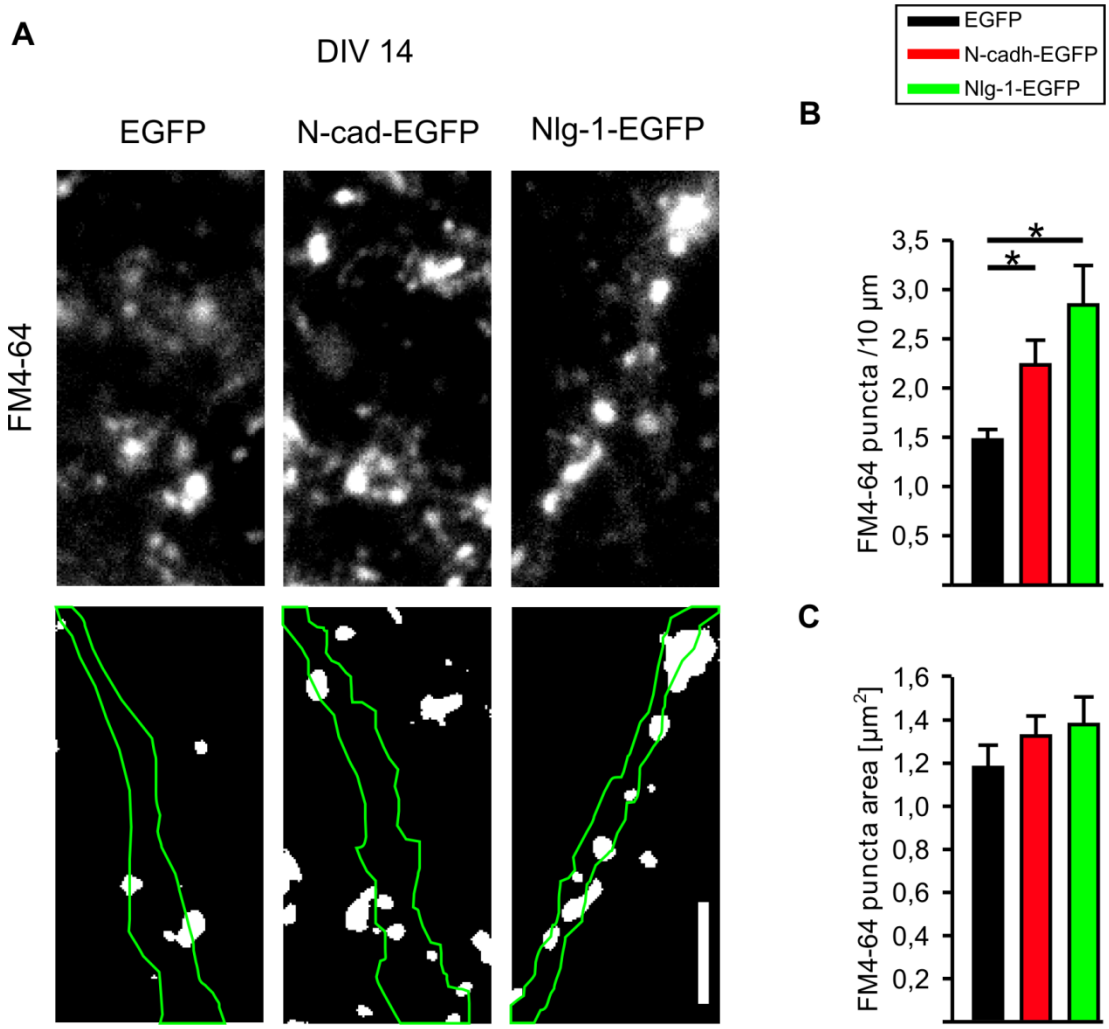

Figure 3.4 Induction of synaptic vesicle cycling by N-cadherin and neuroligin-1 in neurons at DIV 14
Overexpression of N-cadherin-EGFP and neuroligin-1-EGFP enhanced staining of active vesicle cluster with FM4-64 in mature neurons (DIV 14). Vesicle cycling was induced by extracellular application of 90 mM K^+ for 2 min. (**A**) Grey-scale (upper panel) and thresholded (lower panel) fluorescence images of FM4-64 labelled vesicle cluster. Left: FM4-64 signal of EGFP expressing control cells. Middle: FM4-64 signal of N-cadherin-EGFP expressing cells. Right: FM4-64 signal of neuroligin-1-EGFP expressing cells. Dendrites are outlined in thresholded images. Scale bar: 5 µm. (**B**) Quantification of FM4-64 puncta density. (**C**) Quantification of FM4-64 puncta size. EGFP: n= 26; N-cadherin-EGFP: n= 15; neuroligin-1-EGFP: n= 18 (n represents number of cells). Error bars represent S.E.M. * P< 0,05 (Kruskal-Wallis One Way Analysis of Variance on Ranks with Dunn`s Post Hoc Test).

For a more physiological FM4-64 staining, vesicle cycling was stimulated by electrical field stimulation (400 stimuli at 20 Hz; Fig. 3.5A) in the presence of FM4-64 (10 µM).

After washing out of unspecific FM staining, synaptic vesicle cluster were visible as distinct puncta on dendrites. For a better visualization of dendrites, cells in the treated groups were cotransfected with EGFP.

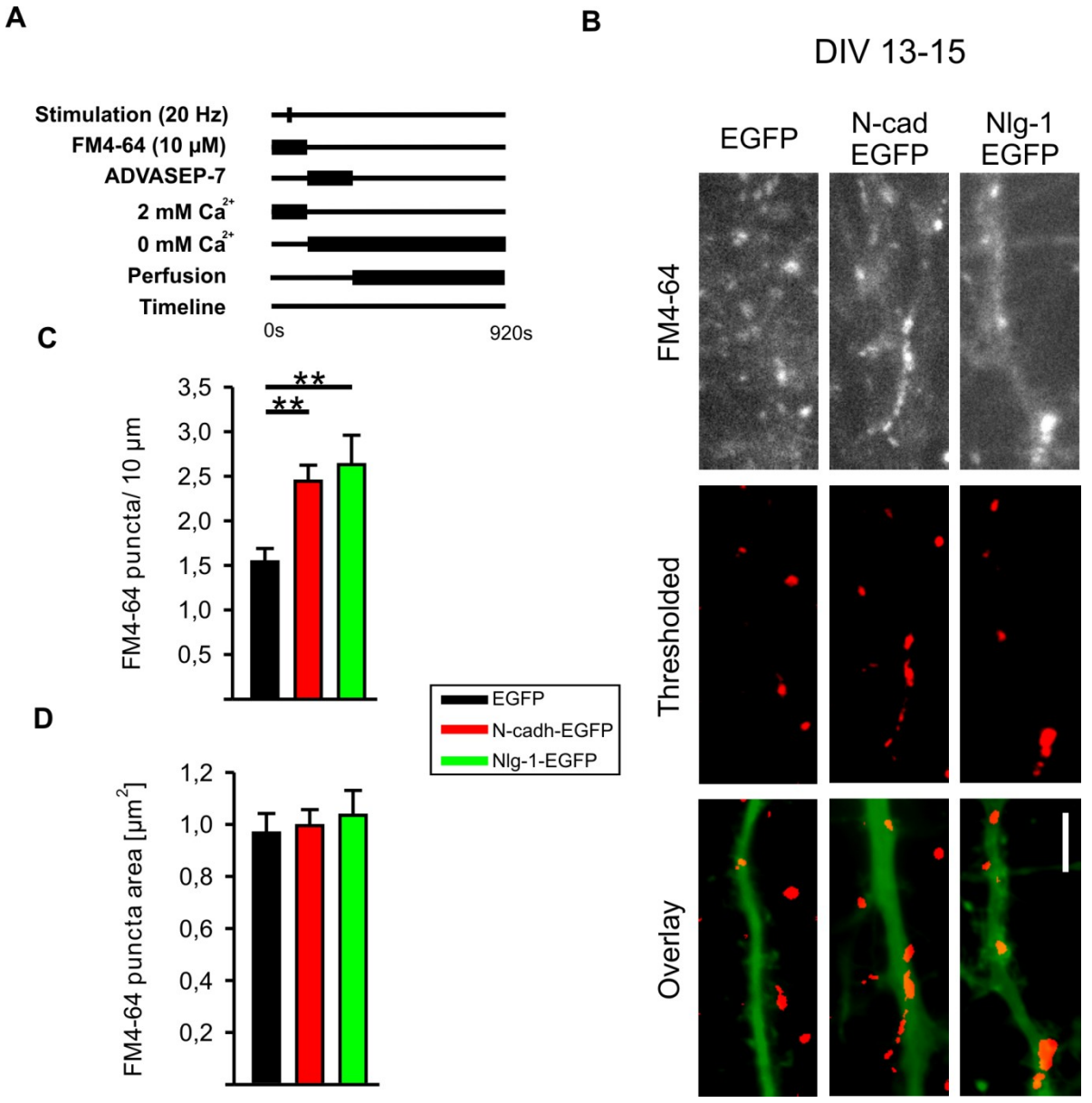

Figure 3.5 Increased presynaptic vesicle cycling enhanced by electrical stimulation in N-cadherin-EGFP and neuroligin-1-EGFP expressing neurons at DIV 13-15
(**A**) Cycling vesicles were labelled by 400 stimuli at 20 Hz in the presence of FM4-64. (**B**) Fluorescence images of FM4-64 labelled vesicle cluster at DIV 13-15. Grey-scale FM4-64 signal (upper panel) was thresholded (middle panel) and merged with the corresponding EGFP signal (lower panel) to visualize dendrites. Left: FM4-64 signal of EGFP expressing control cells. Middle: FM4-64 signal of N-cadherin-EGFP + EGFP expressing cells. Right: FM4-64 signal of neuroligin-1-EGFP + EGFP expressing cells. Scale bar: 5 µm. (**C**) Quantification of FM4-64 puncta density on dendrites. (**D**) Quantification of average FM4-64 puncta size. EGFP: n= 11; N-cadherin-EGFP + EGFP: n= 9; neuroligin-1-EGFP +

EGFP: n= 6 (n represents number of cells). Error bars represent S.E.M. ** P< 0,01 (One Way Anova with Holm-Sidak Post Hoc Test).

Overlay images indicated an increase in FM4-64 puncta density in N-cadherin-EGFP and neuroligin-1-EGFP expressing cells at DIV 13-15 (Fig. 3.5B). The overexpression of N-cadherin-EGFP + EGFP (2,44 ± 0,18 puncta/10 µm dendrite, n= 9 cells) and the overexpression of neuroligin-1-EGFP + EGFP (2,63 ± 0,33 puncta/10 µm dendrite, n= 6 cells) significantly (P< 0,01) increased FM4-64 puncta density compared to control cells expressing EGFP (1,54 ± 0,15 puncta/10 µm dendrite, n= 11 cells; Fig. 3.5C). FM4-64 puncta size was not altered (EGFP: 0,97 ± 0,08 μm^2, n= 11 cells; N-cadherin-EGFP + EGFP: 1,0 ± 0,06 μm^2, n= 9 cells; neuroligin-1-EGFP + EGFP: 1,04 ± 0,10 μm^2, n= 6 cells; Fig. 3.5D).
In summary, the overexpression of N-cadherin-EGFP and neuroligin-1-EGFP enhanced synaptic vesicle cycling in mature neurons (DIV 13-15) both, upon high $[K^+]$-treatment and induced by physiological electrical stimulation.

3.1.3 Effects of N-cadherin and neuroligin-1 expression on presynaptic vesicle release in neurons at DIV 13-15

Initial FM4-64 staining experiments had revealed an increased vesicle cycling by postsynaptic overexpression of N-cadherin-EGFP or neuroligin-1-EGFP in mature cortical neurons. Vesicle cycling was measured through the endocytotic uptake of membrane-bound FM4-64 upon stimulation. Since the uptake of FM dye depends on both, vesicular exo- and endocytosis, further experiments had to be done for a more precise characterization of the observed effects of N-cadherin and neuroligin-1. In a subsequent experimental approach, FM destaining experiments were performed for a separate analysis of vesicular exocytosis.

3.1.3.1 Analysis of vesicular exocytosis with FM4-64 destaining experiments

FM dye destaining is an established method for kinetic measurements of vesicle exocytosis. In a first step, synaptic vesicle cluster were labeled with FM4-64 analogously to the previous experiments (400 stimuli at 20 Hz; Fig. 3.6A+B). After

intense washing in Ca^{2+}-free extracellular solution, vesicle exocytosis was induced by a second stimulation (1200 stimuli at 20 Hz) in the absence of extracellular FM4-64. During the whole destaining experiment, time-lapse sequences were acquired to record FM puncta fluorescence intensities over time (Fig. 3.6C). Exocytosis of FM4-64 labeled vesicles led to a strong loss in fluorescence. In thresholded images, this loss in fluorescence gets better visible by the disappearance of FM puncta when FM4-64 puncta intensities undercut the threshold level (Fig. 3.6D). FM destaining kinetics were analyzed offline in MetaVue software. To correct for variations in staining strengths, average pixel intensity values of individual vesicle cluster at each time point were background subtracted and normalized to baseline level (Fig. 3.6E). Averaging normalized destaining kinetics of several puncta gives the mean destaining curve of one experiment (Fig. 3.6F).

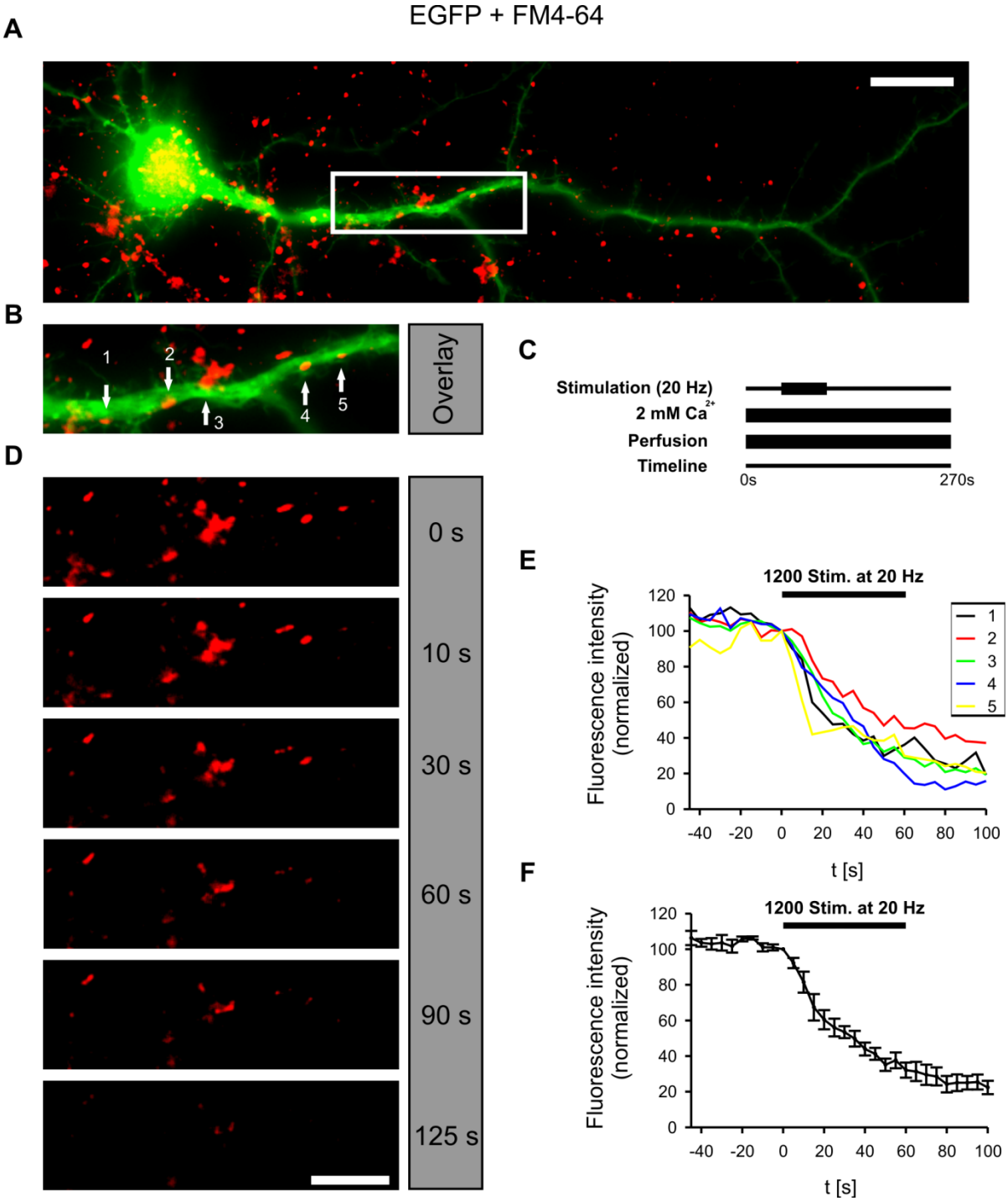

Figure 3.6 Measuring synaptic vesicle exocytosis with FM destaining experiments
Illustration of a typical FM destaining experiment. Neurons were transfected with EGFP for a better assignment of individual vesicle cluster. After FM staining and washing, FM4-64 signal was thresholded and active vesicle cluster appear as distinct puncta. (**A**) Overlay image of the thresholded FM4-64 signal with the corresponding EGFP signal showing several individual presynaptic puncta of one neuron. Scale bar: 20 µm (**B**) FM4-64 puncta (arrows) that overlap with a dendrite of the EGFP expressing neuron were analyzed. (**C**) Destaining was induced by 1200 stimulations at 20 Hz with continuous perfusion of extracellular solution containing 2 mM Ca^{2+}. Time-lapse images were acquired during the whole experiment. (**D**) Thresholded fluorescence images of FM4-64

labelled vesicle cluster from (**B**). Decrease in fluorescence over time by exocytosis leads to the loss of puncta that undercut the threshold. Scale bar: 10 µm. (**E**) Fluorescence intensities over time of individual puncta were background subtracted and normalized to baseline level. (**F**) Destaining curves from individual puncta were averaged to obtain the mean destaining curve.

3.1.3.2 The influence of N-cadherin and neuroligin-1 expression on exocytosis as determined by FM4-64 destaining

Next, FM4-64 destaining experiments were analyzed to examine the roles of N-cadherin and neuroligin-1 in vesicular exocytosis. To do so, destaining curves from cortical neurons at DIV 13-15 (from Fig. 3.5) transfected with N-cadherin-EGFP or neuroligin-1-EGFP, respectively (DIV 9-10) were compared with control cells expressing EGFP. Additionally, EGFP was cotransfected in the treated groups for a better visualization of neuronal processes. Individual vesicle cluster (FM4-64 puncta) from several experiments (for each treatment) were analyzed and averaged to one destaining curve. The overexpression of N-cadherin-EGFP and neuroligin-1-EGFP showed no effect in FM4-64 destaining experiments. The destaining curves of the three groups overlapped and showed no kinetic differences in the fluorescence decline after stimulation (Fig. 3.7A). Also the quantification of the percentage decrease in fluorescence at the end of the stimulus (60 seconds) was unaltered (EGFP: 70,1 ± 0,6 %, n= 308 puncta; N-cadherin-EGFP + EGFP: 68,8 ± 0,9 %, n= 370 puncta; neuroligin-1-EGFP + EGFP: 68,2 ± 0,7 %, n= 300 puncta; Fig. 3.7B). For a better evaluation, I therefore checked the sensitivity of FM destaining experiments by changing the extracellular Ca^{2+}-concentration stepwise between 0,5 and 5 mM. Because synaptic exocytosis highly depends on extracellular Ca^{2+}, differences in destaining kinetics should get visible in FM4-64 destaining experiments. Upon stimulation, destaining curves showed faster fluorescence decline with increasing Ca^{2+}-concentrations from 0,5 to 2 mM (Fig. 3.7C). Interestingly, increasing the Ca^{2+} level from 2 up to 5 mM did not further change destaining kinetics. The destaining curves of 2 mM Ca^{2+} (green) and 5 mM Ca^{2+} (blue) overlapped indicating insufficient sensitivity of FM destaining at higher release probabilities.

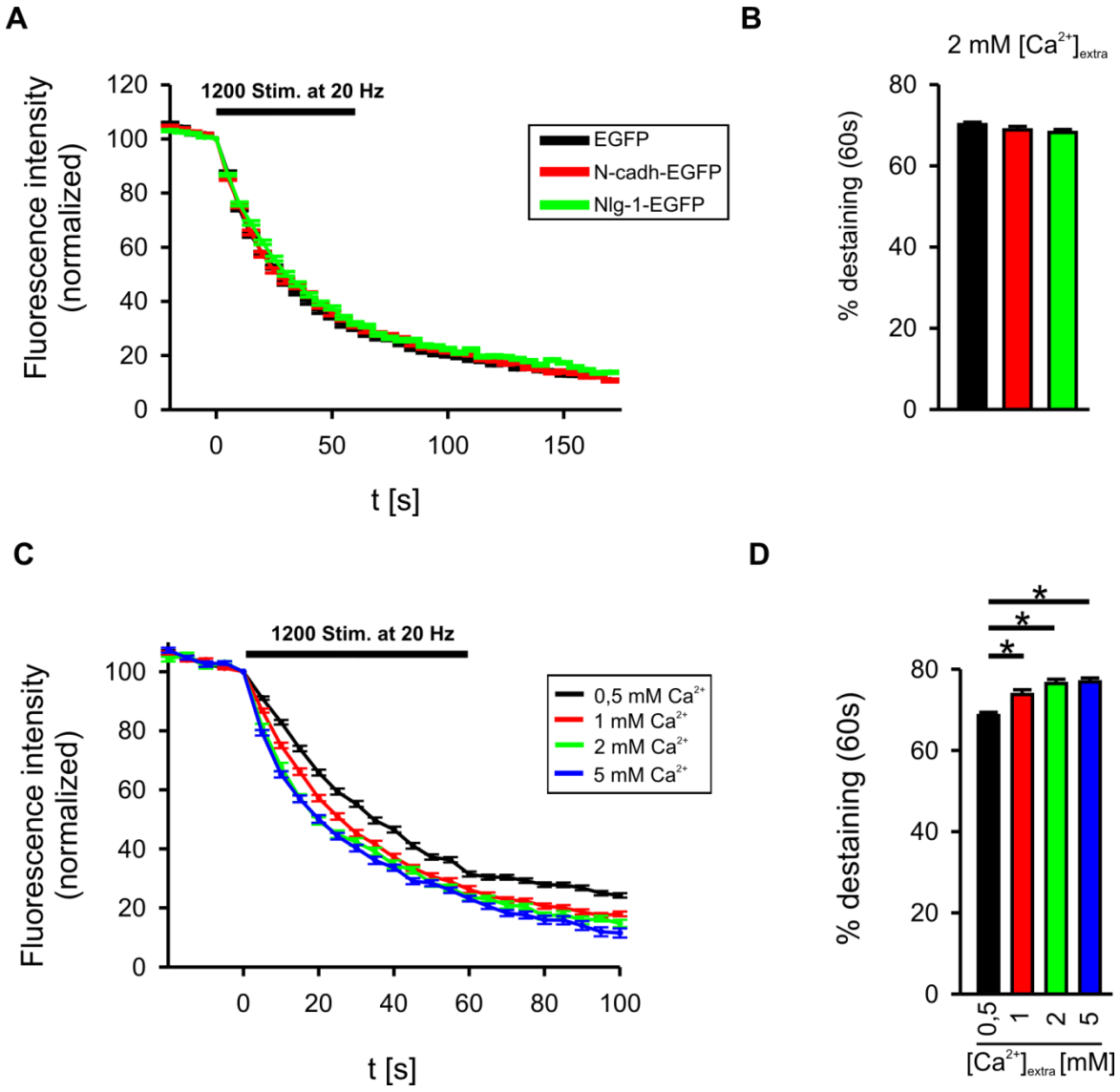

Figure 3.7 FM4-64 destaining upon overexpression of N-cadherin-EGFP and neuroligin-1-EGFP
FM4-64 destaining experiments revealed no effect of N-cadherin-EGFP or neuroligin-1-EGFP overexpression. (**A**) Mean destaining curves of individual puncta. (**B**) Quantification of percentage destaining at the end of the stimulation. EGFP: n= 308; N-cadherin-EGFP + EGFP: n= 370; neuroligin-1-EGFP + EGFP: n= 300 (n represents number of puncta). Error bars represent S.E.M. (**C**) Mean destaining curves of individual puncta upon altered extracellular Ca^{2+}-concentrations. (**D**) Quantification of percentage destaining upon altered extracellular Ca^{2+}-concentrations. 0,5 mM Ca^{2+}: n= 276; 1 mM Ca^{2+}: n= 322; 2 mM Ca^{2+}: n= 247; 5 mM Ca^{2+}: n= 268 (n represents number of puncta). Error bars represent S.E.M. * P< 0,05 (Kruskal-Wallis One Way Analysis of Variance on Ranks with Dunn`s Post Hoc Test).

Quantification of the fluorescence decline upon stimulation revealed a significant (P< 0,05) increase of exocytosis from 0,5 mM Ca^{2+} (68,5 ± 0,8 %; n= 276 puncta) to higher Ca^{2+}-concentrations (1 mM: 73,8 ± 1,2 %, n= 322 puncta; 2 mM: 76,4 ± 1,0 %,

n= 247 puncta; 5 mM: 76,8 ± 1,0 %, n= 268 puncta). However, within the range of 1 mM to 5 mM Ca^{2+}, FM4-64 destaining experiments were not able to detect changes of vesicular exocytosis.

In summary, FM destaining experiments revealed no changes in synaptic vesicle exocytosis by overexpression of N-cadherin-EGFP or neuroligin-1-EGFP. Control experiments indicated a limited sensitivity of FM4-64 destaining experiments to changes of extracellular [Ca^{2+}], especially at high release probabilities. This might possibly explain the lack of an exocytotic effect of N-cadherin-EGFP or neuroligin-1-EGFP as determined by FM4-64 destaining experiments. Because FM destaining was already strong in control conditions (EGFP expression), further increase in destaining might be difficult to achieve.

3.1.4 Synaptic vesicle cycling in conditional N-cadherin knockout neurons

In addition to overexpression experiments, the role of N-cadherin in synaptic vesicle cycling was examined in a “loss-of-function”-approach. To knock out the postsynaptic expression of N-cadherin, individual neurons in primary cortical cultures dissociated from homozygous floxed N-cadherin mice ($Ncad^{flox}$; Kostetskii et al., 2005) were transfected with a CreEGFP expression vector. For a better visualization of transfected neurons, cultures were cotransfected with EGFP. First, the knockout of N-cadherin upon long-term expression of CreEGFP was verified on the protein level using immunocytochemistry. Next, FM4-64 staining and destaining experiments were performed to further examine the role of N-cadherin in vesicle cycling.

3.1.4.1 Cre-induced changes of N-cadherin expression resulting in conditional N-cadherin knockout neurons

To demonstrate the loss of N-cadherin in CreEGFP transfected neurons, the expression of N-cadherin protein was checked by immunocytochemistry (ICC) for N-cadherin (Pielarski et al., 2013). Two different antibodies, mouse anti-N-cadherin and rabbit anti-N-cadherin, were used in this study. Fluorescence images (rabbit anti N-cadherin) revealed N-cadherin expression in cell bodies as well as in processes of

cultured neurons (Fig. 3.8A,B). For quantification, the expression level of N-cadherin (mouse anti N-cadherin) in the soma of individual CreEGFP transfected neurons was determined. Regions of interest were drawn around the cell body of transfected neurons to measure the average pixel intensity. Background fluorescence was determined and subtracted individually for each neuron to correct for unspecific staining. At DIV 7, control neurons transfected with EGFP (at DIV 5) showed a strong expression of N-cadherin (Fig. 3.8A, upper panel). Neurons expressing CreEGFP + EGFP for 2 days showed a similar expression of N-cadherin at DIV 7, revealing no significant knockout of N-cadherin protein (Fig. 3.8A, lower panel). In the next step, CreEGFP expression time was increased to 7 days. Therefore, neurons were transfected at DIV 7 with CreEGFP + EGFP and compared with control cells transfected with EGFP at DIV 14. EGFP transfected neurons showed a strong N-cadherin expression at the cell soma (Fig. 3.8B, upper panel). In contrast, N-cadherin expression was almost absent in neurons expressing CreEGFP + EGFP for 7 days indicating functional knockout of N-cadherin protein after longer expression of CreEGFP. Quantification of N-cadherin fluorescence confirmed the observed knockout of N-cadherin protein at DIV 14. The average pixel intensity was highly significantly ($P< 0,001$) decreased from 100 ± 11,5 % (n= 16 cells) in control cells to 23,5 ± 5,8 % (n= 16 cells) in N-cadherin knockout neurons (Fig. 3.8C).

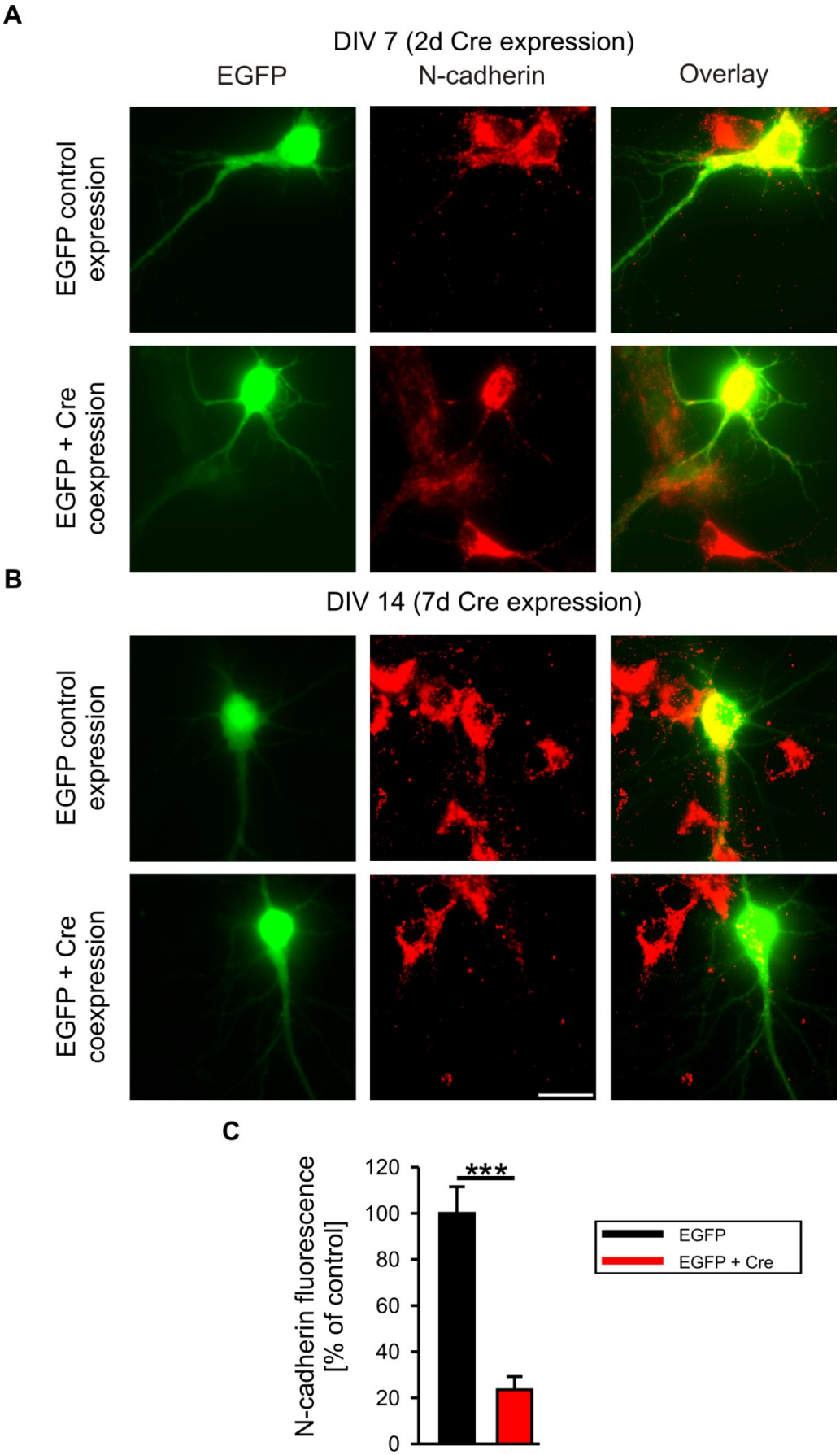
A
DIV 7 (2d Cre expression)
EGFP
N-cadherin
Overlay
EGFP control expression
EGFP + Cre coexpression
B
DIV 14 (7d Cre expression)
EGFP control expression
EGFP + Cre coexpression
C
N-cadherin fluorescence [% of control]
120
100
80
60
40
20
0
***
EGFP
EGFP + Cre

Figure 3.8 Loss of N-cadherin protein upon CreEGFP expression in neurons from homozygous Ncad^{flox} mice
(**A**) Fluorescence images of ICC with antibodies against N-cadherin after 2 days CreEGFP expression (DIV 7). Upper panel: Control cells expressing EGFP. Lower panel: Neurons expressing EGFP + CreEGFP. Left: EGFP signal; Middle: N-cadherin signal; Right: Overlay. (**B**) Analogous to (**A**) but after 7 days CreEGFP expression (DIV 14). (**C**) Quantification of N-cadherin fluorescence intensity at the soma of transfected cells. EGFP: n= 16; EGFP + CreEGFP: n= 16 (n represents number of cells). Error bars represent S.E.M. *** P< 0,001 (Student`s t-test).

3.1.4.2 Synaptic vesicle exocytosis in N-cadherin knockout neurons

Next, conditional N-cadherin knockout neurons were used to examine the role of N-cadherin in synaptic vesicle exocytosis. Individual neurons from Ncad^{flox} mice were transfected at DIV 9 with CreEGFP + EGFP and control cells with EGFP. FM4-64 staining and destaining was performed at DIV 12-15. Neurons were stained with 400 stimuli at 20 Hz in the presence of FM4-64 (10 µM). After intense washing, presynaptic vesicle cluster were visible as distinct puncta (Fig. 3.9A,B). For quantification, FM4-64 puncta on EGFP expressing postsynaptic dendrites were analyzed. Postsynaptic N-cadherin knockout showed no effect on the density of presynaptic FM4-64 puncta (EGFP: 2,53 ± 1,12 puncta/10 µm dendrite, n= 4 cells; EGFP + CreEGFP: 2,13 ± 0,30 puncta/10 µm dendrite, n= 6 cells; Fig. 3.9C). However, long-term expression of CreEGFP significantly (P< 0,001) decreased the size of individual FM4-64 puncta from 1,43 ± 0,17 µm^2 (n= 82 puncta) in control cells to 0,71 ± 0,06 µm^2 (n= 105 puncta) in conditional N-cadherin knockout neurons, indicating a vesicle cycling defect in the absence of N-cadherin (Fig. 3.9D). Next, FM destaining experiments were performed to examine effects of N-cadherin knockout on vesicle exocytosis. Therefore, previously FM4-64 labeled presynaptic vesicle cluster were stimulated with 1200 stimuli and time-lapse sequences were acquired to monitor FM4-64 fluorescence decay upon stimulation (Fig. 3.9E). For quantification, FM4-64 fluorescence intensities over time of individual puncta were background corrected and normalized to its baseline level prior to averaging. Postsynaptic N-cadherin knockout resulted in a distinct slowdown of FM4-64 destaining compared to control (Fig. 3.9F), indicating impaired synaptic vesicle exocytosis. Quantification of the amount of destaining at the end of the stimulation (60 s) revealed a significant

(P< 0,001) decrease from 73,8 ± 1,1 % (n= 91 puncta) in control cells to 66,7 ± 0,6 % (n= 165 puncta) in N-cadherin knockout cells (Fig. 3.9G).

In summary, FM4-64 staining and destaining experiments in conditional N-cadherin knockout neurons confirmed a role of N-cadherin in vesicle cycling as observed in overexpression experiments. Furthermore, N-cadherin knockout experiments revealed an enhancing effect of N-cadherin on vesicle exocytosis in mature neurons.

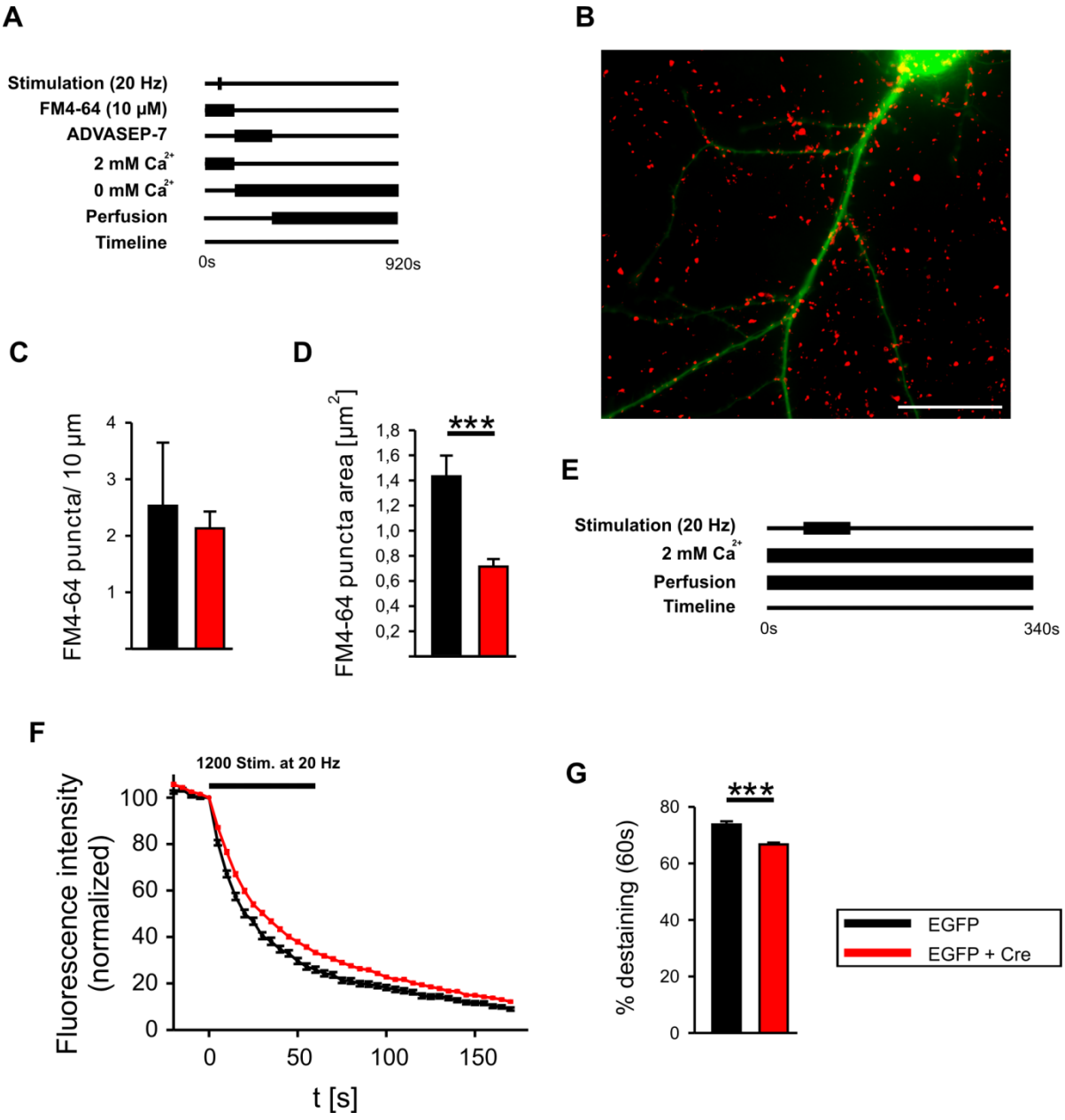

Figure 3.9 FM4-64 staining and destaining in N-cadherin knockout neurons
(**A**) Scheme of FM4-64 staining and washing procedure. (**B**) Example overlay image of FM4-64 labelled vesicle cluster (red) and an EGFP expressing neuron (green). (**C**)

Quantification of FM4-64 puncta density. EGFP: n= 4; EGFP + CreEGFP: n= 6 (n represents number of cells). (**D**) Quantification of FM4-64 puncta area. EGFP: n= 82; EGFP + CreEGFP: n= 105 (n represents number of puncta). (**E**) Scheme of FM destaining experiment. (**F**) Mean destaining curves of puncta from control neurons expressing EGFP and from knockout neurons expressing EGFP + CreEGFP. (**G**) Quantification of amount of destaining (relative to baseline). EGFP: n= 91; EGFP + CreEGFP: n= 165 (n represents number of puncta). Error bars represent S.E.M. *** P< 0,001 (Student`s t-test).

3.1.5 Cooperation of N-cadherin and neuroligin-1 in transsynaptic regulation of vesicle cycling

The experiments described above demonstrated enhancing effects of the cell adhesion molecules N-cadherin and neuroligin-1 on the cycling of synaptic vesicles. Postsynaptic overexpression of N-cadherin as well as neuroligin-1 enhanced the activity dependent staining of presynaptic vesicle cluster with FM4-64 in mature neurons. Simultaneously, ICC for the vesicle membrane associated protein VAMP2 revealed no synaptogenic effect of these cell adhesion molecules conversely indicating a specific role in vesicle exo- and endocytosis. FM4-64 destaining experiments in N-cadherin knockout neurons demonstrated the impact of N-cadherin for synaptic vesicle exocytosis. The next step was to examine a potential cooperation of N-cadherin and neuroligin-1 in the transsynaptic induction of presynaptic vesicle cycling in mature neurons.

3.1.5.1 Interaction of N-cadherin and neuroligin-1 in the modulation of synaptic vesicle cycling

FM4-64 staining was performed to test whether N-cadherin and neuroligin-1 cooperate to induce vesicle cycling. For this, cortical neurons dissociated from homozygous $Ncad^{flox}$ mice were transfected simultaneously with neuroligin-1-EGFP + CreEGFP (DIV 9) to create neuroligin-1 overexpression on an N-cadherin knockout background. For control, neurons were transfected with EGFP or neuroligin-1-EGFP without CreEGFP. In addition, CreEGFP was cotransfected with EGFP. Between DIV 12-14, transfected neurons were labeled with FM4-64 by electrical stimulation (400 stimuli at 20 Hz) and staining was quantified as previously described. In the presence of N-cadherin (Fig. 3.10A, 2 left images), the postsynaptic overexpression of

neuroligin-1-EGFP increased the density of FM4-64 puncta on dendrites. In contrast, neuroligin-1-EGFP overexpression in N-cadherin knockout neurons (Fig. 3.10A, 2 right images) showed no effect on FM4-64 staining. Quantification of FM4-64 puncta density revealed a significant ($P< 0,01$) increase from 1,91 ± 0,18 puncta/10 µm dendrite (n= 14 cells) in control cells expressing EGFP to 4,85 ± 0,48 puncta/10 µm dendrite (n= 6 cells) in neuroligin-1-EGFP overexpressing cells. The overexpression of neuroligin-1-EGFP in N-cadherin knockout neurons showed no changes in FM4-64 puncta density (1,97 ± 0,34 puncta/10 µm dendrite, n= 12 cells). N-cadherin knockout without overexpression slightly but not significantly decreased the density of FM4-64 puncta on dendrites (1,38 ± 0,22 puncta/10 µm dendrite (n= 12 cells; Fig. 3.10B). Consistently, the knockout of N-cadherin significantly ($P<0,01$) reduced the vesicle cycling inducing effect of neuroligin-1. The comparison of the neuroligin-1 effect size on synaptic vesicle cycling revealed a significant decrease ($P< 0,05$) from 153,5 ± 25,2 % (n= 6 cells) in the presence of N-cadherin to 43,3 ± 24,8 % (n= 12 cells) in the absence of N-cadherin (Fig. 3.10C). FM4-64 puncta area was not affected in all four conditions (EGFP: 1,02 ± 0,07 μm^2, n= 14 cells; neuroligin-1-EGFP: 1,09 ± 0,16 μm^2, n= 6 cells; EGFP + CreEGFP: 1,39 ± 0,27 μm^2, n= 12 cells; neuroligin-1-EGFP + CreEGFP: 1,20 ± 0,21 μm^2, n= 12 cells; Fig. 3.10D).

These data indicate a dependence of the vesicle cycling inducing effect of neuroligin-1 on the presence of N-cadherin hence implying a functional cooperation of both cell adhesion molecules.

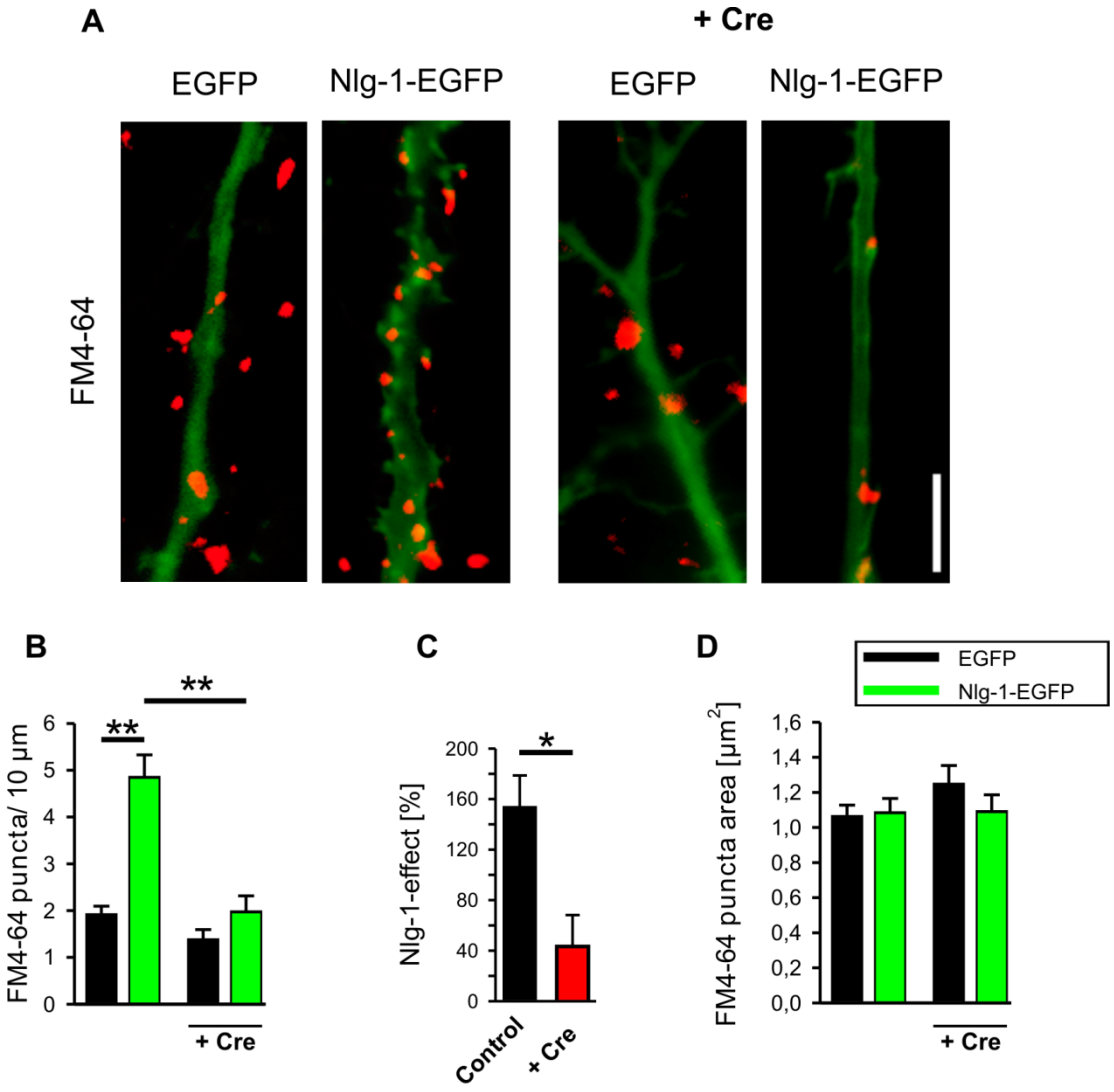

Figure 3.10 Cooperation of N-cadherin and neuroligin-1 in the modulation of vesicle cycling

Vesicle cycling inducing effect of neuroligin-1 depends on N-cadherin. (**A**) Fluorescence images of thresholded FM4-64 puncta (red) on proximal dendrites (EGFP, green) in the presence of N-cadherin (2 left images) and in N-cadherin knockout neurons (2 right images). Scale bar: 5 µm. (**B**) Quantification of FM4-64 puncta density. ** P< 0,01 (One Way Anova with Holm-Sidak Post Hoc Test). (**C**) Quantification of the effect size of neuroligin-1-EGFP overexpression on FM4-64 puncta density in the presence (control) and absence (+Cre) of N-cadherin. * P< 0,05 (Student`s t-test). (**D**) Quantification of FM4-64 puncta area. EGFP: n= 14; neuroligin-1-EGFP: n= 6; EGFP + CreEGFP: n= 12; neuroligin-1-EGFP + CreEGFP: n= 12 (n represents number of cells). Error bars represent S.E.M.

3.1.5.2 The role of N-cadherin in synaptic and dendritic neuroligin-1 localization

Next, the impact of N-cadherin on the distribution of neuroligin-1-EGFP was investigated. Therefore, cortical neurons dissociated from homozygous $Ncad^{flox}$ mice were transfected (DIV 9) with neuroligin-1-EGFP as control group or cotransfected with neuroligin-1-EGFP + CreEGFP. At DIV 14, z-stack images of the neuroligin-1-EGFP signal were acquired. After deconvolution, maximum intensity images were analyzed. Neuroligin-1-EGFP cluster were analyzed in thresholded images related to puncta density, average intensity and size. Additionally, diffuse neuroligin-1-EGFP fluorescence was determined by averaging the pixel intensities of 3 regions of interest offside neuroligin-1-EGFP puncta. After background subtraction, these values describe the amount of non-synaptic, non-clustered neuroligin-1-EGFP signal within dendrites. Postsynaptic N-cadherin knockout decreased the clustering of neuroligin-1-EGFP (Fig. 3.11A). The density of neuroligin-1-EGFP puncta was highly significantly ($P< 0,001$) decreased from 5,67 ± 0,42 puncta/10 µm dendrite (n= 30 cells) in control cells to 2,71 ± 0,31 puncta/10 µm dendrite (n= 33 cells) in neuroligin-1-EGFP + CreEGFP expressing cells (Fig. 3.11B). The size of neuroligin-1-EGFP puncta significantly ($P< 0,001$) decreased from 0,80 ± 0,05 μm^2 (n= 30 cells) to 0,55 ± 0,05 μm^2 (n= 33 cells; Fig. 3.11C). Also the average pixel intensity downsized ($P< 0,001$) from 1130,4 ± 94,8 a.u. (n= 30 cells) in control cells to 575,5 ± 43,6 a.u. (n= 33 cells) in the absence of N-cadherin (Fig. 3.11D). In addition, the average pixel intensity of diffuse, non-clustered neuroligin-1-EGFP significantly ($P< 0,001$) changed from 100,0 ± 14,3 % (n= 30 cells) in control cells to 35,1 ± 6,1 % (n= 33 cells) in N-cadherin knockout neurons (Fig. 3.11E). Furthermore, control experiments in cortical neurons dissociated from C57/BL6 mice showed no changes of neuroligin-1 localization (data not shown).

These data indicate a connection between postsynaptic N-cadherin and the localization of neuroligin-1 in dendrites. They show a direct correlation between the availability of N-cadherin and the clustering of neuroligin-1 within dendrites.

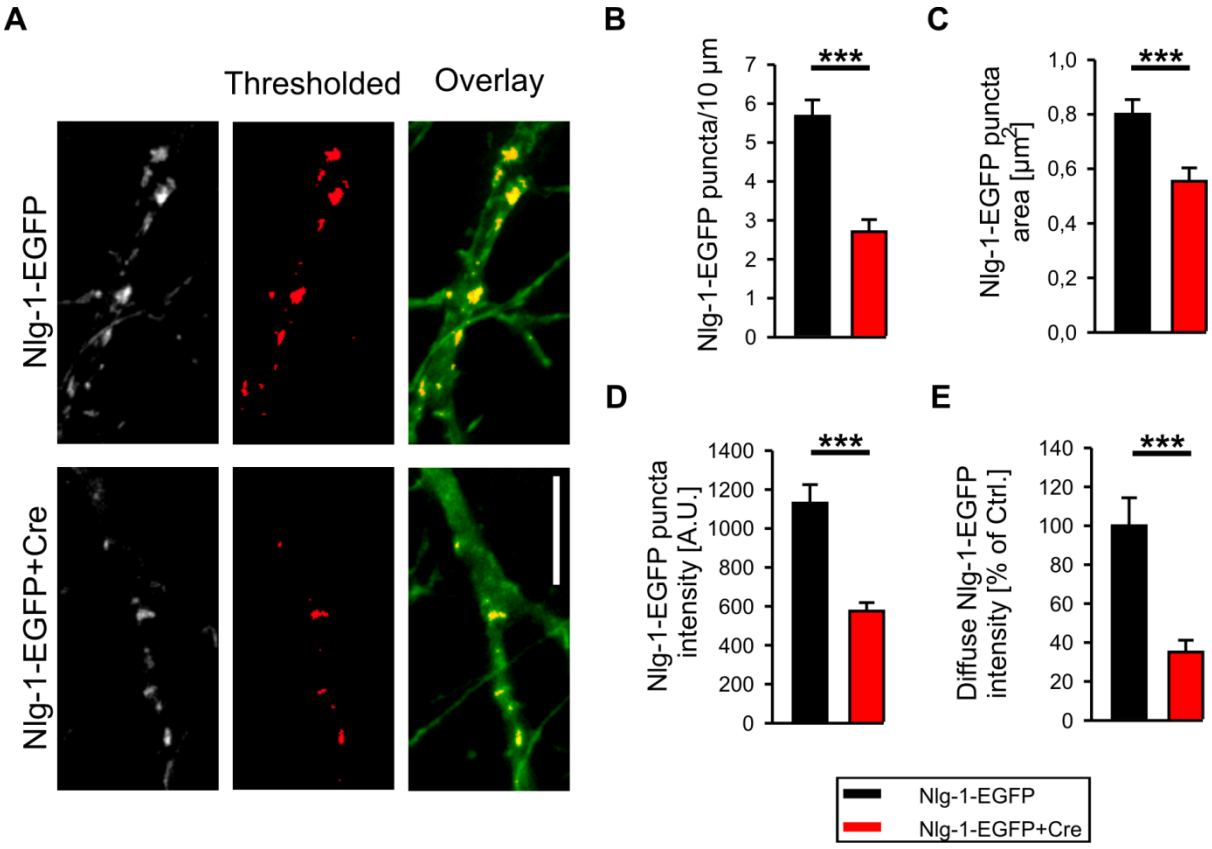

Figure 3.11 Neuroligin-1-EGFP clustering in N-cadherin knockout neurons
N-cadherin affects clustering of neuroligin-1-EGFP in mature (DIV 14) neurons. (**A**) Fluorescence images of neuroligin-1-EGFP. Left: Grey-scale image; Middle: Thresholded neuroligin-1-EGFP signal; Right: Lower thresholding of neuroligin-1-EGFP for visualisation of neuronal processes. (Upper panel) Control neuron expressing neuroligin-1-EGFP. (Lower panel) Neuroligin-1-EGFP expressing N-cadherin knockout neuron. Scale bar: 5 µm. (**B**) Quantification of neuroligin-1-EGFP puncta density. (**C**) Quantification of mean neuroligin-1-EGFP puncta area. (**D**) Quantification of clustered neuroligin-1-EGFP puncta intensity. (**E**) Quantification of non-clustered, diffuse neuroligin-1-EGFP intensity. Neuroligin-1-EGFP: n= 30; neuroligin-1-EGFP + CreEGFP: n= 33 (n represents number of cells). Error bars represent S.E.M. *** P< 0,001 (Student`s t-test).

3.2 Analysis of modulation of vesicle cycling by N-cadherin and neuroligin-1 with Synaptophysin-pHluorin

The styryl dye FM4-64 was used to basically characterize the role of N-cadherin and neuroligin-1 in the modulation of cycling of presynaptic vesicles. Due to the fact that FM4-64 is taken up by vesicular endocytosis of pre-exocytosed vesicles, FM staining depends on the strength of both, vesicle exo- and endocytosis. Hence, FM staining is not suitable for a differential analysis of vesicle exo- and endocytosis. Furthermore, FM destaining experiments in varying extracellular Ca^{2+}-concentrations revealed a limited sensitivity of FM4-64 in the detection of changes in vesicle exocytosis, especially in conditions of higher release probabilities. In subsequent experiments, the genetically encoded probe synaptophysin-pHluorin was used to get a detailed view about the role of N-cadherin and neuroligin-1 in the modulation of synaptic vesicle turnover.

3.2.1 Functionality and characteristics of synaptophysin-pHluorin for differential analysis of vesicular exo- and endocytosis

Since its development in 1998, pH-sensitive GFP constructs (pHluorins) were used to study synaptic vesicle cycling (Miesenböck et al., 1998). To do so, pHluorins can be fused to diverse molecules within synaptic vesicles like synaptobrevin, vGlut1 or synaptophysin. In this study, a fusion protein of pHluorin with the vesicle membrane associated molecule synaptophysin (abbreviated to SypHy; Granseth et al., 2006) was used for the differential examination of exo- and endocytosis of presynaptic vesicles.

3.2.1.1 Dissecting vesicular exo- and endocytosis using SypHy in autaptic glial microisland cultures

In an advanced experimental approach, vesicle cycling was examined with SypHy in an autaptic glial microisland system. SypHy was expressed in neurons from DIV 9 together with the fluorescence marker DsRed2. SypHy experiments were performed in mature, post-synaptogenic neurons (from DIV 12).

In the resting state nearly all SypHy fluorescence is quenched because of the low pH within synaptic vesicles (Fig. 3.12A-1). Upon stimulation, vesicles fuse with the presynaptic membrane and SypHy fluorescence gets unquenched because of the higher pH within the extracellular solution. The increase in fluorescence characterizes the kinetic parameters of vesicle exocytosis (Fig. 3.12A-2). After exocytosis, parts of the presynaptic membrane get endocytosed again and SypHy fluorescence decreases upon reacidification of newly formed vesicles. The decline in fluorescence describes the speed of endocytosis (Fig. 3.12A-3+4). At the end of the experiment, the cultures were incubated with 50 mM NH_4Cl (Fig. 3.12B) to alkalize the complete vesicle cluster and to unquench all SypHy molecules (NH_4Cl-signal). Hence, this quantifies the total expression of SypHy, which is needed for the normalization of SypHy fluorescence signals. Furthermore, the NH_4Cl signal was used to create ROIs around autaptic vesicle cluster. For this, the thresholded SypHy signal was merged with the corresponding DsRed2 image to detect SypHy puncta on dendrites (Fig. 3.12C). Because of the very low transfection efficiency of mature primary neurons in autaptic cultures, SypHy puncta on dendrites in the same field of view arise from the same neuron and represent autaptic contacts. For the analysis of autapses, only SypHy puncta on dendrites of the DsRed2 expressing neuron (white arrows) were processed. Axonal contacts with other neurons (yellow arrowheads) were excluded from analysis (Fig. 3.12D).

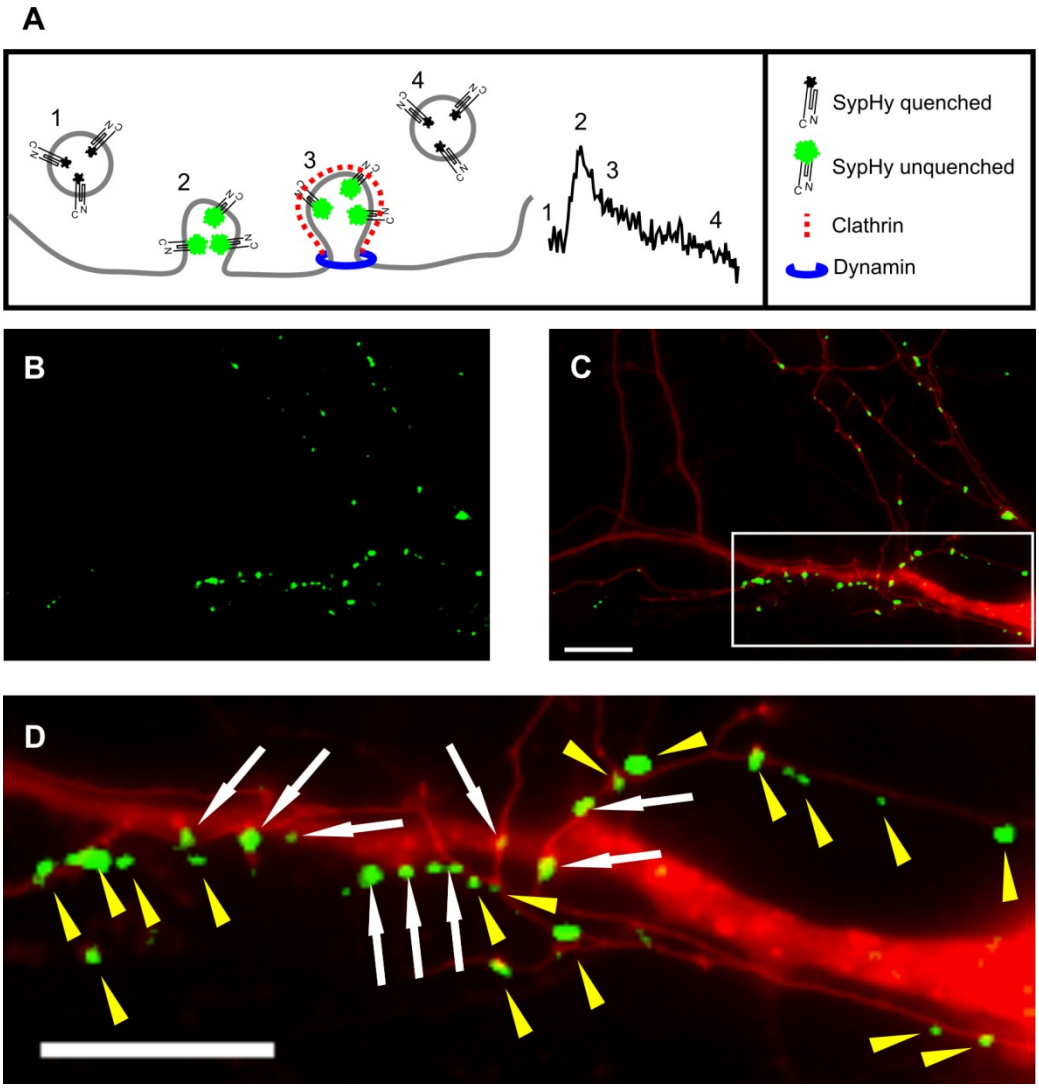

Figure 3.12 Measuring synaptic vesicle cycling in autaptic microisland cultures using SypHy
(**A**) Schematic illustration of SypHy-based imaging (modified after Royle et al., 2008). In the resting state the SypHy signal is quenched (1). Upon stimulation, vesicles fuse, protons distribute into the synaptic cleft and SypHy fluorescence gets unquenched (2). SypHy gets requenched during vesicle endocytosis and vesicle reacidification (3+4). (**B**) NH_4Cl-induced SypHy signal shows the level of SypHy expression in the respective experiment. (**C**) Overlay image of NH_4Cl-induced SypHy fluorescence (green) with the corresponding DsRed2 signal (red). (**D**) Enlarged cutting of (**C**). Autapses (white arrows) can be clearly distinguished from other axonal contacts (yellow arrowheads). Scale bars: 10 µm.

Time-lapse sequences were acquired during the experiments to record fluorescence intensities over time. SypHy signal before stimulation (0 sec) was determined as baseline level (Fig. 3.13A). Upon stimulation, the fluorescence intensities of several SypHy puncta increased (4-30 sec). After stimulation the SypHy signal declined back to the baseline level because of synaptic endocytosis (120-232 sec). Offline analysis

of the time-lapse sequences gave traces of SypHy fluorescence intensities over time for each punctum in (A) (Fig. 3.13B). Averaging all traces of individual puncta resulted in the mean curve of the experiment (Fig. 3.13C).

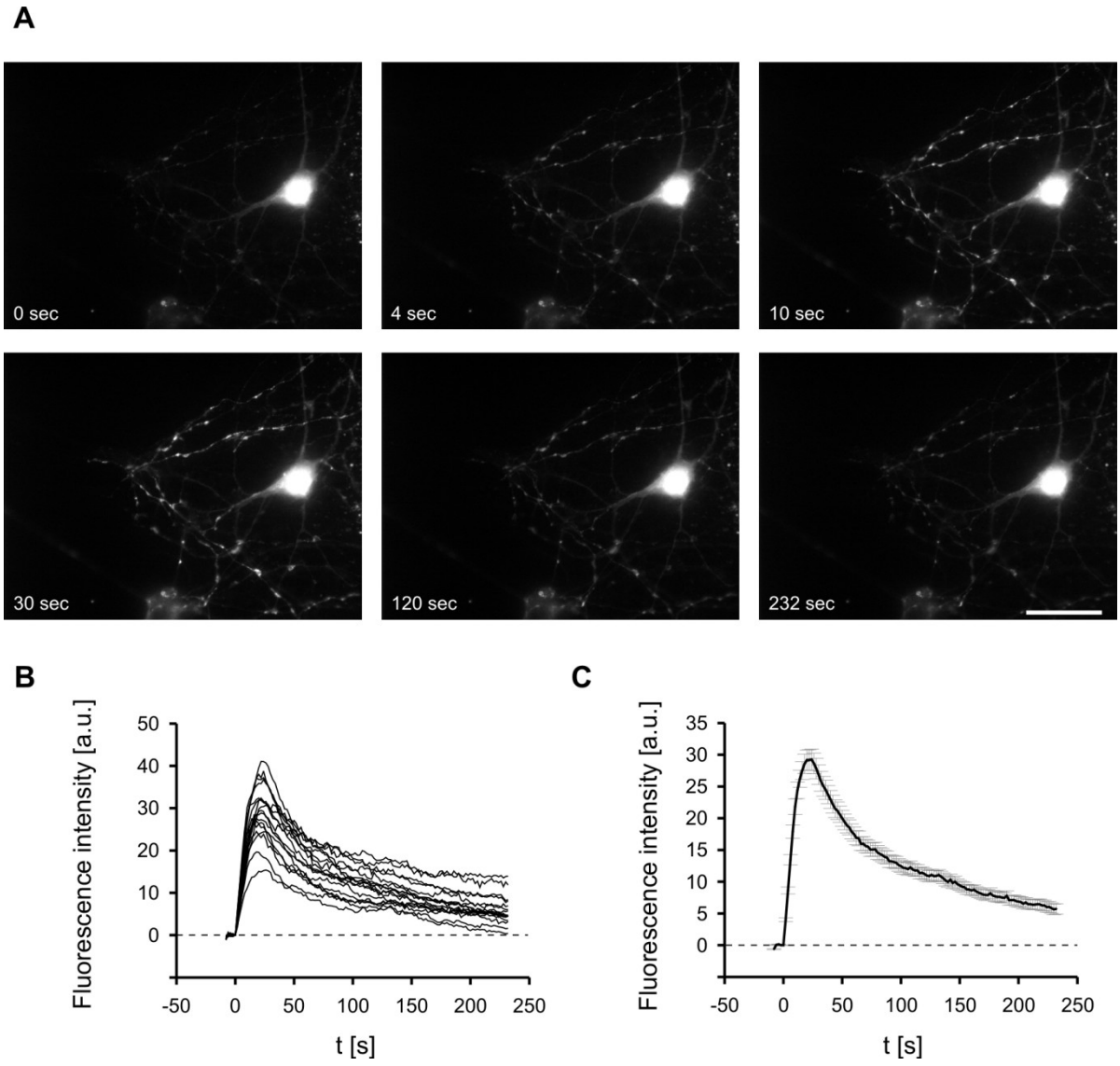

Figure 3.13 Example images and fluorescence intensity analysis of a SypHy expressing neuron during and after stimulation
(**A**) Electrical stimulation induces vesicle exocytosis from presynaptic terminals that leads to a fast increase of the SypHy fluorescence followed by a slower decline in fluorescence while vesicles get endocytosed and reacidified. Scale bar: 30 µm. (**B**) SypHy puncta intensities over time of individual vesicle cluster from (A). (**C**) Mean fluorescence intensity averaged from (B) over time.

To summarize, SypHy experiments in autaptic microisland cultures enabled the time-resolved measurement of synaptic vesicle exo- and endocytosis. DsRed2

cotransfection helped to distinguish between autapses and synapses. Furthermore, autaptic cultures lead to a simultaneous overexpression on the pre- and postsynaptic site. This makes them interesting especially for the examination of a homophilic CAM like N-cadherin. Glial microisland cultures also enable the simultaneous analysis of several autapses with one measurement as they show numerous SypHy puncta within one field of view.

3.2.1.2 SypHy as a probe to study vesicular endocytosis

Control experiments were performed to confirm SypHy as a specific indicator of synaptic exo- and endocytosis. For this, SypHy experiments were performed in the presence of chemicals that are known to alter distinct steps of vesicle endocytosis and kinetics were compared with control neurons. In control cells, electrical stimulation led to increased SypHy fluorescence representing exocytosis followed by a slower decline representing endocytosis (Fig. 3.14A upper panel). The example traces of two puncta (encircled in red; Fig. 3.14B) as well as the average signal from several puncta (Fig. 3.14C) showed the typical kinetics of SypHy fluorescence upon stimulation. First, the ability of SypHy to measure synaptic endocytosis was examined. Cultures were incubated with bafilomycin A1 (1 µM), an inhibitor of the v-type ATPase that assures vesicle reacidification after endocytosis (Bowman et al., 1988). In the presence of bafilomycin A1, electrical stimulation increased the SypHy signal comparable to control cells indicating unaltered vesicle exocytosis (Fig. 3.14A middle panel). However, in contrast to control no decline of the SypHy signal after electrical stimulation was observed confirming the specific block of vesicle reacidification by bafilomycin A1. Furthermore, the curves showed a further, very slow increase in fluorescence after stimulation (Fig. 3.14D,E). SypHy experiments were repeated in the presence of dynasore (80 µM), which is known as a non-competitive inhibitor of the GTPase activity of dynamin 1/2; hence it can be used to block clathrin-mediated endocytosis (Thompson and McNiven, 2006). Similar to bafilomycin A1 treatment, the incubation with dynasore did not significantly change the increase of SypHy fluorescence triggered by exocytosis (Fig. 3.14A lower panel).

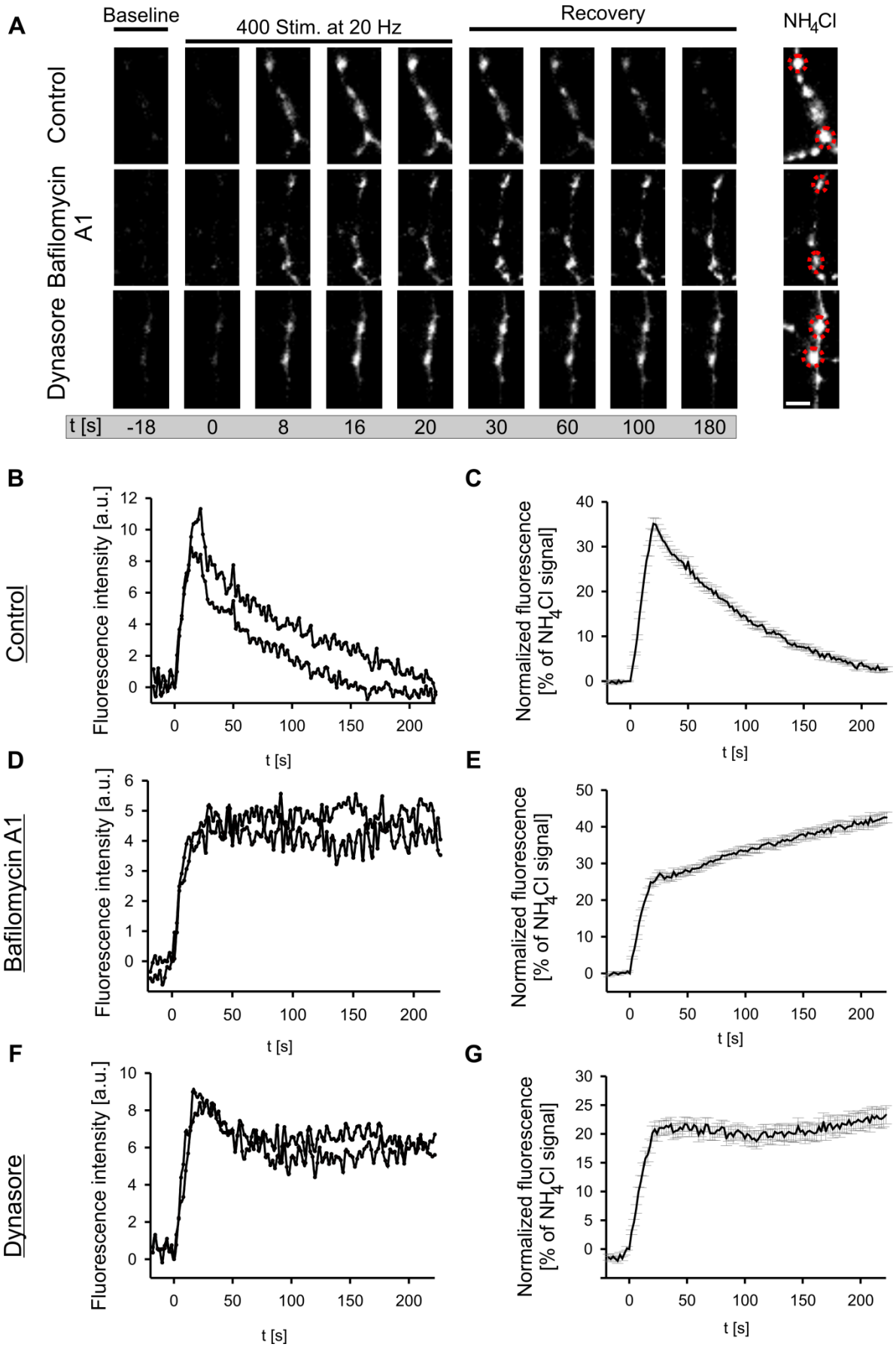
A
Baseline
400 Stim. at 20 Hz
Recovery
NH4Cl
Control
Bafilomycin A1
Dynasore
t [s] -18 0 8 16 20 30 60 100 180
B
Control
Fluorescence intensity [a.u.]
t [s]
C
Normalized fluorescence [% of NH4Cl signal]
t [s]
D
Bafilomycin A1
Fluorescence intensity [a.u.]
t [s]
E
Normalized fluorescence [% of NH4Cl signal]
t [s]
F
Dynasore
Fluorescence intensity [a.u.]
t [s]
G
Normalized fluorescence [% of NH4Cl signal]
t [s]

Figure 3.14 Measuring vesicle endocytosis using SypHy
SypHy experiments upon chemical treatment of synaptic endocytosis. (**A**) Example image sequences of SypHy fluorescence upon electrical stimulation with 400 stimuli at 20 Hz of control, bafilomycin A1 and dynasore treated cells. Scale bar: 2 µm. Time course of fluorescence intensity of red encircled puncta are shown in (**B**), (**D**) and (**F**). Average curves from several puncta are shown in (**C**), (**E**) and (**G**). Control: 243 puncta; bafilomycin A1: 179 puncta; dynasore: 76 puncta (each from 4 experiments). Error bars represent S.E.M.

But in contrast to control, the SypHy signal showed no decline, indicating the specific block of vesicle endocytosis in these cells (Fig. 3.14F,G).
In summary, these experiments confirm SypHy as a specific probe to directly measure vesicular endocytosis.

3.2.1.3 Ca^{2+}-dependence of synaptic exo- and endocytosis as studied by SypHy imaging

SypHy imaging makes it possible to examine exo- and endocytosis separately with one experiment. Control experiments with alterations of key steps of vesicle turnover confirmed its suitability for the precise measurement of synaptic endocytosis. Next, control experiments were performed to confirm SypHy as a specific probe of vesicular exocytosis. For this, SypHy experiments were carried out in different extracellular Ca^{2+}-concentrations to vary the rate of presynaptic exocytosis. Changed extracellular Ca^{2+}-concentrations strongly influenced synaptic vesicle exocytosis in SypHy experiments. The amplitude of the SypHy fluorescence signal clearly increased with higher Ca^{2+}-concentrations. The decline in fluorescence after stimulation was not significantly changed (Fig. 3.15A). The maximum fluorescence increase (relative to baseline signal) rose step by step from 69,3 ± 14,8 % in 0,5 mM Ca^{2+} to 86,6 ± 15,4 % in 1 mM Ca^{2+} and 109,4 ± 20,3% in 2 mM Ca^{2+} to 172,7 ± 18,6 % in 5 mM Ca^{2+} (Fig. 3.15B). In contrast, the decay time constant showed no significant changes (39,7 ± 6,8 s in 0,5 mM Ca^{2+}; 37,8 ± 5,3 s in 1 mM Ca^{2+}; 37,8 ± 6,6 s in 2 mM Ca^{2+}; 50,6 ± 7,6 s in 5 mM Ca^{2+}; Fig. 3.15C).
These observations showed a clear dependence of SypHy fluorescence increases to extracellular Ca^{2+}-concentrations. Hence, they indicated a higher sensitivity of SypHy compared to FM4-64 destaining to measure synaptic exocytosis (data from 3.1.3.2 were analyzed for single cells; Fig. 3.15D+E). Here, only the destaining in 0,5 mM

Ca^{2+} was significantly different and no step by step increase of vesicular exocytosis from 0,5 to 5 mM Ca^{2+} was obvious (68,5 ± 1,6 % in 0,5 mM Ca^{2+}; 71,5 ± 3,7 % in 1 mM Ca^{2+}; 75,6 ± 1,8 % in 2 mM Ca^{2+}; 76,3 ± 2,1 % in 5mM Ca^{2+}; Fig. 3.15E).

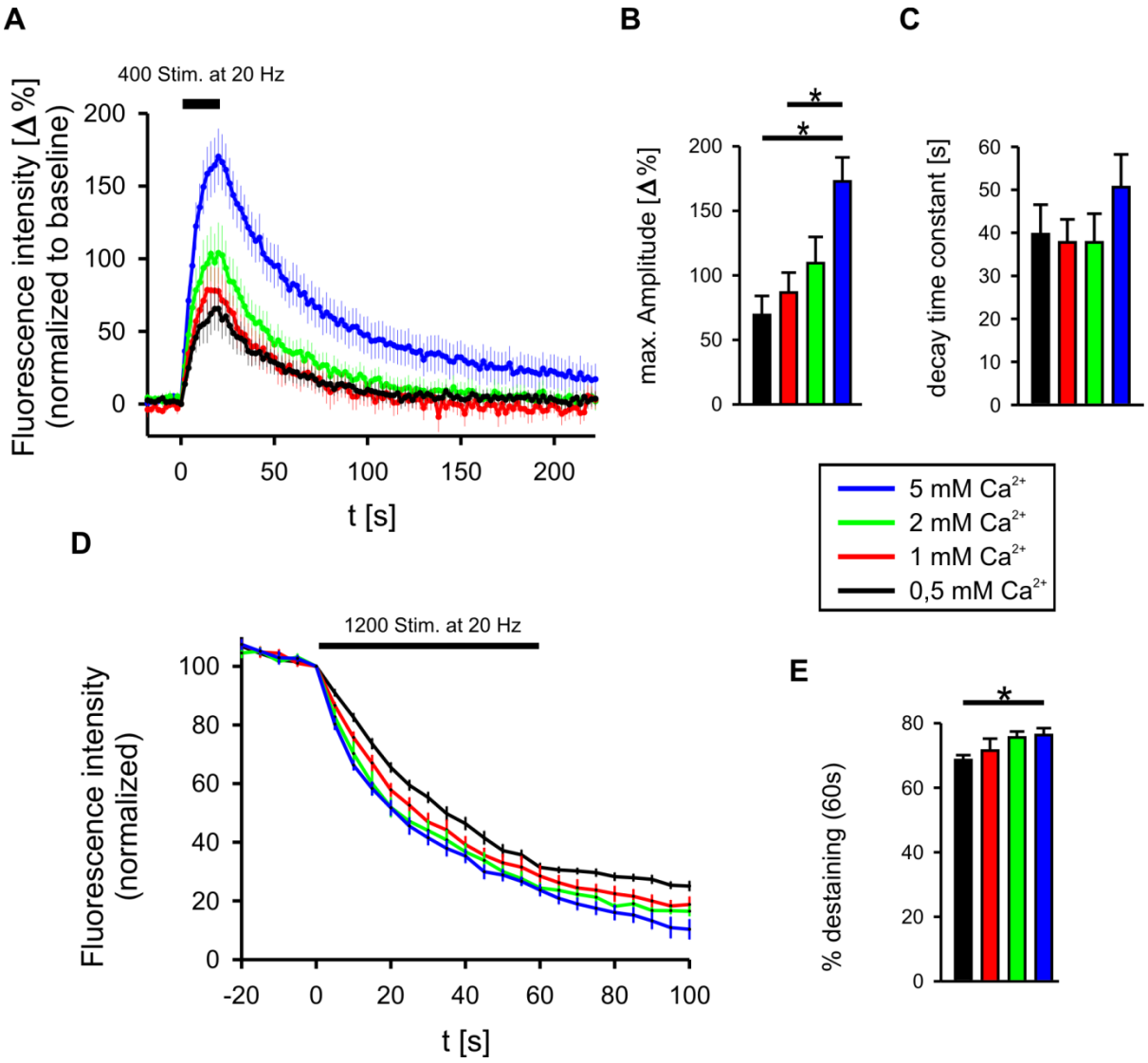

Figure 3.15 Ca^{2+}-dependence of SypHy fluorescence imaging compared to FM4-64 destaining experiments
(**A**) SypHy fluorescence upon electrical stimulation (400 stimuli at 20 Hz) in different extracellular Ca^{2+}-concentrations. Signals from individual puncta were averaged for each cell and then cells were averaged. (**B**) Quantification of vesicle exocytosis. (**C**) Quantification of vesicle endocytosis. 0,5 mM Ca^{2+}: n= 9; 1 mM Ca^{2+}: n= 8; 2 mM Ca^{2+}: n=7; 5 mM Ca^{2+}: n= 9 (n represents number of cells). (**D**) FM4-64 destaining upon electrical stimulation (1200 stimuli at 20 Hz) in different extracellular Ca^{2+}-concentrations (data from experiment 3.1.3.2). Destainings of individual puncta were averaged for each cell and then cells were averaged. (**E**) Quantification of percentage FM4-64 destaining. 0,5 mM Ca^{2+}: n= 8; 1 mM Ca^{2+}: n= 12; 2 mM Ca^{2+}: n=8; 5 mM Ca^{2+}: n= 9 (n represents number of cells). Error bars represent S.E.M. * P< 0,05 (Kruskal-Wallis One Way Analysis of Variance on Ranks with Dunn`s Post Hoc Test).

3.2.2 The roles of N-cadherin and neuroligin-1 in presynaptic vesicle exo- and endocytosis

The above described FM4-64 experiments demonstrated a vesicle cycling inducing effect of N-cadherin and neuroligin-1. Furthermore, FM4-64 destaining experiments in N-cadherin knockout neurons indicated an important role of N-cadherin in vesicle exocytosis. However, because of its limited sensitivity FM4-64 destainings in N-cadherin and neuroligin-1 overexpressing neurons showed no clear changes in vesicle exocytosis. In the next step SypHy experiments were performed to further analyze the distinct roles of N-cadherin and neuroligin-1 in synaptic exo- and endocytosis.

3.2.2.1 SypHy-based analysis of vesicle turnover in N-cadherin and neuroligin-1 overexpressing cortical neurons

SypHy experiments were performed in autaptic microisland cultures in neurons that overexpressed N-cadherin or neuroligin-1, and in control cells. For control, individual neurons were cotransfected (DIV 9) with SypHy and DsRed2 as a marker for transfected cells. For overexpressions, neurons were additionally cotransfected with pCMV-Neuroligin-1 (neuroligin-1 plasmid) or pMS149.1-N-cadherin (N-cadherin plasmid). SypHy experiments were performed at DIV 12-14. Vesicle cycling was induced by 400 stimuli at 20 Hz. Autaptic puncta were analyzed and cycling vesicle cluster were averaged for each cell. Overexpression of N-cadherin and neuroligin-1 enhanced the exocytosis of synaptic vesicles. The amplitudes of stimulation-induced SypHy fluorescence signals were significantly ($P< 0,05$) increased in neurons overexpressing N-cadherin (35,9 ± 6,9 % of NH_4Cl signal, n= 11 cells) and neuroligin-1 (37,0 ± 5,0 % of NH_4Cl signal, n= 8 cells) as compared to control (19,5 ± 1,3 % of NH_4Cl signal, n= 10 cells; Fig. 3.16A,B). Additionally, the endocytosis-related decline in SypHy fluorescence after stimulation was much faster in neurons overexpressing N-cadherin (Fig. 3.16A).

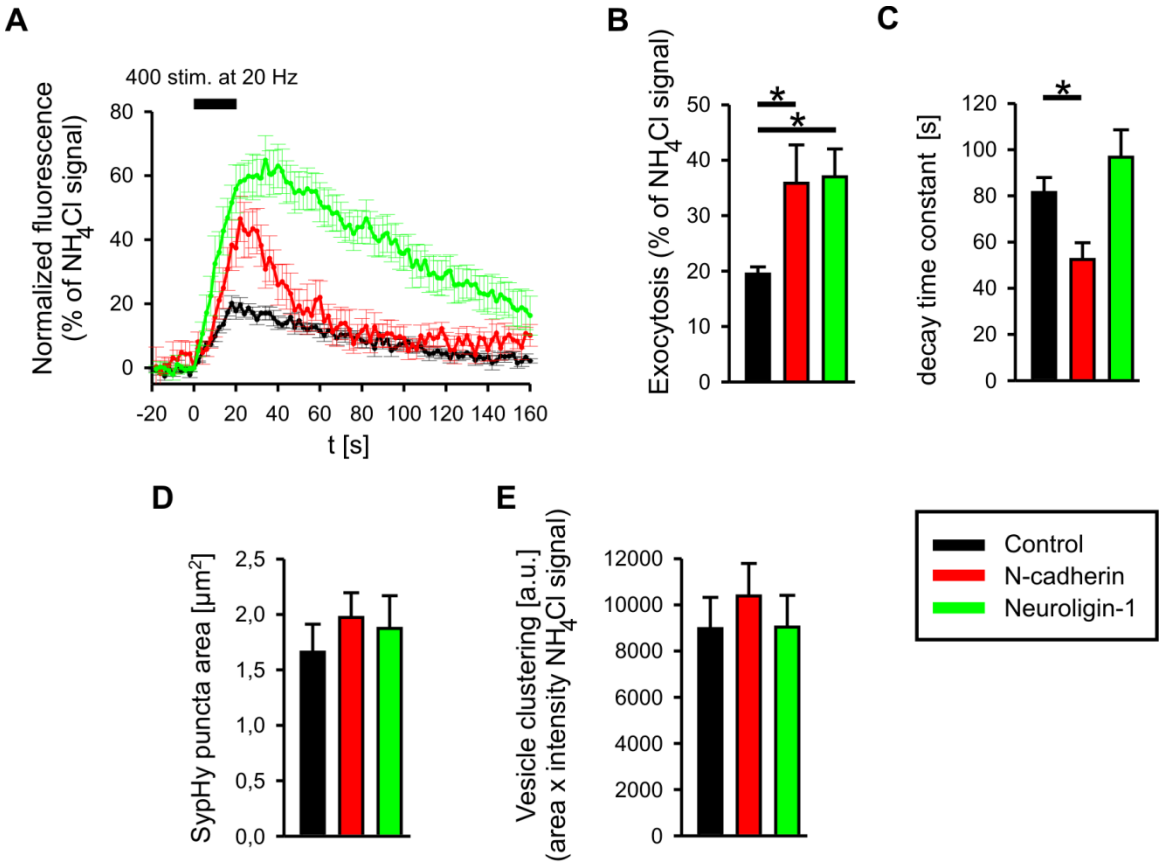

Figure 3.16 Enhancement of synaptic vesicle cycling by overexpression of N-cadherin and neuroligin-1 as analysed by SypHy experiments
SypHy experiments on N-cadherin and neuroligin-1 overexpressing neurons at DIV 12-14. (**A**) Example traces of mean SypHy puncta fluorescence of individual cells. (**B**) Quantification of vesicle exocytosis. (**C**) Quantification of vesicle endocytosis. (**D**) Quantification of SypHy puncta size. (**E**) Quantification of vesicle clustering. Control: n= 10; N-cadherin: n= 11; neuroligin-1: n= 8 (n represents number of cells). Error bars represent S.E.M. * P< 0,05 (One Way Anova with Holm-Sidak Post Hoc Test).

The decay time constant significantly (P< 0,05) decreased from 81,4 ± 6,5 s (n= 10 cells) in control cells to 52,4 ± 7,3 s (n= 11 cells) in cells overexpressing N-cadherin. The decay time constant of cells overexpressing neuroligin-1 was not altered compared to control (96,7 ± 11,9 s, n= 8 cells; Fig. 3.16C). The size of the NH_4Cl-induced SypHy puncta was not altered (control: 1,66 ± 0,25 µm^2, n= 10 cells; N-cadherin: 1,97 ± 0,22 µm^2, n= 11 cells; neuroligin-1: 1,87 ± 0,29 µm^2, n= 8 cells; Fig. 3.16D). Also the integrated intensity (area x pixel intensity) of NH_4Cl-induced SypHy signals was not changed (control: 8968,2 ± 1353,9 a.u., n= 10 cells; N-cadherin: 10385,0 ± 1411,5 a.u., n= 11 cells; neuroligin-1: 9038,3 ± 1372,6 a.u., n= 8 cells; Fig. 3.16E). These findings confirmed the lack of synaptogenesis induced by N-cadherin

or neuroligin-1 in this mature culture system that was previously observed by immunocytochemistry.

In an additional experiment, the enhancement of synaptic exocytosis by neuroligin-1 was further analyzed. Therefore, the transsynaptic interaction of postsynaptic neuroligin-1 with presynaptic β-neurexin was blocked to test whether this interaction is necessary for the effect of neuroligin-1 on exocytosis.

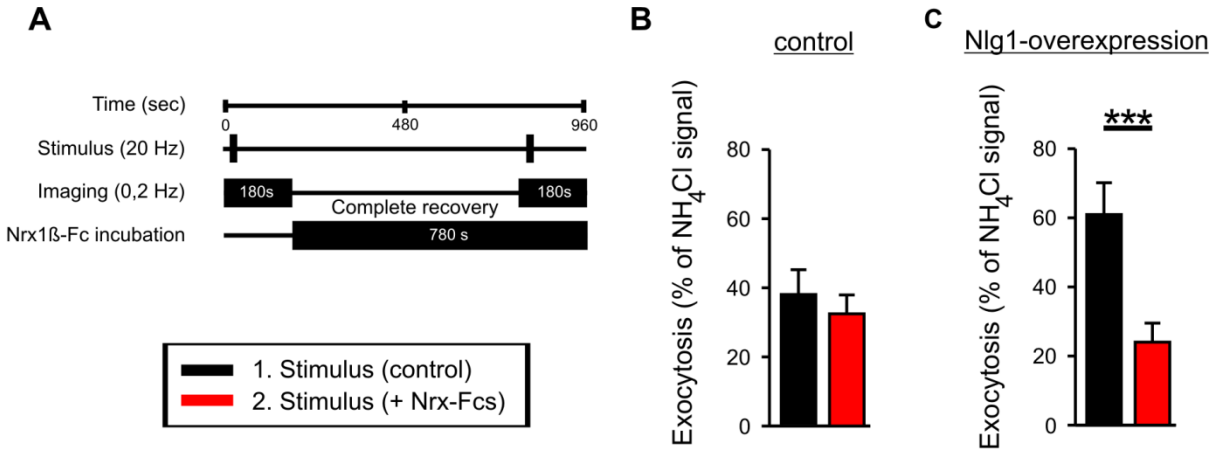

Figure 3.17 The enhancing effect of neuroligin-1 on exocytosis depends on neuroligin-1/β-neurexin interaction
(**A**) Schematic illustration of double-stimulation experiments combined with neurexin 1β/Fc chimera incubation. (**B**) Quantification of vesicle exocytosis in control cells. (**C**) Quantification of vesicle exocytosis in neuroligin-1-overexpressing cells. Control: n= 17 puncta from 6 cells; neuroligin-1-overexpression: n= 14 puncta from 5 cells. Error bars represent S.E.M. *** P< 0,001 (Student`s t-test).

SypHy experiments (as described above) were performed in control cells and upon overexpression of neuroligin-1 at DIV 12-14. Neuroligin-1/β-neurexin interaction was blocked by extracellular application of recombinant human neurexin 1β/Fc chimera (R&D Systems) in a concentration of 2 µg/ml. For the direct observation of functional changes upon blocking this transsynaptic interaction, double-stimulation experiments were performed. SypHy expressing neurons were stimulated twice with 400 stimuli at 20 Hz. The first pulse was followed by a pause for the complete recovery of fused vesicle membrane. Simultaneously, cultures were incubated with neurexin 1β/Fc chimera for 10 min prior to the second pulse. Finally, the second stimulation (in the presence of neurexin 1β/Fc chimera) was applied to measure exocytosis upon blockade of neuroligin-1/β-neurexin interaction (Fig. 3.17A). For analysis, only initially

intact vesicle cluster (≥ 50 % fluorescence decay after 1. stimulus) were quantified. In control cells, the block of neuroligin-1/β-neurexin interaction had only a slight effect on synaptic exocytosis (1. stimulus: 38,0 ± 7,2 % of NH_4Cl signal; 2. stimulus: 32,8 ± 5,5 % of NH_4Cl signal, n=17 puncta; Fig. 3.17B). In contrast, application of neurexin 1β/Fc chimera significantly ($P< 0,001$) decreased vesicle exocytosis in neurons overexpressing neuroligin-1. Exocytosis signals decreased from 61,1 ± 9,2 % of NH_4Cl signal (1. stimulus) to 24,0 ± 5,5 % of NH_4Cl signal (2. stimulus) in the presence of neurexin 1β/Fc chimera (Fig. 3.17C, n= 14 puncta).
In summary, these data indicated the enhancement of presynaptic vesicle exocytosis by N-cadherin and neuroligin-1. Furthermore, it indicated an important role of N-cadherin in the endocytosis of presynaptic vesicles. In addition, it was shown that the enhancing effect on exocytosis by postsynaptic neuroligin-1 depends on the transsynaptic interaction with presynaptic β-neurexin.

3.2.2.2 N-cadherin modulates endocytosis upon strong synaptic activity

Next, the effect of N-cadherin on endocytosis was analyzed in more detail, especially in terms of synaptic activity. Therefore, “loss-of-function”-experiments were performed in N-cadherin knockout neurons from homozygous $Ncad^{flox}$ mice using SypHy. Neurons were cotransfected (DIV 9) with SypHy and DsRed2 and N-cadherin knockout was induced by additional expression of CreEGFP. SypHy experiments were performed (DIV 13-14) in control and N-cadherin knockout neurons in different extracellular Ca^{2+}-concentrations (2 mM and 5 mM) and cultures were stimulated with 200 to 800 stimuli (20 Hz) to get variation of synaptic activity (exocytosis). SypHy fluorescence intensities of individual puncta were analyzed to get a correlation between the amount of exocytosis and the strength of compensatory endocytosis of the respective vesicle cluster. Puncta were grouped due to their exocytosis signal into strongly active (high exocytosis; amplitude 60-80 % of NH_4Cl signal) and less active (low exocytosis; amplitude 10-30 % of NH_4Cl signal) vesicle cluster. Upon low and high exocytosis, the knockout of N-cadherin affected vesicle endocytosis differentially.

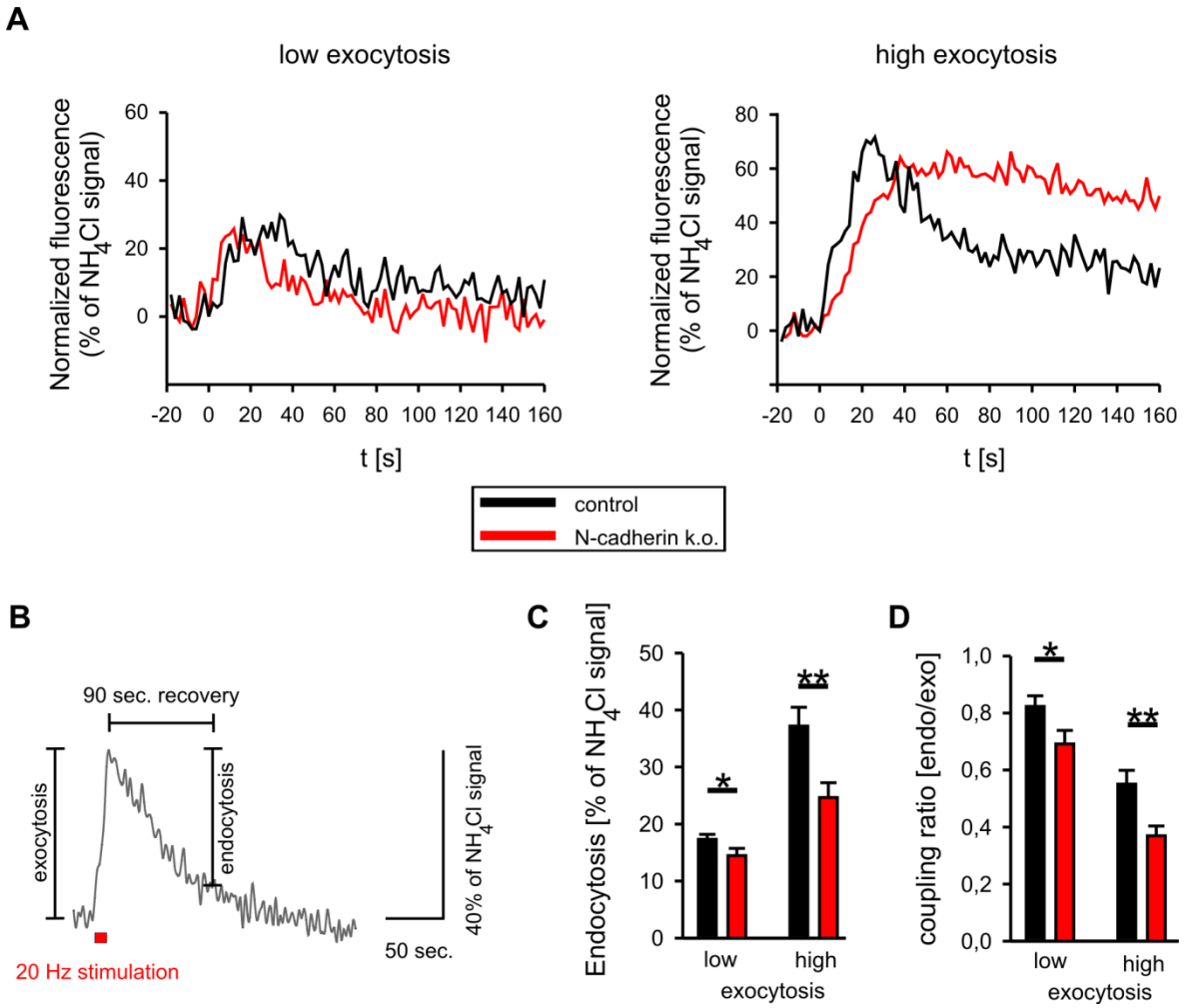

Figure 3.18 Activity-dependent role of N-cadherin in compensatory vesicle endocytosis
N-cadherin is important for coupling of exo- and endocytosis. Vesicle cluster were grouped based on their exocytotic activity. (**A**) Example SypHy traces of single vesicle cluster with low (left) and high (right) exocytosis of control (black) and N-cadherin knockout cells (red). Stimulation starts at 0 s. (**B**) Illustration of quantitative analysis of vesicle exo- and endocytosis from single vesicle cluster. (**C**) Quantification of endocytosis in control and N-cadherin knockout neurons. (**D**) Quantification of coupling ratios. Control (low exocytosis): n= 46 puncta from 19 cells; N-cadherin knockout (low exocytosis): n= 41 puncta from 10 cells; Control (high exocytosis): n=10 puncta from 7 cells; N-cadherin knockout (high exocytosis): n= 9 puncta from 6 cells. Error bars indicate S.E.M. * P< 0,05; ** P< 0,01 (Student`s t-test).

In the absence of N-cadherin, vesicle cluster with high exocytosis showed a strongly inhibited decline of SypHy fluorescence. Comparison of the N-cadherin knockout effect upon low and high exocytosis indicated a stronger defect of synaptic endocytosis in highly active vesicle cluster (Fig. 3.18A). To prevent imprecise curve fitting of noisy single puncta traces, analysis of endocytosis in individual SypHy puncta differed from whole cell analysis. In these experiments, endocytosis was

quantified by determining the decay of fluorescence 90 seconds after the end of stimulation (Fig. 3.18B). N-cadherin knockout reduced synaptic vesicle endocytosis in less active vesicle cluster (low exocytosis) and in highly active puncta (high exocytosis). In synapses with low exocytosis, compensatory endocytosis slightly decreased ($P< 0,05$) from 17,3 ± 0,9 % of NH_4Cl signal (n= 46 puncta) in control to 14,4 ± 1,3 % of NH_4Cl signal (n= 41 puncta) in N-cadherin knockout neurons. In highly active synapses, compensatory endocytosis strongly decreased ($P< 0,01$) from 37,2 ± 3,3 % of NH_4Cl signal (n= 10 puncta) in control cells to 24,6 ± 2,6 % of NH_4Cl signal (n= 9 puncta) in the absence of N-cadherin (Fig. 3.18C). Quantification of the corresponding coupling ratios confirmed these observations. The coupling ratio (endocytosis/exocytosis) correlates endocytosis with previous exocytosis. It should help to correct for individual puncta variation in vesicle exocytosis. A ratio of 1 means that all exocytosed vesicles were subsequently endocytosed. Lower ratios indicate an incomplete compensation of exocytosis by endocytosis. After low exocytosis, the coupling ratio slightly ($P< 0,05$) decreased from 0,82 ± 0,04 in control cells to 0,69 ± 0,05 in N-cadherin knockout cells. In highly active vesicle cluster, the ratio strongly ($P< 0,01$) decreased from 0,55 ± 0,05 in control to 0,37 ± 0,03 in the absence of N-cadherin (Fig. 3.18D).

In summary, these experiments indicated a crucial role of N-cadherin in the compensation of vesicle exocytosis by subsequent endocytosis. Particularly in highly active synapses, N-cadherin is needed to maintain proper synaptic function.

In a more elaborated experimental setup, SypHy double-stimulation experiments were performed. In this approach, individual vesicle cluster were stimulated twice with two different protocols. First, cells were stimulated with 200 stimuli at 20 Hz to induce weak exocytosis followed by a break of 3 min without taking images to prevent photobleaching and to enable recovery of exocytosed vesicles as indicated by quenched SypHy signals. Finally, a second longer stimulus (800 stimuli at 20 Hz) induced strong exocytosis (Fig. 3.19A). Both stimuli were given in 5 mM Ca^{2+} to induce a strong exocytosis with the second stimulus. In contrast to the previous experiment, SypHy signals were not grouped by the amount of exocytosis but by the strength of the stimulus. Vesicle cluster with less than 10 % increase of exocytosis from the first to the second pulse were not analyzed. Here, vesicle exocytosis was

already saturated by the weak stimulation or synaptic contacts got damaged because of phototoxicity during the first stimulus. The quantitative analysis was analogous to the previous experiment. The advantage of this double-stimulation experiment was that it enabled to measure alterations of vesicle turnover upon changes of synaptic activity directly at individual vesicle cluster. Knockout of N-cadherin reduced exocytosis upon weak stimulation (200 stimuli at 20 Hz). The SypHy signal amplitude significantly ($P< 0,05$) decreased from 33,8 ± 3,5 % of NH_4Cl signal (n= 22 puncta) in control to 25,4 ± 1,9 % of NH_4Cl signal (n= 25 puncta) in N-cadherin knockout neurons. Upon longer stimulation (800 stimuli at 20 Hz) the effect of N-cadherin knockout on vesicle exocytosis was not significant (control: 47,7 ± 3,9 % of NH_4Cl signal, n= 22 puncta; N-cadherin knockout: 44,2 ± 3,0 % of NH_4Cl signal, n= 25 puncta; Fig. 3.19B). Quantification of exocytosis in knockout neurons relative to control confirmed this observation. The relative vesicle exocytosis in N-cadherin knockout was significantly ($p< 0,05$) lower upon weak stimulation (75,2 ± 5,5 %, n= 25 puncta) than upon stronger stimulation (92,7 ± 6,4 %, n= 25 puncta; Fig. 3.19C). This indicated that the effect of N-cadherin knockout on synaptic exocytosis gets compensated upon longer stimulation. In contrast to this, an effect of N-cadherin knockout on vesicle endocytosis was absent upon weak stimulation but clearly arised upon strong stimulation. With 200 stimuli at 20 Hz, the endocytosis-related SypHy signal decline was not different in N-cadherin knockout cells (22,7 ± 1,5 % of NH_4Cl signal, n= 25 puncta) compared to control (25,0 ± 3,0 % of NH_4Cl signal, n= 22 puncta). With a stronger stimulation, the vesicle endocytosis-related SypHy signal decreased significantly ($P< 0,01$) from 25,7 ± 2,5 % of NH_4Cl signal (n= 22 puncta) in control cells to 17,0 ± 2,0 % of NH_4Cl signal (n= 25 puncta) in N-cadherin knockout neurons (Fig. 3.19D). In this case, the endocytosis signal relative to control was significantly smaller ($P< 0,05$) upon strong stimulation (66,1 ± 7,9 %, n= 25 puncta) compared to weak stimulation (90,5 ± 6,2 %, n= 25 puncta; Fig. 3.19E). Also the coupling ratio (endocytosis/exocytosis) indicated no endocytotic defect in N-cadherin knockout cells upon weak stimulation (control: 0,78 ± 0,06, n= 22 puncta; N-cadherin knockout: 0,94 ± 0,06, n= 25 puncta). In contrast, upon strong stimulation the coupling ratio significantly ($P< 0,05$) decreased from 0,54 ± 0,03 % (n= 22 puncta) in control to 0,41 ± 0,04 % (n= 25 puncta) in N-cadherin knockout cells (Fig. 3.19F).

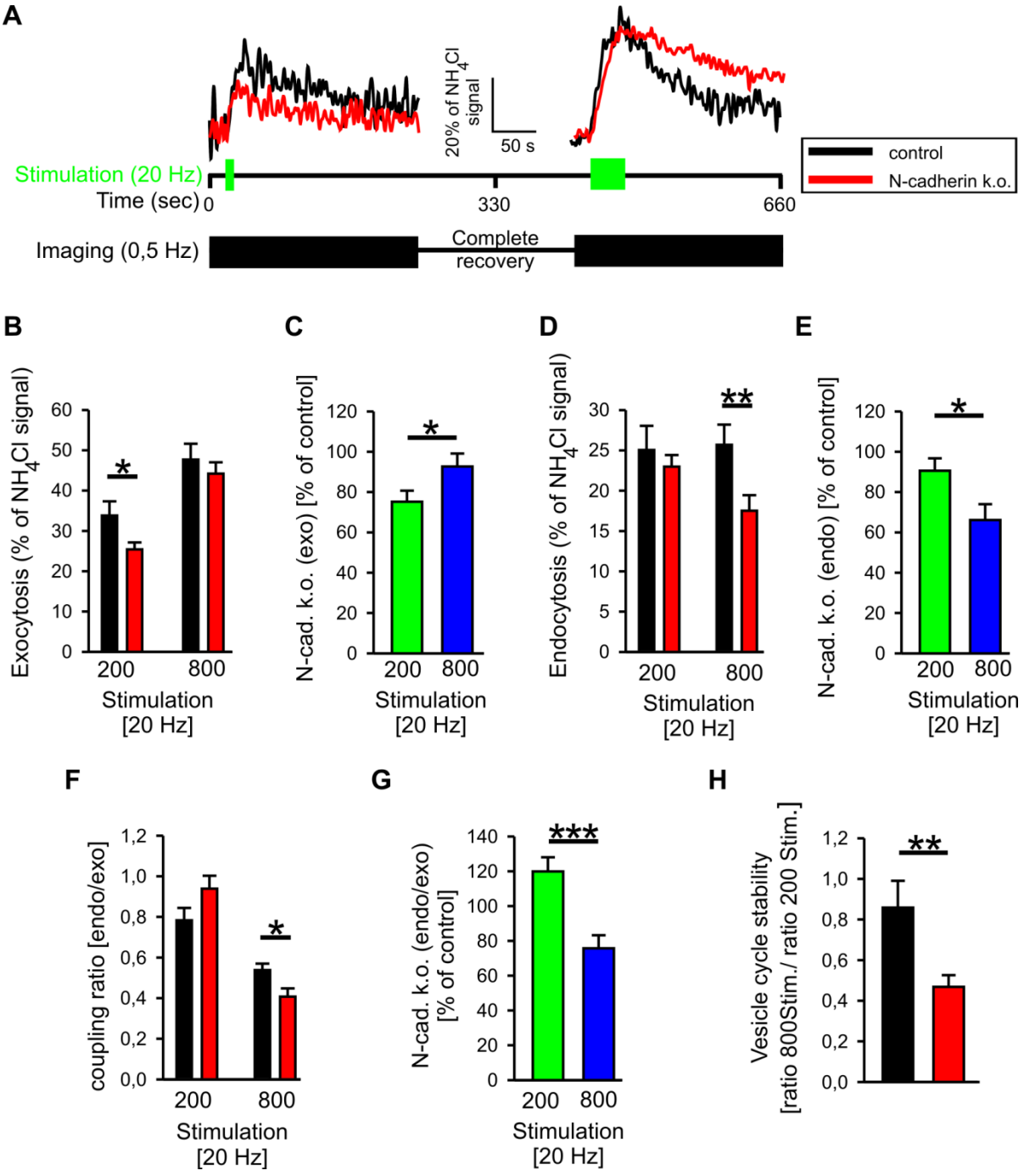

Figure 3.19 Dependence of compensative endocytosis on N-cadherin upon strong synaptic activity
(**A**) Illustration of double-stimulation experiments and example traces from control (black) and N-cadherin knockout (red) cells. (**B**) Quantification of vesicle exocytosis. (**C**) Relative vesicle exocytosis (compared to control) in N-cadherin knockout cells upon weak (green) and strong (blue) stimulation. (**D**) Quantification of vesicle endocytosis. (**E**) Relative vesicle endocytosis (compared to control) in N-cadherin knockout cells upon weak (green) and strong (blue) stimulation. (**F**) Quantification of the coupling ratio. (**G**) Relative coupling ratio (compared to control) upon weak (green) and strong (blue) stimulation. (**H**) Quantification of vesicle cycle stability in control (black) and N-cadherin knockout (red)

cells. Control: n= 22 puncta from 11 cells; N-cadherin knockout: n= 25 puncta from 5 cells. Error bars indicate S.E.M. * P< 0,05; ** P< 0,01, *** P< 0,001 (Student`s t-test).

Quantification of the relative coupling ratio (knockout ratio/control ratio) further supported the observation that a defect of compensatory endocytosis in the absence of N-cadherin depends on the activity level. The relative coupling ratio significantly decreased (P< 0,001) from 119,9 ± 8,1 % (n= 25 puncta) upon weak stimulation to 75,7 ± 7,5 % (n= 25 puncta) after strong exocytosis (Fig. 3.19G). Finally, the stability of the vesicle cycle was quantified to measure the ability of the vesicle cluster to compensate strong exocytosis with subsequent endocytosis. The ratio also includes the condition of the vesicle cluster at weak stimulation to describe changes upon increased synaptic activity. Vesicle cycle stability significantly (P< 0,01) decreased from 0,86 ± 0,13 (n= 22 puncta) in control to 0,47 ± 0,06 (n= 25 puncta) in N-cadherin knockout neurons (Fig. 3.19H).

In summary, the double-stimulation experiments confirmed the observations of the previous data. They demonstrated that the effect of N-cadherin on synaptic endocytosis depends on the activity pattern of the vesicle cluster. N-cadherin is less important to compensate weak synaptic exocytosis with subsequent endocytosis. In contrast, N-cadherin is essential to compensate strong exocytosis with increased endocytosis. This indicates an important role of N-cadherin in maintaining the coupling between exo- and endocytosis that is indispensable for proper synaptic function.

3.2.2.3 Isolated analysis of synaptic exocytosis by blocking vesicle reacidification

The next experiment concentrated on the enhancing effects of N-cadherin and neuroligin-1 on vesicle exocytosis that was previously observed by the overexpression of these cell adhesion molecules (Fig. 3.16). In SypHy experiments, the maximum amplitude of the fluorescence signal gives a good approximation of vesicle exocytosis. However, endocytosis followed by vesicle reacidification also occurs (in small amounts) during the rise time of SypHy fluorescence signal. Hence, quenching of SypHy fluorescence by reacidification was blocked for the correct

measurement of vesicle exocytosis. Vesicle reacidification was blocked with bafilomycin A1, an inhibitor of the vesicular H^+-ATPase and thus synaptic vesicles were trapped in an alkaline state. Hence, SypHy fluorescence was kept unquenched (Fig. 3.20A).

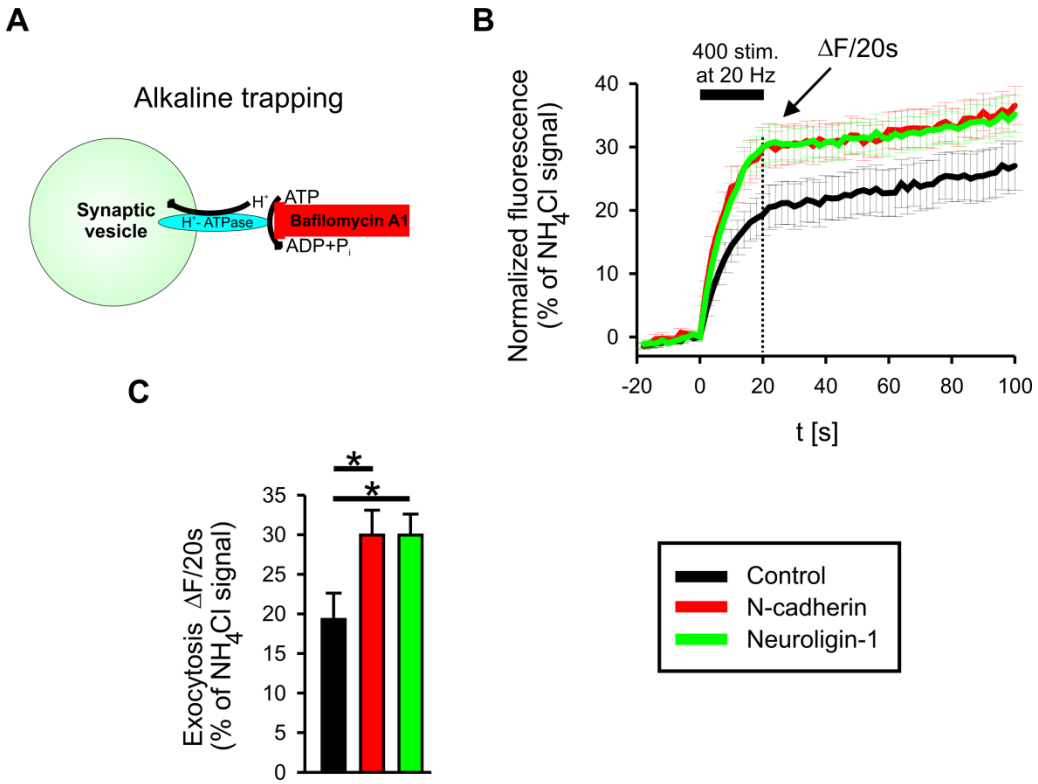

Figure 3.20 Overexpression of N-cadherin and neuroligin-1 induce enhanced synaptic vesicle exocytosis
(**A**) Illustration of blocking reacidification with bafilomycin A1. (**B**) Example traces of SypHy experiments in the presence of bafilomycin A1. (**C**) Quantification of synaptic vesicle exocytosis. Control: n= 13; N-cadherin: n= 16; neuroligin-1: n= 11 (n represents number of cells). Error bars represent S.E.M. * P< 0,05 (Kruskal-Wallis One Way Analysis of Variance on Ranks with Dunn`s Post Hoc Test).

For SypHy experiments, cells were transfected as previously described (Fig. 3.16). Cultures were stimulated (400 stimuli at 20 Hz) in the presence of bafilomycin A1 (1 µM). As expected, overexpression of N-cadherin and neuroligin-1 induced exocytosis of synaptic vesicles. The mean amplitude of SypHy fluorescence signal at the end of the stimulation was significantly (P< 0,05) increased in cells overexpressing N-cadherin (30,0 ± 3,1 % of NH_4Cl signal, n= 16 cells) or neuroligin-1 (30,0 ± 2,6 % of

NH_4Cl signal, n= 11 cells) compared to control (19,3 ± 3,3 % of NH_4Cl signal, n= 13 cells; Fig. 3.20B,C).

These data confirm the previous observations that N-cadherin and neuroligin-1 induce enhanced exocytosis of presynaptic vesicles.

3.3 Structural relocalization of synaptic components upon intense synaptic activity

FM4-64 and SypHy experiments demonstrated a crucial regulatory role of N-cadherin and neuroligin-1 in synaptic vesicle cycling. Both cell adhesion molecules enhance exocytosis at presynaptic terminals. Furthermore, it was shown that N-cadherin is important for vesicle endocytosis, particularly upon high synaptic activity. These observations also indicated a specific role of N-cadherin in the coupling of vesicular exo- and endocytosis that is essential to maintain proper synaptic function in highly active networks. Next, structural changes of several pre- and postsynaptic molecules associated with strong synaptic activity were examined. In a previous study it has been shown that N-cadherin spreads out from the active zone during strong exocytosis induced by high [K^+]-treatment (Tanaka et al., 2000). In a similar experimental approach, the structural characteristics of N-cadherin, neuroligin-1 and PSD95 upon high synaptic activity were analyzed.

3.3.1 Spatial distribution of N-cadherin, neuroligin-1 and PSD95 during strong synaptic stimulation

Immunocytochemical stainings with antibodies against N-cadherin were performed to investigate potential changes in its spatial distribution upon strong synaptic activity. Furthermore, the distribution of PSD95 and neuroligin-1 was analyzed. Therefore, cortical neurons were transfected (DIV 9) with neuroligin-1-EGFP and experiments were done at DIV 12-14. Cultures were stimulated with high [K^+] (50 mM) for 5 min and immediately fixed with 4 % PFA. For control, cultures were kept in normal extracellular solution for 5 min and fixed. To check for reversibility, stimulated cultures were subsequently kept in normal extracellular solution for 30 min to enable recovery of distributed molecules. Then, immunocytochemical stainings were performed with antibodies against N-cadherin or PSD95. The distribution of neuroligin-1 was visualized via neuroligin-1-EGFP fluorescence. In a further experiment, the impact of PSD95 overexpression on neuroligin-1 distribution was analyzed. Therefore, PSD95-DsRed2 was cotransfected (DIV 9) with neuroligin-1-EGFP and cells were treated as described (DIV 12-14).

3.3.1.1 Effects of high [K^+]-treatment on the distribution of N-cadherin and PSD95

First, the distributions of N-cadherin and PSD95 were analyzed with immunocytochemistry. For quantification, z-stack images were deconvolved with AutoDeblur and further processed with the autothreshold function and the low-pass filter option in MetaMorph. Immunocytochemical stainings revealed an altered localization of N-cadherin upon strong synaptic activity. The size of N-cadherin puncta increased in K^+-stimulated cells and recovered to smaller sizes comparable to control cells (Fig. 3.21A, 2 upper panels). In contrast, the postsynaptic scaffolding molecule PSD95 showed no obvious changes upon stimulation (Fig. 3.21A, 2 lower panels). The mean N-cadherin puncta area significantly ($P< 0,05$) increased from 0,38 ± 0,07 μm^2 (n= 8 cells) in control to 0,97 ± 0,20 μm^2 (n= 8 cells) in stimulated cells. The N-cadherin puncta size recovered to 0,44 ± 0,07 μm^2 (n= 7 cells) (Fig. 3.21B). The size of PSD95 puncta did not change upon stimulation (control: 0,36 ± 0,06 μm^2, n= 6 cells; K^+-stimulated: 0,45 ± 0,08 μm^2, n= 10 cells; Recovery: 0,51 ± 0,14 μm^2, n= 8 cells; Fig. 3.21B). The percentage change in puncta area upon stimulation was significant ($P< 0,05$) larger for N-cadherin puncta (157,6 ± 52,4 %, n= 8 cells) compared to PSD95 puncta (26 ± 22,9 %, n= 10 cells; Fig. 3.21C).

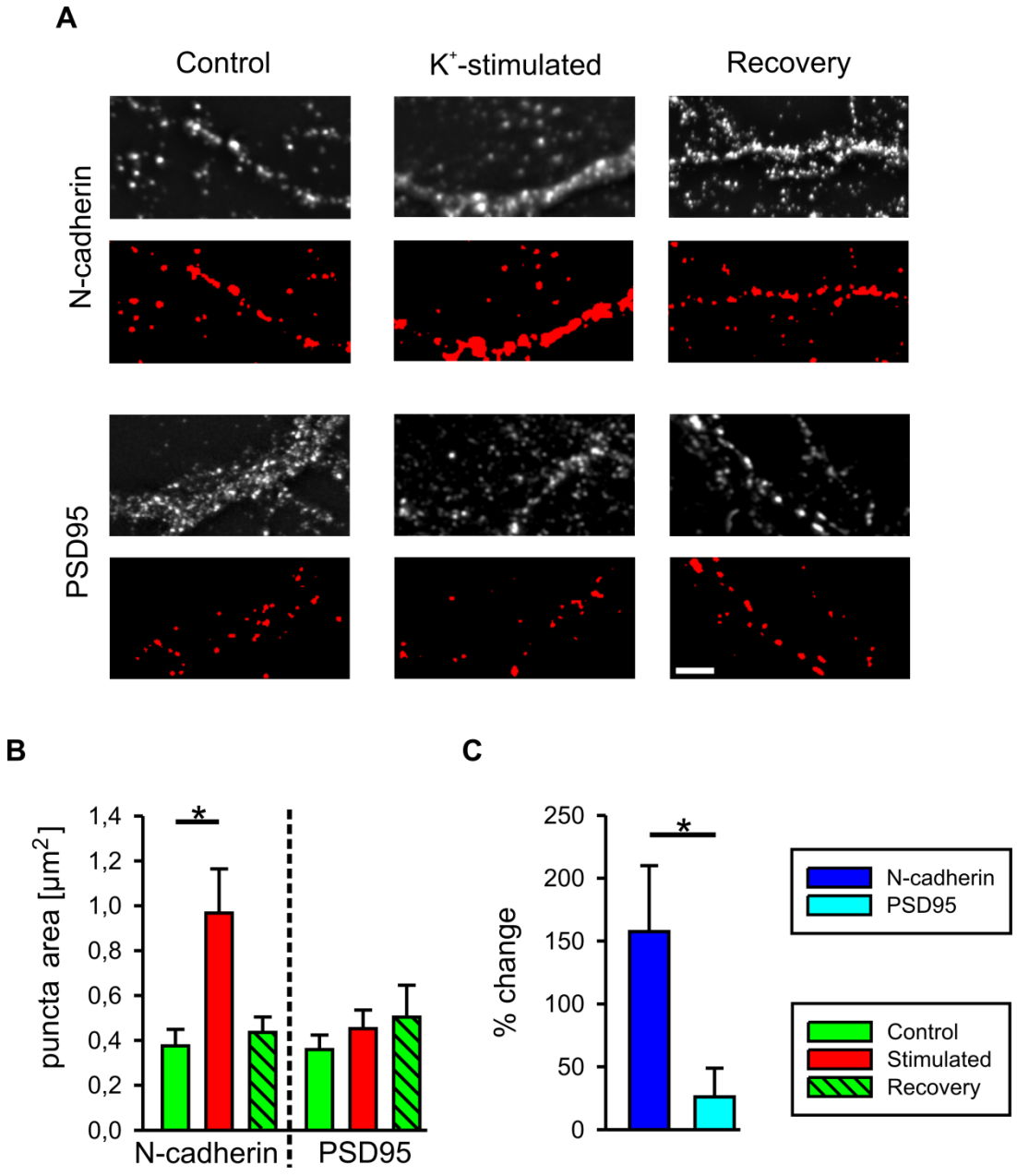

Figure 3.21 Spatial redistribution of N-cadherin upon intense vesicle release
(**A**) Example images of immunocytochemical stainings for N-cadherin (2 upper panels) and PSD95 (2 lower panels). Grey-scale images are shown in white and autothresholded images in red. Scale bar: 5 µm. (**B**) Mean area of N-cadherin and PSD95 puncta. (**C**) Comparison of percentage change of N-cadherin and PSD95 puncta area. N-cadherin (Control: n= 8; K^+-stimulated: n= 8; Recovery: n= 7). PSD95 (Control: n= 6; K^+-stimulated: n= 10; Recovery: n= 8). n represents number of cells. Error bars represent S.E.M. * P< 0,05 (Kruskal-Wallis One Way Analysis of Variance on Ranks with Dunn`s Post Hoc Test for B). * P< 0,05 (Student`s t-test for C).

Next, the experiments were repeated and SIM images were acquired in cooperation with Prof. Dr. Hermann Aberle (University of Düsseldorf) with kind assistance of Rebekka Ochs. Qualitatively, superresolution images revealed enlarged N-cadherin

puncta of oval shape in stimulated cultures (Fig. 3.22B) compared to round shaped puncta in control cultures (Fig. 3.22A). N-cadherin puncta of recovered cultures mainly appeared round (Fig. 3.22C upper images) with few oval shaped structures (Fig. 3.22C lower images).

In summary, these data demonstrated the redistribution of N-cadherin upon intense vesicle cycling. In contrast, the localization of postsynaptic PSD95 remained unaffected. SIM images further indicated structural changes of N-cadherin from round to rod-shaped cluster.

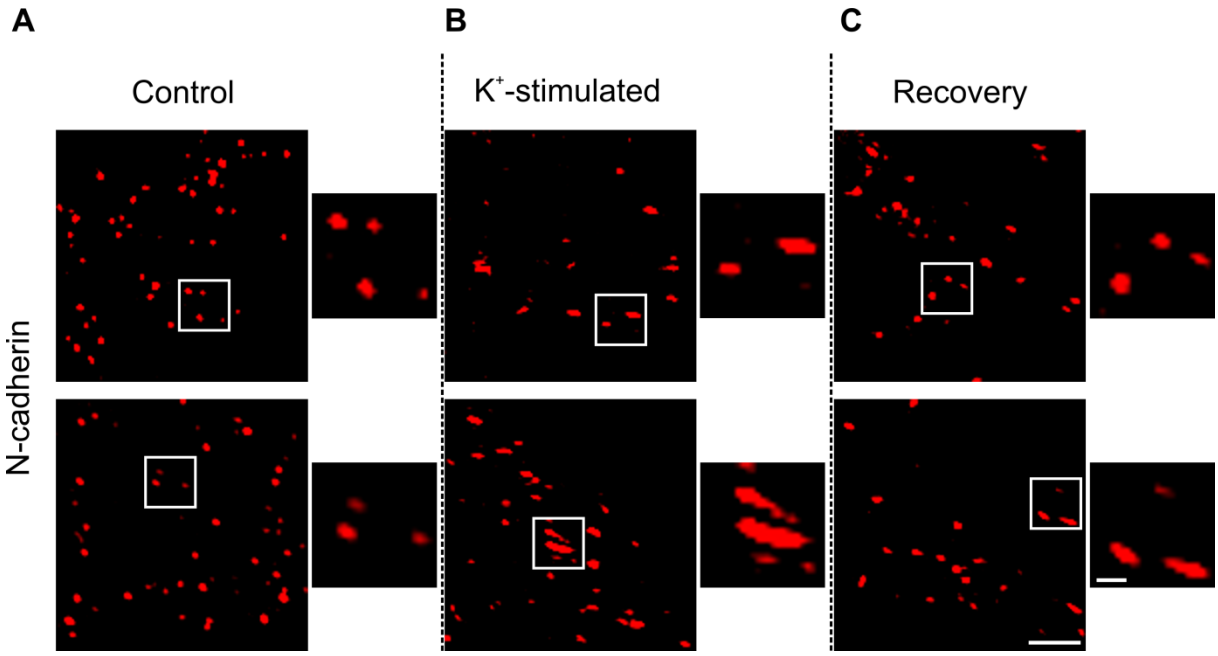

Figure 3.22 SIM imaging of N-cadherin upon strong synaptic stimulation
Example superresolution images of immunocytochemical stainings for N-cadherin. Two example images per condition are shown. Control (**A**), K^+-stimulated (**B**) and Recovery (**C**). Boxed areas are enlarged on the right. Scale bars: 1 µm (overview images), 200 nm (magnified images).

3.3.1.2 Redistribution of neuroligin-1 after strong synaptic stimulation

Previous experiments confirmed spatial changes of N-cadherin upon strong synaptic stimulation that was first described by Tanaka et al. in 2000. Furthermore, it was shown in this work that N-cadherin influences the clustering of neuroligin-1 (3.1.5.2). Therefore, the spatial localization of neuroligin-1 upon strong stimulation was examined. Neurons were transfected with neuroligin-1-EGFP (DIV 9) and expression

patterns were analyzed after stimulation and recovery by fluorescence imaging (Fig. 3.23).

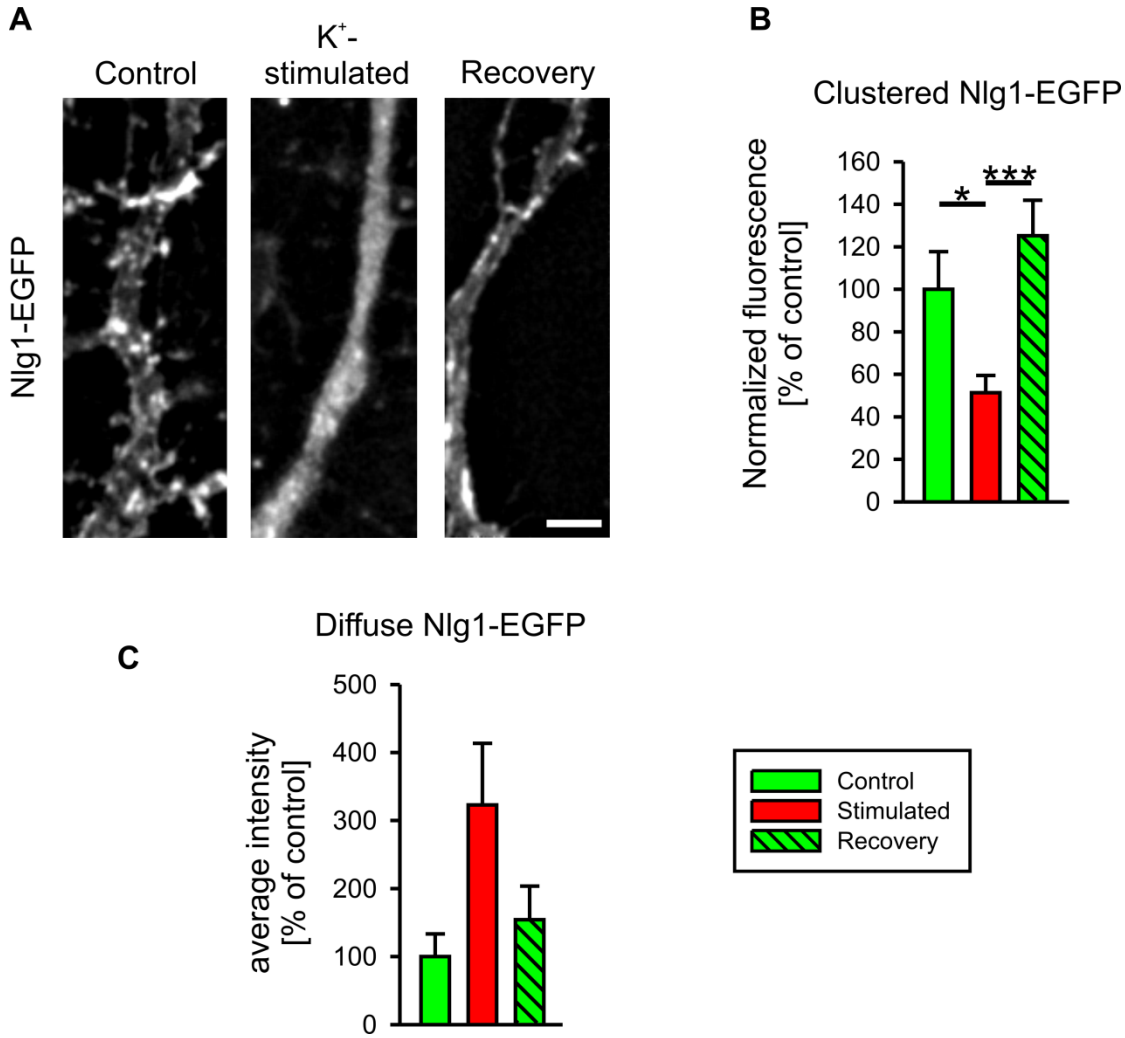

Figure 3.23 Spatial changes of neuroligin-1-EGFP localization upon strong synaptic activity
Localization of neuroligin-1-EGFP upon high [K^+]-treatment. (**A**) Example images of neuroligin-1-EGFP fluorescence in dendrites of control, K^+-stimulated and recovered neurons. Scale bar: 5 µm. (**B**) Quantification of clustered neuroligin-1-EGFP fluorescence. (**C**) Average intensity of diffuse neuroligin-1-EGFP fluorescence. Control: n= 17; K^+-stimulated: n= 23, Recovery: n= 18 (n represents number of cells). Error bars represent S.E.M. * P< 0,05 and *** P< 0,001 (One Way Anova with Holm-Sidak Post Hoc Test).

High [K^+]-treatment induced the dispersal of neuroligin-1-EGFP puncta in dendrites. In control conditions, neuroligin-1-EGFP was clustered in small puncta with some diffuse expression in the entire dendrite. Upon high [K^+]-stimulation, neuroligin-1-EGFP puncta disappeared and the signal was distributed all over the dendrite.

Neuroligin-1-EGFP reclustered after recovery (Fig. 3.23A). Spatial changes of neuroligin-1 localization were quantified by the ratio of clustered to diffusely distributed neuroligin-1-EGFP fluorescence to include differences in neuroligin-1-EGFP expression between individual neurons. High [K^+]-treatment significantly ($P< 0,05$) decreased clustering of neuroligin-1-EGFP from 100 ± 17,7 % (n= 17 cells) in control to 51,4 ± 8,1 % (n= 23 cells) in K^+-stimulated cells. Recovery after stimulation significantly ($P< 0,001$) increased neuroligin-1-EGFP clustering back to control level (125,2 ± 16,4 %, n = 18 cells; Fig. 3.23B). Simultaneously, the average intensity of diffuse neuroligin-1-EGFP fluorescence was increased upon synaptic stimulation and recovered back to control values (Control: 100 ± 33,2 %, n= 17 cells; K^+-stimulated: 322,9 ± 90,5 %, n= 23 cells; Recovery: 154,2 ± 49,2 %, n= 18 cells; Fig. 3.23C).
These data indicate a dispersal of neuroligin-1 along the dendrite upon strong synaptic activity comparable to N-cadherin.

3.3.1.3 Impact of PSD95 on neuroligin-1 distribution during high [K^+]-treatment

The previous approach was extended to study the impact of PSD95 on the localization of neuroligin-1. Therefore the experiment was repeated in neurons that coexpressed DsRed2-PSD95 and neuroligin-1-EGFP. High [K^+]-treatment showed no effect on the size of DsRed2-PSD95 puncta (Fig. 3.24A). The area of DsRed2-PSD95 puncta on dendrites was not significantly altered (Control: 0,40 ± 0,04 μm^2, n= 7 cells; K^+-stimulated: 0,57 ± 0,12 μm^2, n= 9 cells; Recovery: 0,44 ± 0,05 μm^2, n= 6 cells; Fig. 3.24B). However, overexpression of DsRed2-PSD95 reduced the dispersal of neuroligin-1-EGFP upon strong synaptic stimulation (Control: 100,0 ± 12,0 %, n= 9 cells; K^+-stimulated: 67,3 ± 10,1 %, n= 11 cells; Recovery: 98,4 ± 19,8 %, n= 7 cells; Fig. 3.24C). Also the high [K^+]-stimulation induced increase in diffuse neuroligin-1-EGFP fluorescence was reduced upon overexpression of DsRed2-PSD95 (Control: 100,0 ± 25,8 %, n= 9 cells; [K^+]-stimulated: 140,2 ± 41,9 %, n= 11 cells; Recovery: 96,7 ± 28,2 %, n= 7 cells; Fig. 3.24D).
In summary, these data indicate a stabilizing effect of PSD95 on neuroligin-1 clustering during strong synaptic stimulation.

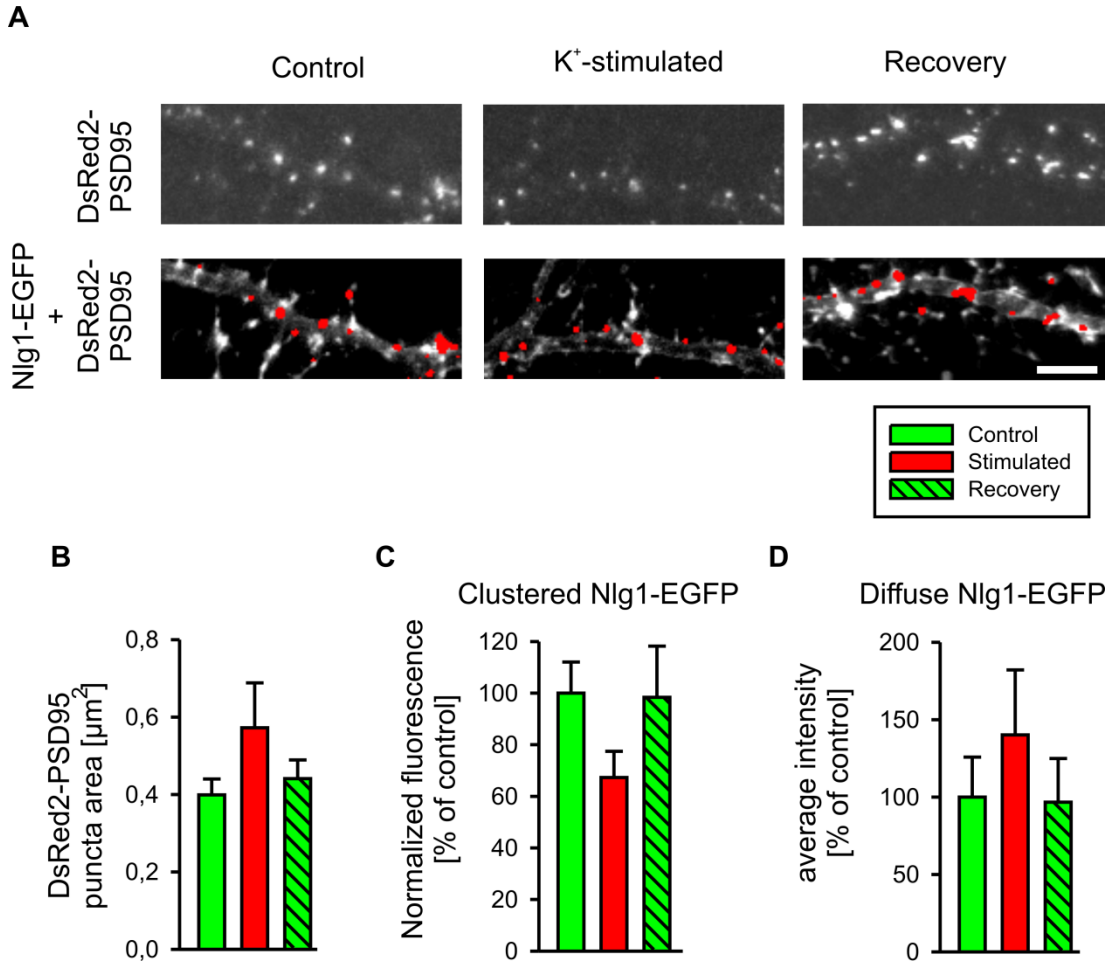

Figure 3.24 PSD95 overexpression stabilizes neuroligin-1 during strong synaptic activity
(**A**) Example images of DsRed2-PSD95 and neuroligin-1-EGFP fluorescence in dendrites of control, K^+-stimulated and recovered neurons. Upper panel: Grey-scale images of DsRed2-PSD95 fluorescence. Lower panel: Overlay of thresholded DsRed2-PSD95 signal (red) and Grey-scale neuroligin-1-EGFP fluorescence (white). Scale bar: 5 µm. (**B**) Quantification of DsRed2-PSD95 puncta area. Control: n= 7; K^+-stimulated: n= 9, Recovery: n= 6 (n represents number of cells). (**C**) Quantification of clustered neuroligin-1-EGFP fluorescence. (**D**) Average intensity of diffuse neuroligin-1-EGFP fluorescence. Control: n= 9; K^+-stimulated: n= 11, Recovery: n= 7 (n represents number of cells). Error bars represent S.E.M.

3.3.2 Superresolution microscopy analysis of pre- and postsynaptic molecules

The resolution of conventional fluorescence microscopy is limited by the diffraction limit. Hence, a detailed analysis of the spatial distribution of pre- and postsynaptic molecules is restricted. However, upcoming superresolution microscopy techniques

enable greatly improved analysis. In preliminary experiments, SIM was used to get a closer look at the spatial redistribution of synaptic molecules upon strong stimulation.

3.3.2.1 Limits of conventional fluorescence microscopy for analyzing synaptic structures

For a detailed analysis of structural changes, cultures were treated analogously to 3.3.1. Additionally, synaptic vesicle endocytosis was blocked by the presence of dynasore (80 µM) to inhibit vesicle endocytosis. Subsequently, cultures (DIV 10) were fixed and labeled with antibodies for the dendritic marker MAP2, the vesicle membrane associated molecule synaptobrevin2 (VAMP2) and N-cadherin. First, immunocytochemical stainings were studied with conventional deconvolution fluorescence microscopy (Axiovert 200M). In control cells, presynaptic VAMP2 and N-cadherin appeared as clear distinct puncta that were placed side by side or overlaid on dendrites (Fig. 3.25, left). High [K^+]-treatment induced intense release of presynaptic vesicles in the presence of dynasore that resulted in outspreading of VAMP2 puncta. In consequence, nearly the entire postsynaptic dendrite was covered. Similar to previous experiments, high [K^+]-treatment induced dispersion of N-cadherin that was observed as an increase in puncta size (Fig. 3.25, right). Although conventional fluorescence microscopy enabled the analysis of basic spatial redistribution of VAMP2 and N-cadherin, details about structural alignments of these molecules remain unclear. Therefore, SIM was used next to circumvent these technical limitations.

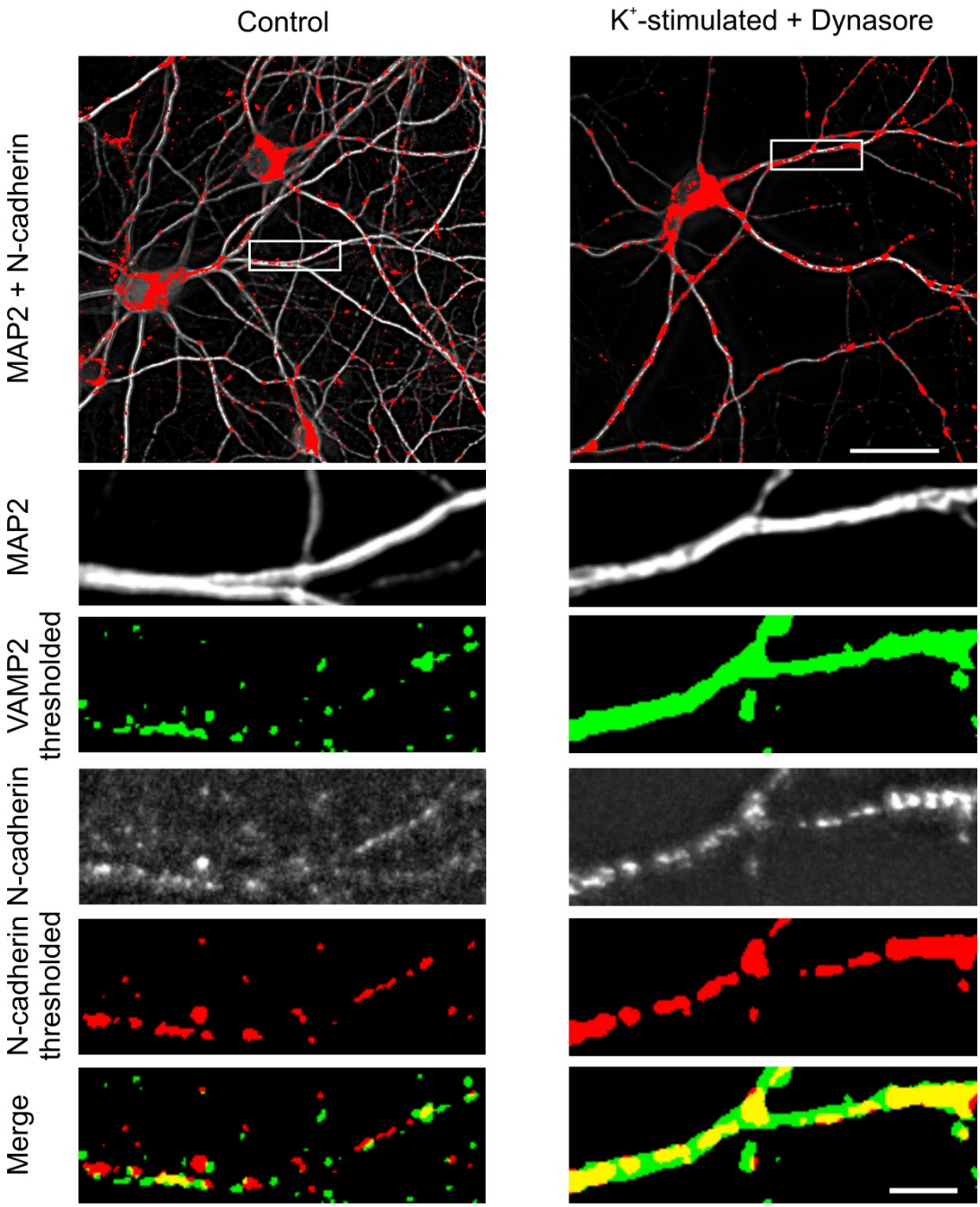

Figure 3.25 Redistribution of N-cadherin and VAMP2 upon intense vesicle exocytosis
Vesicle exocytosis was induced by high [K^+]-treatment and endocytosis was blocked with dynasore. Immunocytochemical stainings were performed with antibodies against synaptobrevin2 (VAMP2), MAP2 and N-cadherin. High [K^+]-treatment induced spreading of VAMP2 and N-cadherin. MAP2 was used as a dendritic marker. Scale bars: 30 µm (large images) and 5 µm (small images).

3.3.2.2 Superresolution examination of pre- and postsynaptic molecules with SIM

Cortical neurons (DIV 10) were immunolabeled with antibodies against VAMP2, N-cadherin and PSD95 and superresolution images were acquired on a SIM setup (Zeiss Elyra PS). After processing, images were scanned for structures with all three pre- and postsynaptic molecules within one focal plane (Fig. 3.26).

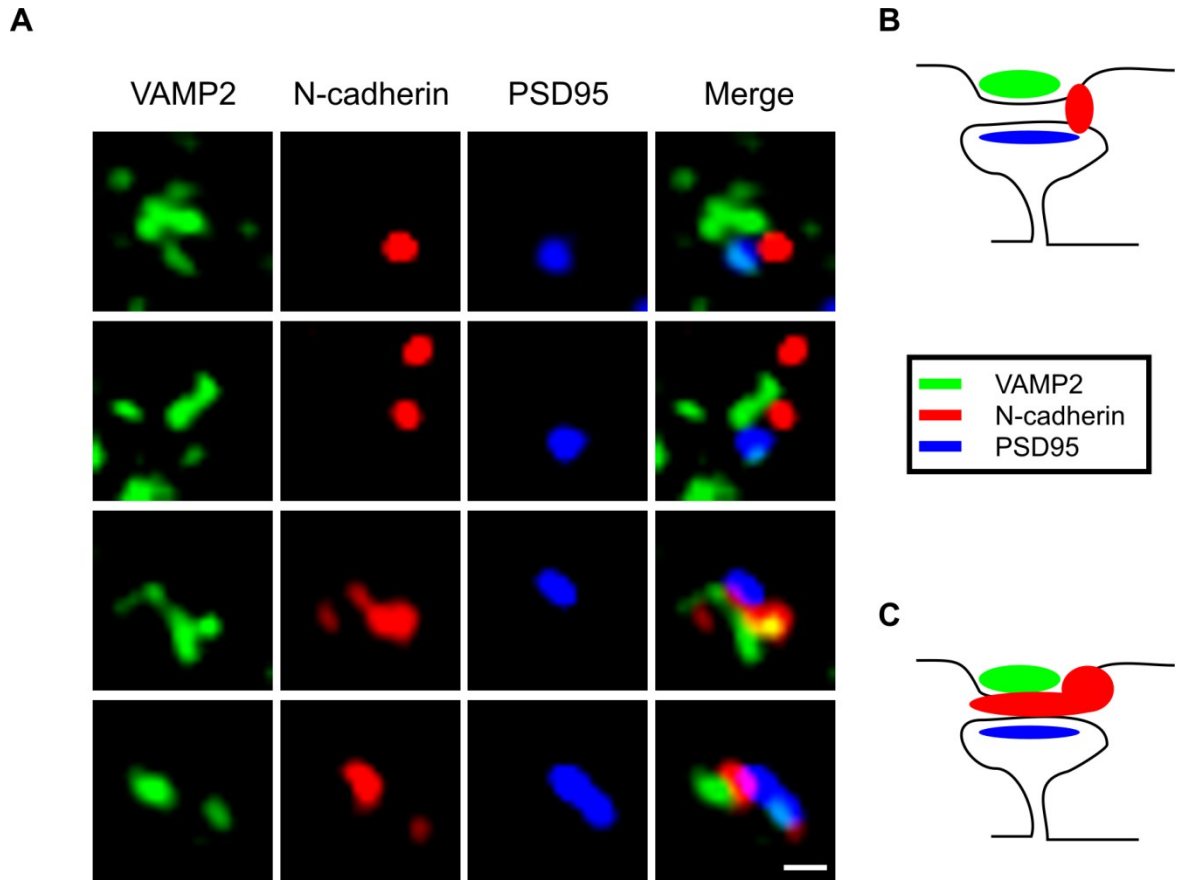

Figure 3.26 Spatial organisation of synaptic molecules revealed by SIM
Alignment of pre- and postsynaptic molecules within synaptic contacts. (**A**) Example SIM images of three-part synaptic structures of VAMP2 (presynaptic, green), N-cadherin (pre- and postsynaptic, red) and PSD95 (postsynaptic, blue). Scale bar: 100 nm. (**B**) Schematic drawing of protein organisation within synapses. (**C**) Schematic drawing of N-cadherin localization between VAMP2 and PSD95 within the synaptic cleft.

These synapses composed of VAMP2, N-cadherin and PSD95 were organized in a side by side manner (Fig. 3.26A, upper two panels and drawing B). N-cadherin was generally not located all over the active zone underneath the VAMP2 signal. Rather it was flanking one side of the active zone. In some cases, N-cadherin was also found

within the synaptic cleft and separated the presynaptic VAMP2 from the postsynaptic PSD95 signal (Fig. 3.26A, lower two panels and drawing C).
Compared to conventional fluorescence microscopy, SIM enables more precise examination of spatial alignments of pre- and postsynaptic molecules. Triple-stainings revealed a large variety of different arrangements of synaptic molecules. In general, N-cadherin was located perisynaptic beside VAMP2 and PSD95. Exceptional, N-cadherin was located within the synaptic cleft between VAMP2 and PSD95 areas.

3.3.2.3 Superresolution observation of synaptic molecules after strong stimulation and simultaneous blocking of vesicular endocytosis

Next, structural changes of synaptic molecules upon strong stimulation were examined with SIM. Similar to 3.3.2.1, neurons were stimulated for 5 min with 50 mM K^+ in the presence of dynasore (80 µM) and immediately fixed and immunolabeled for VAMP2, PSD95 and N-cadherin. In non-stimulated control cells, synapses showed the typical alignment of VAMP2, N-cadherin and PSD95 as described in 3.3.2.2 (Fig. 3.27B and drawing A). Qualitatively, high [K^+]-stimulation induced spreading of distinct VAMP2 cluster to a more diffuse distribution. Similarly, N-cadherin puncta also spread out and merged with each other to larger oval structures (Fig. 3.27C and drawing A). In contrast, postsynaptic PSD95 showed no obvious changes upon stimulation.
In summary, these first superresolution data qualitatively confirmed the observation that N-cadherin redistributes upon strong synaptic stimulation. Furthermore, SIM images gave additional information about the spatial changes. They demonstrated that N-cadherin spread out upon strong synaptic activity and merged with surrounded cluster to form large accumulations. VAMP2 stainings also showed a dispersion of vesicle cluster upon stimulation and concurrent blocking of compensatory endocytosis. This could readily be explained by the dissolution of vesicle membrane associated VAMP2 molecules when vesicles fuse with the presynaptic membrane by exocytosis. In addition, PSD95 stainings confirmed previous data done with

conventional fluorescence microscopy. In this case, high [K^+]-stimulation did not obviously change spatial localization or puncta size.

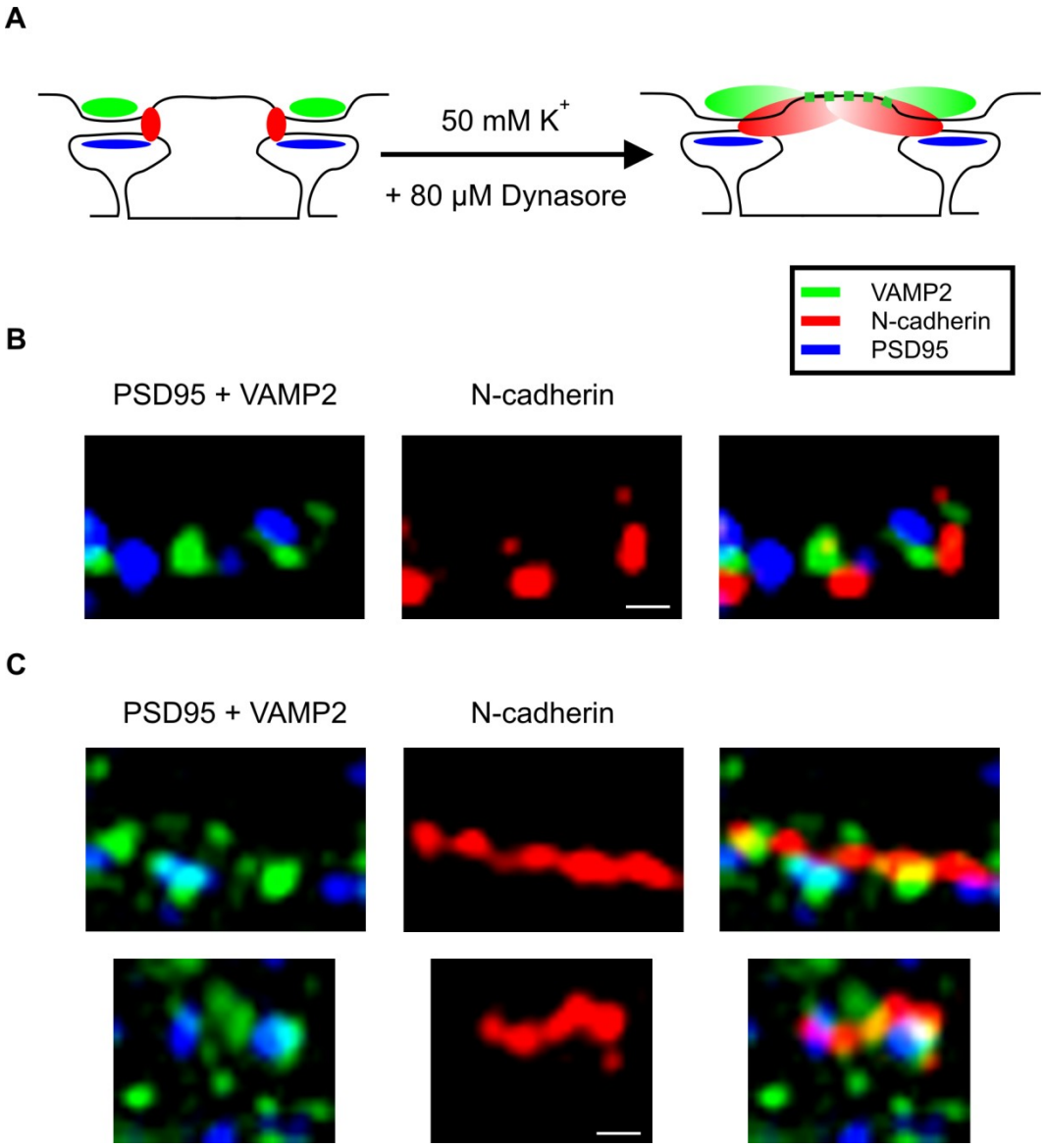

Figure 3.27 Spatial changes of synaptic molecules upon strong stimulation and blocked endocytosis
(**A**) Schematic drawing of spatial organisation of synaptic molecules and changes upon strong activity and block of vesicle endocytosis. (**B**) Example SIM images of non-stimulated control synapses. (**C**) Example images upon high [K^+]-treatment in the presence of dynasore. Scale bars: 100 nm.

3.4 Human iPS cell derived neurons as a model system for Alzheimer`s disease

Alzheimer`s disease (AD) is characterized by the formation of oligomers of amyloid-β (Aβ) peptides. The recent establishment of neurons derived from human induced pluripotent stem cells (hiPSC derived neurons) enables direct examination of pathological effects of Aβ on human synapses, in addition to analysis in animal models systems.

3.4.1 The effect of Aβ on synaptic function

The following experiments were performed as part of a study that established a highly reproducible AD model based on hiPSC derived neurons. Neurons were obtained by in vitro differentiation of human iPS cells including an innovative immunopanning step to achieve a higher density of immature human neurons compared to other methods. To examine the toxic effects of Aβ on human synapses, presynaptic vesicle cluster of hiPSC derived neurons were labeled with the activity-dependent dye FM4-64. Extracellular application of Aβ was performed by incubation of neuronal cell cultures with an Aβ containing conditioned medium from the CHO cell line 7PA2 (7PA2-CM) that expresses mutant human APP. To exclude potential toxic effects of other components, 7PA2-CM was immunodepleted with antibodies against Aβ. For this study, Aβ treated hiPSC derived neurons were provided by Dr. Katja Nieweg (University of Marburg). Fluorescence microscopy was performed 8 days after Aβ incubation.

3.4.1.1 Potential effects of 7PA2-CM incubation on the viability of hiPS cell derived neurons

To examine effects of Aβ on synaptic contacts, cultured cortical neurons derived from human iPS cells were incubated for 8 days with 7PA2-CM. To check the general toxicity of Aβ, the density of cells and neuronal processes after incubation with 7PA2-CM was determined. Therefore, neurons were stained with the membrane-permeable

fluorescence dye calcein-AM by extracellular application (dilution 1/2000) at the end of each experiment.

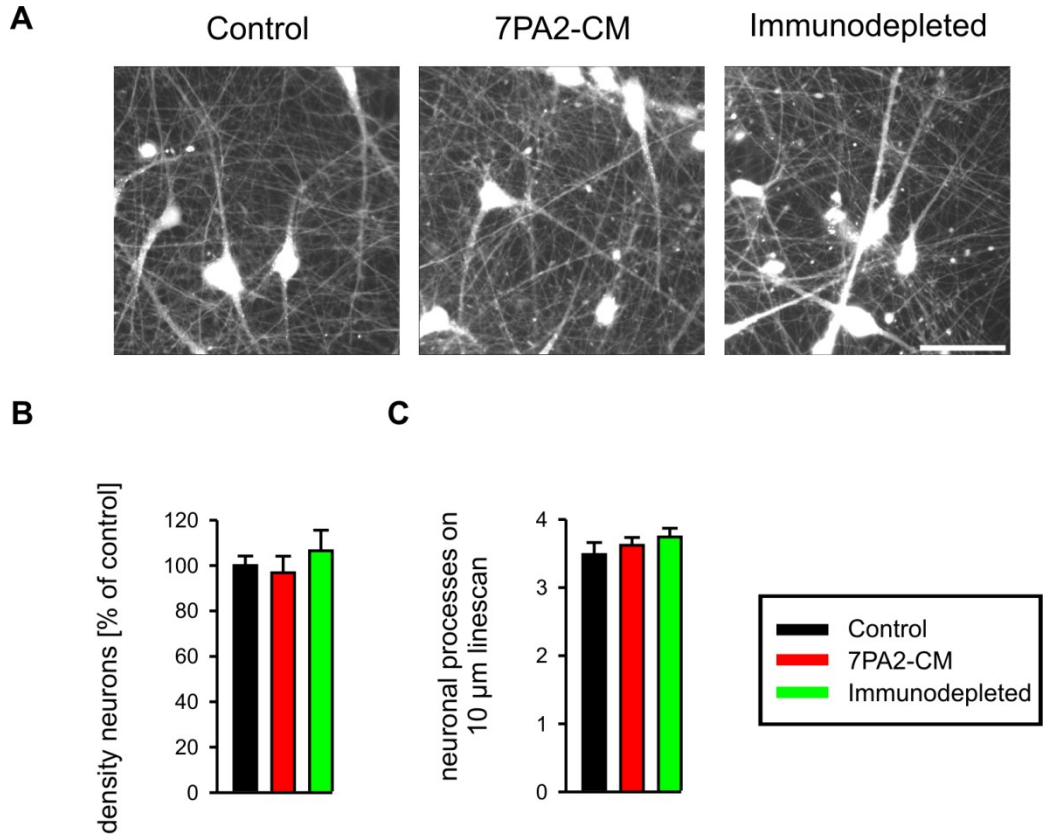

Figure 3.28 Cell viability of hiPSC derived neurons upon incubation with 7PA2 conditioned medium
Incubation of neuronal cultures derived from iPS cells with 7PA2-CM for 8 days showed no effect on cell viability or number of processes. (**A**) Example fluorescence images of neuronal cultures labelled with calcein-AM. Scale bar: 50 µm. (**B**) Quantification of neuron density by counting calcein-AM labelled cell bodies. (**C**) Quantification of neuronal processes crossing a linescan. Control: n= 10; 7PA2-CM: n= 10; Immunodepleted: n= 8 (n indicates number of cultures). Error bars represent S.E.M.

8 days incubation with Aβ had no effect on the cell density or on the number of neuronal processes. Also the incubation with Aβ immunodepleted medium showed no effect on cell viability (Fig. 3.28A). The normalized density of cell bodies was not altered (Control: 100,0 ± 4,2 %, n= 10 cultures; 7PA2-CM: 96,8 ± 7,4 %, n= 10 cultures; Immunodepleted: 106,5 ± 9,1 %, n= 8 cultures; Fig. 3.28B). Also the quantification of neuronal processes by determining the number of neurites that cross randomly chosen lines within the fluorescence image showed no differences between the experimental groups (Control: 3,48 ± 0,18/10 µm, n= 10 cultures; 7PA2-CM: 3,62

± 0,12/10 µm, n= 10 cultures; Immunodepleted: 3,74 ± 0,13/10 µm, n= 8 cultures; Fig. 3.28C).

These observations showed that incubation with 7PA2-CM for 8 days did not affect cell viability of the neuronal culture. Hence, the incubation of hiPSC derived neurons with 7PA2-CM enables the study of functional defects induced by Aβ on human synapses in a physiological model system.

3.4.1.2 Effects of Aβ peptides on synaptic vesicle cluster

Next, the role of Aβ on the functionality of presynaptic vesicle cluster was examined. Cycling vesicles were labeled with the activity-dependent dye FM4-64 by electrical stimulation with 400 stimuli at 20 Hz as previously described. Actively cycling vesicle cluster got visible as distinct puncta using fluorescence microscopy. 8 days incubation with 7PA2-CM decreased the overall FM4-64 puncta density compared to control and immunodepleted cultures (Fig. 3.29A). To determine the total amount of FM4-64 labeled vesicles, the density of FM puncta of each staining was multiplied with the average integrated intensity (area x pixel intensity) per punctum. Quantification revealed a significant ($P< 0,01$) reduction of the normalized overall FM4-64 signal in cultures that were treated with 7PA2-CM (56,9 ± 7,6 % of control, n= 10 experiments) compared to control (100,0 ± 9,9 %, n= 10 experiments). Cultures that were incubated with Aβ immunodepleted medium were not affected as compared to control (92,2 ± 8,0 % of control, n= 9 experiments), and overall FM4-64 staining was significantly ($P< 0,05$) increased in comparison with 7PA2-CM treatment (Fig. 3.29B). Plotting FM4-64 puncta density versus integrated intensity revealed that the Aβ induced effect on the overall FM4-64 puncta staining was largely due to a reduced density of cycling vesicle cluster (Fig. 3.29C). In addition, effects of 7PA2-CM on vesicular exocytosis were examined by FM destaining experiments. Therefore, FM4-64 stained cultures were stimulated with 1200 stimuli at 20 Hz in the absence of dye. A second longer stimulation (2000 stimuli at 20 Hz) was used to determine the background level after complete FM4-64 destaining. Extracellular application of Aβ had no effect on destaining kinetics (Fig. 3.29D).

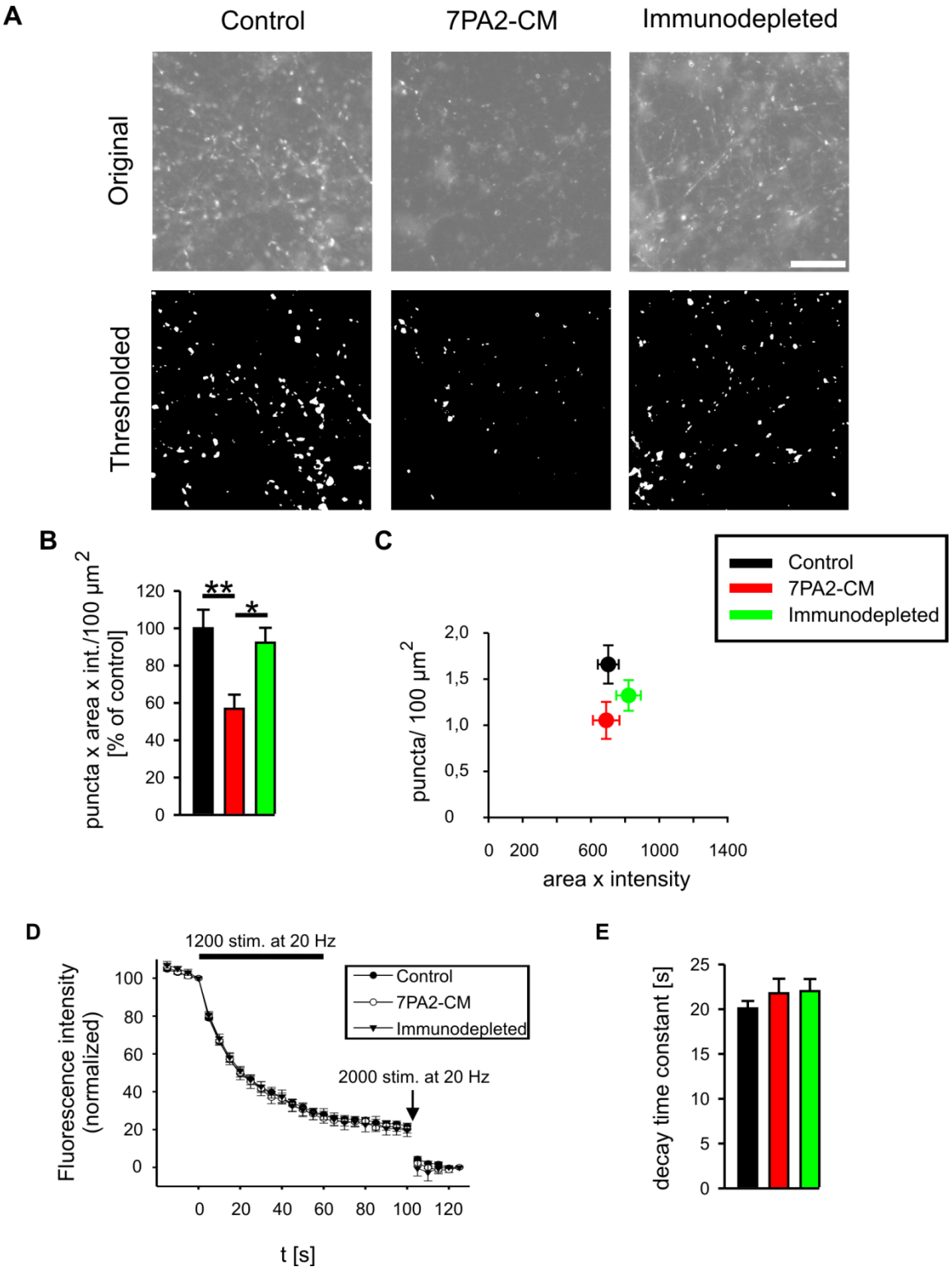

Figure 3.29 Incubation with 7PA2 conditioned medium impaired cycling vesicle cluster in neurons derived from hiPSCs

(**A**) Grey-scale (upper panel) and thresholded (lower panel) images of FM4-64 labeled vesicle cluster. Scale bar: 20 µm. (**B**) Quantification of total FM4-64 fluorescence. (**C**) Puncta density versus integrated intensity of thresholded FM4-64 puncta. (**D**) Mean normalized fluorescence decay caused by stimulation-induced vesicle exocytosis. (**E**)

Quantification of decay time constants of destaining curves. Control: n= 10; 7PA2-CM: n= 10; Immunodepleted: n= 9 (n indicates number of experiments). Error bars represent S.E.M. * P< 0,05 and ** P< 0,01 (One Way Anova with Holm-Sidak Post Hoc Test).

The decay time constant was not significantly altered (Control: 20,1 ± 0,8 s, n= 10 experiments; 7PA2-CM: 21,8 ± 1,6 s, n= 10 experiments; Immunodepleted: 22,0 ± 1,4 s, n= 9 experiments; Fig. 3.29E).

In summary, these experiments demonstrated a strong reduction of actively cycling vesicle cluster in neurites (axons and dendrites) of hiPSC derived neurons by short-term (8 days) incubation with Aβ peptides.

3.4.1.3 Effects of Aβ peptides on presynaptic vesicle cycling

Next, the impact of Aβ on bona fide synapses was studied. Therefore, FM4-64 stainings were analyzed for presynaptic vesicle cluster that contacted postsynaptic dendrites. Dendrites were visualized by calcein-AM staining. Incubation for 8 days with 7PA2-CM did not change the density of presynaptic FM4-64 puncta on proximal dendrites (Fig. 3.30A). Quantification of the normalized total amount of presynaptic FM4-64 fluorescence revealed no significant changes (Control: 100,0 ± 12,7 %, n= 32 cells; 7PA2-CM: 89,2 ± 11,1 %, n= 37 cells; Immunodepleted: 107,7 ± 18,9 %, n= 32 cells; Fig. 3.30B). Neither a change in presynaptic FM4-64 puncta density, nor a clear reduction of the integrated intensity was found (Fig. 3.30C). Also FM4-64 destaining experiments revealed no significant alterations of vesicular exocytosis in presynaptic vesicle cluster (Fig. 3.30D+E). Quantification of the mean decay time constant revealed no effects of Aβ on synaptic exocytosis (Control: 25,9 ± 2,0 s, n= 32 cells; 7PA2-CM: 28,2 ± 2,5 s, n= 37 cells; Immunodepleted: 29,9 ± 2,9 s, n= 32 cells; Fig. 3.30F).

Summing up, analysis of bona fide synapses revealed no significant change in the functionality of presynaptic vesicle cluster upon short-term incubation with Aβ.

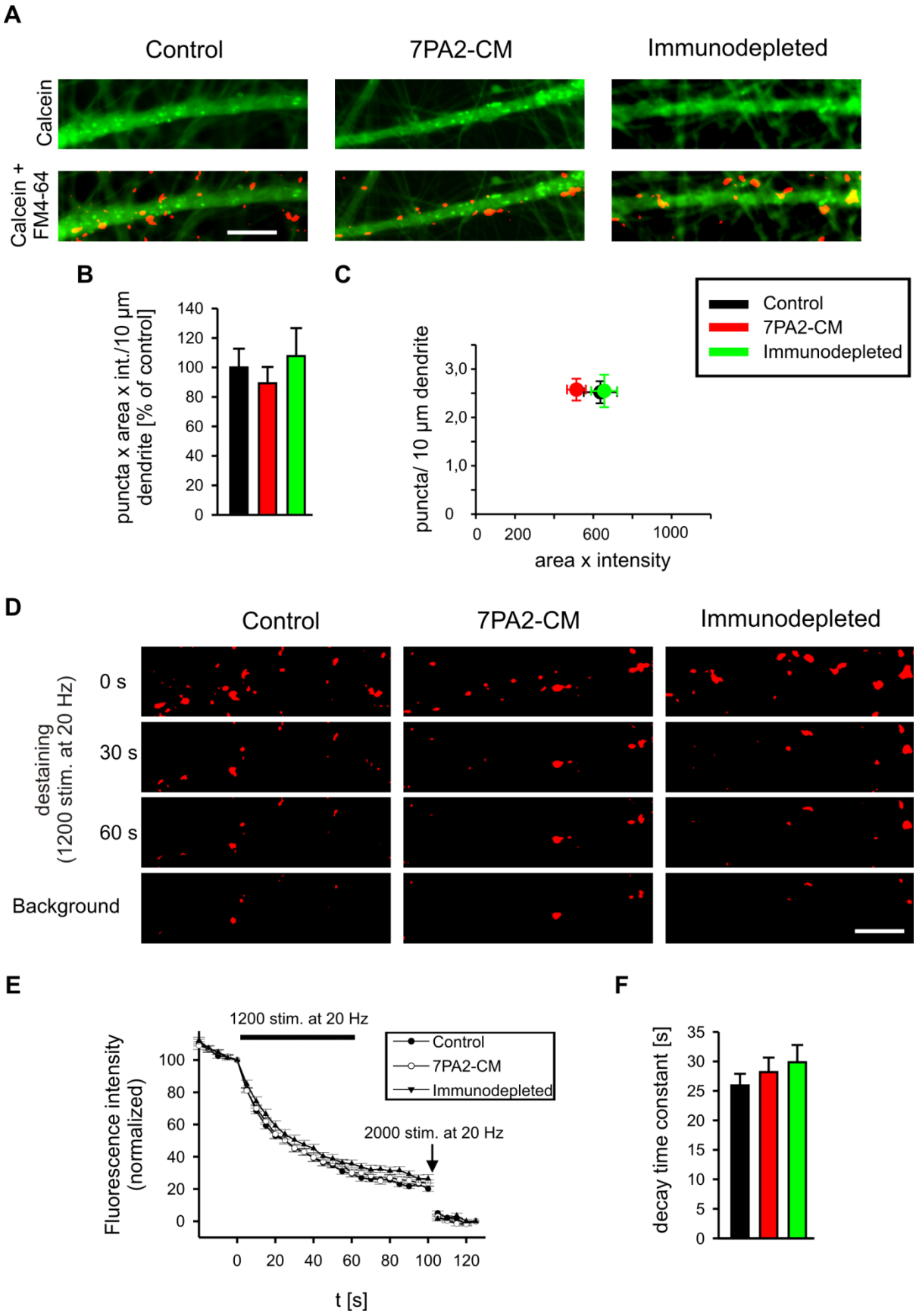
A
Control
7PA2-CM
Immunodepleted
Calcein
Calcein + FM4-64
B
puncta x area x int./10 µm dendrite [% of control]
140
120
100
80
60
40
20
0
C
Control
7PA2-CM
Immunodepleted
puncta/ 10 µm dendrite
3,0
2,0
1,0
0
0
200
600
1000
area x intensity
D
Control
7PA2-CM
Immunodepleted
destaining (1200 stim. at 20 Hz)
0 s
30 s
60 s
Background
E
1200 stim. at 20 Hz
Control
7PA2-CM
Immunodepleted
2000 stim. at 20 Hz
Fluorescence intensity (normalized)
100
80
60
40
20
0
0
20
40
60
80
100
120
t [s]
F
decay time constant [s]
35
30
25
20
15
10
5
0

Figure 3.30 Absence of effects of Aβ on presynaptic function in hiPSC derived cortical neurons
(**A**) Example fluorescence images of calcein-AM stained proximal dendrites and thresholded presynaptic FM4-64 puncta. (**B**) Quantification of total FM4-64 fluorescence signal on proximal dendrites. (**C**) Presynaptic FM4-64 puncta density versus integrated intensity of FM4-64 puncta on proximal dendrites. (**D**) Example images of thresholded FM4-64 puncta during destaining. Loss in FM4-64 fluorescence gets visible by disappearance of FM puncta that undercut the threshold. (**E**) Mean fluorescence decay of stimulation-induced vesicle destaining of FM4-64 puncta on proximal dendrites. (**F**) Quantification of decay time constants. Control: n= 32; 7PA2-CM: n= 37; Immunodepleted: n= 32 (n indicates number of cells). Error bars represent S.E.M.

4 Discussion

Previous studies showed a functional cooperation of N-cadherin and neuroligin-1 in presynaptic vesicle accumulation at nascent synapses in immature neurons (Stan et al., 2010; Aiga et al., 2011). The aim of this work was to examine the role of the cell adhesion molecules N-cadherin and neuroligin-1 in vesicle cycling in more mature neurons. Therefore, mainly activity-dependent imaging methods like FM4-64 staining/destaining and SypHy imaging were used to measure synaptic vesicle exo- and endocytosis. Additionally, immunocytochemical stainings were performed to characterize structural properties of pre- and postsynaptic structures.

4.1 Role of N-cadherin and neuroligin-1 in presynaptic vesicle cycling

For a basic examination of the role of N-cadherin and neuroligin-1 in vesicular exo- and endocytosis in mature neurons, FM4-64 stainings and destainings were performed in a “gain-of-function”-approach in cortical neurons overexpressing N-cadherin-EGFP or neuroligin-1-EGFP. Control cells were transfected with EGFP. Immunocytochemical stainings were done to verify synaptogenic effects of N-cadherin and neuroligin-1 in initial experiments in immature neurons (DIV 7) to test the functionality of the used plasmids. Immunocytochemical stainings for VAMP2 revealed an enhanced presynaptic vesicle clustering by postsynaptic expression of N-cadherin-EGFP or neuroligin-1-EGFP in immature neurons (Fig. 3.1). These observations confirm previous studies that showed a crucial role of N-cadherin and neuroligin-1 in synaptogenic vesicle clustering in immature neurons (Scheiffele et al., 2000; Togashi et al., 2002; Bozdagi et al., 2004; Graf et al., 2006; Stan et al., 2010; Aiga et al., 2011). Next, vesicle cluster were labeled with FM4-64 in immature neurons. In contrast to VAMP2 immunostainings that mark all synaptobrevin-2 molecules, FM4-64 is taken up exclusively by cycling vesicles via endocytosis. Thus, FM4-64 stainings give additional information about the functionality of the presynaptic vesicle cluster. Postsynaptic expression of N-cadherin and neuroligin-1 strongly increased the density of active vesicle cluster (Fig. 3.2). This demonstrates that the postsynaptic expression of N-cadherin-EGFP and neuroligin-1-EGFP induced the

formation of functional vesicle cluster on the presynaptic site. Thus, these observations indicated the proper expression and functionality of the used plasmids in dissociated neurons and enable their application in further experimental approaches. To examine the influence of N-cadherin and neuroligin-1 on the functionality of mature presynaptic vesicle cluster, experiments were done in more mature neurons to minimize synaptogenic effects of these cell adhesion molecules (as seen in Fig. 3.1). Therefore, the first experiments were repeated in neurons after extended cultivation (DIV 15). VAMP2 immunostainings were performed in N-cadherin and neuroligin-1 overexpressing neurons and compared with EGFP expressing controls. The postsynaptic expression of N-cadherin or neuroligin-1 had no effect on the density or the area of VAMP2 puncta. This showed that neither N-cadherin nor neuroligin-1 induced synaptogenesis in this more mature culture system. The lack of synaptogenesis induced by N-cadherin confirms previous observations in ES cell-derived N-cadherin knockout neurons (Jüngling et al., 2006) or in conditional N-cadherin knockout cells (Kadowaki et al., 2007). In these studies, immunostainings for the presynaptic vesicle associated molecule synapsin I revealed no obvious alteration in synapse formation in the absence of N-cadherin. In contrast, the role of neuroligin-1 in mature neurons is not well characterized. An important role of neuroligin-1 in initial synapse formation has been repeatedly described (Scheiffele et al., 2000; Fu et al., 2003; Sara et al., 2005; Banovic et al., 2010), but its role in mature neurons remained unclear. In line with a previous study (Wittenmayer et al., 2009) the above described results indicate no synaptogenic effect of neuroligin-1 in mature neurons. Next, vesicle cluster were labelled with FM4-64 in mature, primary dissociated cortical neurons (DIV 14). Postsynaptic expression of N-cadherin as well as of neuroligin-1 strongly enhanced the density of FM4-64 puncta (Fig. 3.4). In contrast to immature neurons, this increase in active vesicle cluster could not be explained with synaptogenic effects of these cell adhesion molecules. Rather, it indicated a “cycling” effect of N-cadherin and neuroligin-1 in mature neurons, i.e. the postsynaptic expression of these cell adhesion molecules enhanced presynaptic vesicle function. These data confirm previous studies that examined FM stainings in a N-cadherin function blocking approach (Togashi et al., 2002) or in ES cell-derived N-cadherin deficient neurons (Jüngling et al., 2006). Also the expression of a mutant

N-cadherin construct lacking the extracellular domains strongly decreased FM4-64 uptake (Bozdagi et al., 2004; Vitureira et al., 2011). Conversely, expression of wild-type N-cadherin did not affect FM uptake in one study (Vitureira et al., 2011). One explanation could be a potential lower endogenous expression of p120-catenin as compared to the cell culture system used in this work. In that context, a recent study indicated the requirement of p120-catenin coexpression for proper function of expressed N-cadherin (Flannery and Brusés, 2012). Furthermore, the analysis of integrated fluorescence intensities in Vitureira et al. did not exclude potential effects of N-cadherin on the density of active vesicle cluster as described in this work. Comparison of the VAMP2 puncta density with the FM4-64 puncta density (Fig. 3.4 vs. Fig 3.3) showed a significant portion of non-cycling vesicle cluster in control cells (~ 52% non-cycling vesicle cluster) that got “activated” by N-cadherin (~ 23% non-cycling vesicle cluster) or neuroligin-1 expression (no non-cycling vesicle cluster). This idea of functional activation is supported by a previous study, in which overexpression of neuroligin-1-EGFP in immature neurons (DIV 5) increased FM4-64 uptake to levels of mature neurons (DIV 14; Wittenmayer et al., 2009). Cycling effects were confirmed by a more physiological approach, where FM4-64 uptake was induced by electrical stimulation (Fig. 3.5). Similar to high [K^+]-induced FM4-64 stainings, the cycling effect of N-cadherin and neuroligin-1 was also present upon electrical stimulation.

FM stainings result in basic information about the functionality of presynaptic vesicle cluster. However, they do not distinguish vesicular exo- and endocytosis. Thus a differential analysis of vesicle exo- and endocytosis with FM stainings is problematic. Hence, FM4-64 destaining experiments were performed for the selective analysis of vesicular exocytosis (Fig. 3.6). A second electrical stimulation in the absence of extracellular FM dye induced exocytosis of FM-labeled vesicles and caused the loss of fluorescence. The decrease of puncta fluorescence correlates with the amount of vesicular exocytosis (Hoopmann et al., 2012). Surprisingly, postsynaptic expression of N-cadherin or neuroligin-1 showed no enhanced vesicle exocytosis in FM4-64 destaining experiments (Fig. 3.7). Destaining curves of N-cadherin or neuroligin-1 overexpressing neurons overlapped with EGFP expressing controls. Accordingly, percentage destaining at the end of the electrical stimulation was unaltered (Fig.

3.7A,B). Previous studies showed controversial results with regard to the role of N-cadherin in vesicle exocytosis. Whereas FM experiments in N-cadherin knockout neurons indicated a role of N-cadherin in vesicle exocytosis (Jüngling et al., 2006), overexpression of a dominant-negative N-cadherin mutant showed no exocytotic effect revealed by FM destaining experiments (Vitureira et al., 2011). Electrophysiological experiments showed an important influence of neuroligin-1 on presynaptic release probability (Futai et al., 2007). Contrary, FM destainings demonstrated an exocytotic effect of neuroligin-1 in immature (DIV5) but not in mature (DIV 13) neurons (Wittenmayer et al., 2009). In this work, control experiments were performed for a better evaluation of the significance of these results and for a better comparison with previous observations. Stepwise changes of the extracellular Ca^{2+}-concentration indicated a limited sensitivity of FM destaining experiments in detecting increases in vesicular exocytosis, especially at high release probabilities (Fig. 3.7C,D). In control neurons destaining at 2 mM Ca^{2+} was already close to the maximum at 5 mM Ca^{2+}. This indicated that FM4-64 destaining experiments were unable to resolve further increases of vesicular exocytosis at high release probabilities, that would be expected by overexpression of N-cadherin and neuroligin-1.

4.2 Inhibition of synaptic vesicle cycling in the absence of N-cadherin

To circumvent the limited sensitivity of FM4-64 destaining experiments at high release probabilities, vesicle exocytosis was examined in N-cadherin knockout neurons. Postsynaptic expression of N-cadherin was knocked out by expression of CreEGFP in neurons from homozygous floxed N-cadherin mice (Kostetskii et al., 2005). Immunocytochemistry verified the knockout of N-cadherin protein 7 days after transfection with CreEGFP (Fig. 3.8B,C) whereas short-term expression of CreEGFP for 2 days had no effect on N-cadherin protein level (Fig. 3.8A; Pielarski et al., 2013). Although knockout of N-cadherin showed no effect on FM4-64 puncta density (Fig. 3.9C) it significantly decreased FM4-64 puncta area (Fig. 3.9D). The lack of effect in FM4-64 puncta density could be explained with the low number of experiments (Control: n= 4 cells; N-cadherin knockout: n= 6 cells) and the high standard error.

However, quantification of the FM4-64 puncta area (Fig. 3.9D) confirmed a vesicle cycling defect in the absence of N-cadherin as previously found (Jüngling et al., 2006) or upon overexpression of a dominant-negative mutant N-cadherin (Bozdagi et al., 2004; Vitureira et al., 2011). Destaining experiments also demonstrated an important role of N-cadherin in synaptic vesicle exocytosis. Exocytosis was significantly reduced in N-cadherin knockout neurons (Fig. 3.9F,G). This observation confirms previous findings in N-cadherin deficient neurons (Jüngling et al., 2006). In contrast, FM destaining experiments of a more recent study found no exocytotic effects of the overexpression of a dominat-negative mutant of N-cadherin (Vitureira et al., 2011). A possible explanation is the relatively weak stimulation (2 Hz) in that study compared to this work (20 Hz) or to the study by Jüngling et al. (30 Hz). Probably, interfering with N-cadherin adhesion does not affect vesicle exocytosis at low activity levels, but proper N-cadherin signaling becomes more important during high synaptic activity.

4.3 Cooperation of N-cadherin and neuroligin-1 in the transsynaptic regulation of presynaptic vesicle cycling

Previous studies showed a functional cooperation of N-cadherin and neuroligin-1 in the modulation of presynaptic vesicle clustering at nascent synapses (Stan et al., 2010; Aiga et al., 2011). However, the role of this cooperation on the presynaptic function in mature neurons still needs to be clarified. For this, FM4-64 experiments were performed to test whether the vesicle cycling effect of neuroligin-1 depends on the presence of N-cadherin. Neuroligin-1 was expressed in the presence of N-cadherin (comparable to Fig. 3.5) and in N-cadherin knockout neurons (by coexpression of CreEGFP) in cortical neurons from homozygous floxed N-cadherin mice. A functional cooperation of both cell adhesion molecules would result in a diminished effect size of neuroligin-1-induced vesicle cycling in the absence of N-cadherin. Indeed, postsynaptic knockout of N-cadherin strongly decreased the density of active vesicle cluster in neuroligin-1 expressing neurons (Fig. 3.10A,B). Accordingly, the effect size of neuroligin-1 expression on presynaptic vesicle cycling significantly decreased in the absence of N-cadherin (Fig. 3.10C). These data

strongly indicate a functional cooperation of neuroligin-1 and N-cadherin in the induction of presynaptic vesicle cycling in mature neurons. Furthermore, it shows the importance of N-cadherin and neuroligin-1 also for the maintenance of proper synaptic function in mature neurons. In an additional approach, the role of N-cadherin in the localization of neuroligin-1 was examined. Therefore, neuroligin-1-EGFP fluorescence in synapses and on dendrites was quantified in control cells expressing N-cadherin and in N-cadherin knockout neurons. Changes of neuroligin-1-EGFP expression patterns in N-cadherin knockout neurons would indicate an effect of N-cadherin on the clustering of neuroligin-1 protein. My data indicated a strong correlation between the presence of N-cadherin and the synaptic localization of neuroligin-1. The knockout of N-cadherin diminished the clustering of neuroligin-1 revealed by a significant decrease of neuroligin-1-EGFP puncta density, area and intensity (Fig. 3.11A-D). Simultaneously, the localization of dendritic, non-clustered neuroligin-1 was inhibited in the absence of N-cadherin (Fig. 3.11E). These results indicate a significant role of N-cadherin for synaptic localization of neuroligin-1, hence confirming a functional cooperation of these cell adhesion molecules.

In summary, these results show a cooperation of N-cadherin and neuroligin-1 in the transsynaptic induction of the cycling of presynaptic vesicle cluster. Furthermore, they show the importance of N-cadherin for the proper synaptic localization of neuroligin-1. Based on these findings, it can be proposed that the disturbed clustering of neuroligin-1 in the absence of N-cadherin causes the lack of the vesicle cycling effect of neuroligin-1 in N-cadherin knockout neurons.

4.4 SypHy-based examination of vesicle exo- and endocytosis

FM4-64 experiments indicated a functional role of N-cadherin and neuroligin-1 in the regulation of presynaptic vesicle cycling. However, because FM experiments are affected by several steps of the vesicle cycle, they are not well suited for the differential analysis of vesicular exo- and endocytosis. In contrast, SypHy imaging is an activity-dependent method able to differentiate between vesicle exo- and endocytosis (Fig. 3.12A). The stimulation-induced increase of SypHy fluorescence signal correlates with the amount of vesicle exocytosis. The H^+-ATPase inhibitor

bafilomycin A1 can be used to prevent slight impreciseness by concurrent requenching (through fast vesicle endocytosis) during the rise time of SypHy fluorescence (Fig. 3.14D). The post-stimulus decline of SypHy fluorescence correlates with the speed of vesicle endocytosis and reacidification. Because reacidification is fast compared to endocytosis, the decline of SypHy signal shows endocytosis close to real time (Atluri and Ryan, 2006; Granseth et al., 2006). In this work, SypHy experiments were performed in autaptic glial microisland cultures. Autapses have been shown to exist in vivo and are not only present in in vitro cultures (Bekkers, 2003). This elaborated culture system enabled the simultaneous analysis of several presynaptic SypHy puncta within one field of view because axon growth was limited by the astrocyte. Furthermore, it enabled the simultaneous expression of the homophilic cell adhesion molecule N-cadherin on the pre- and postsynaptic site. To create autaptic cultures, 10-20 neurons were seeded on astrocyte microislands (Fig. 2.1A,B) and individual neurons were transfected using the Magnetofection^{TM} technique. Because SypHy fluorescence is quenched in the resting state, DsRed2 was cotransfected as a marker for transfected cells. For analysis, the NH_4Cl-induced maximal SypHy signal was thresholded and merged with the corresponding DsRed2 signal to separate autapses from other axonal contacts (Fig. 3.12B-D). Electrical stimulation induced a fast increase of SypHy fluorescence signal in autaptic boutons (exocytosis) and was followed by a slower decline in fluorescence (endocytosis; Fig. 3.13A). For analysis at the level of individual cells, SypHy fluorescence intensities over time from individual puncta (Fig. 3.13 B) were averaged to get a mean SypHy signal for each cell (Fig. 3.13C). The combined application of the optical probe SypHy and the autaptic glial microisland culture system turned out as an optimal system for the separate analysis of vesicle exo- and endocytosis. In particular, it enabled simultaneous expression of the homophilic cell adhesion molecule N-cadherin on the pre- and postsynaptic site. Furthermore, the simultaneous analysis of several autapses within one experiment minimized variability and improved the exactness of kinetic measurements. Control experiments confirmed SypHy as a specific probe to measure synaptic exo- and endocytosis. Both, the chemical suppression of endocytosis with dynasore as well as the blocking of vesicle reacidification with bafilomycin A1 revealed a strong inhibition of the SypHy

fluorescence decline (Fig. 3.14). These results confirm the post-stimulation decline of SypHy fluorescence as a specific indicator of vesicle endocytosis. The suitability of SypHy to measure vesicle exocytosis was confirmed in control experiments with stepwise variation of the extracellular Ca^{2+}-concentration ($[Ca^{2+}]_{ex}$; Fig. 3.15). Because it is known that vesicle exocytosis strongly depends on Ca^{2+} influx (Heidelberger et al., 1994), increasing $[Ca^{2+}]_{ex}$ should result in SypHy experiments in stepwise increases in fluorescence intensity. Indeed, SypHy experiments revealed increased vesicular exocytosis in high $[Ca^{2+}]_{ex}$, confirming the suitability of SypHy to measure vesicle exocytosis (Fig. 3.15 A,B). The decay of SypHy fluorescence was not significantly influenced by $[Ca^{2+}]_{ex}$ levels. In contrast to exocytosis, the role of Ca^{2+} in synaptic endocytosis is controversial and unclear. On the one hand, it has been shown that Ca^{2+} is important for the basic formation of the clathrin coat during clathrin-mediated endocytosis (Gad et al., 1998). On the other hand, alterations of the intracellular Ca^{2+}-concentration ($[Ca^{2+}]_i$) with buffers had no effect on vesicular endocytosis supporting the idea that residual Ca^{2+}-levels after stimulation are sufficient to enable vesicle endocytosis (Ryan et al., 1996). In contrast, synapto-pHluorin experiments revealed a tight regulation of vesicle endocytosis by $[Ca^{2+}]_{ex}$ (Sankaranarayanan and Ryan, 2001). Probably, differences in the stimulation pattern revealed an effect of $[Ca^{2+}]_{ex}$ on vesicle endocytosis. It may be hypothesized, that the stimulation-induced increase of $[Ca^{2+}]_i$ was not saturating because of the weaker stimulation in that work (300 stimuli at 10 Hz). Conversely, it might be possible that the stronger stimulation used in my experiments (400 stimuli at 20 Hz) already saturated the $[Ca^{2+}]_i$ at relatively low $[Ca^{2+}]_{ex}$. In that case, $[Ca^{2+}]_i$ would be independent from $[Ca^{2+}]_{ex}$ and thus reveal no effect of Ca^{2+} on synaptic endocytosis.

In summary, the comparison of Ca^{2+}-experiments revealed a higher sensitivity of the SypHy imaging method (Fig. 3.15A,B) compared to FM4-64 destainings (Fig. 3.15D,E) in detecting changes of vesicular exocytosis. SypHy imaging revealed a higher sensitivity especially at high release probabilities (induced by high $[Ca^{2+}]_{ex}$). In contrast, FM4-64 destaining experiments revealed changes only at relatively low release probabilities (induced by 0,5 mM $[Ca^{2+}]_{ex}$). This finding also helps to explain the lack of exocytotic effects upon overexpression of N-cadherin and neuroligin-1 in FM destaining experiments (Fig. 3.7A,B), because expression of these cell adhesion

molecules is expected to increase presynaptic vesicle cycling. Hence, although N-cadherin and neuroligin-1 expression affects vesicular exocytosis as revealed in SypHy experiments (Fig. 3.16 + Fig. 3.20), the enhancement cannot be resolved with FM4-64. In contrast, reducing presynaptic vesicle cycling (by N-cadherin knockout) revealed an exocytotic effect of N-cadherin using FM4-64 destaining (Fig. 3.9). The higher sensitivity of SypHy imaging (compared to FM4-64 destaining experiments) at high release probabilities makes it particularly interesting to study vesicle cycling in "gain-of-function"-experiments, that were carried out in this work by overexpression of N-cadherin or neuroligin-1.

4.5 The specific roles of N-cadherin and neuroligin-1 in synaptic vesicle exo- and endocytosis

SypHy experiments in N-cadherin and neuroligin-1 expressing neurons revealed important roles of these cell adhesion molecules in presynaptic vesicle cycling. N-cadherin as well as neuroligin-1 enhanced synaptic vesicle exocytosis (Fig. 3.16A,B). An additional SypHy experiment upon block of vesicle endocytosis with bafilomycin A1 was performed for an isolated analysis of vesicle exocytosis. This experimental approach confirmed the enhancement of presynaptic vesicle exocytosis by N-cadherin and neuroligin-1 expression (Fig. 3.20). Accordingly, the more sensitive SypHy imaging method revealed exocytotic effects of these cell adhesion molecules that were not visible in FM destainings. Furthermore, quantification of the SypHy signal decay indicated the induction of vesicular endocytosis exclusively by N-cadherin (Fig. 3.16A,C). Vesicle cycling effects of N-cadherin or neuroligin-1 have not been described in pHluorin-based experimental approaches yet. Accordingly, the observations in this work enable a more detailed view about the roles of N-cadherin and neuroligin-1 in presynaptic vesicle cycling. These data confirm an exocytotic effect of N-cadherin that was previously described with FM destaining experiments (Jüngling et al., 2006). Furthermore, these findings confirmed the exocytotic defect that was described above in N-cadherin knockout neurons (Fig. 3.9). The enhancement of vesicle exocytosis by neuroligin-1 was in line with FM destaining experiments in immature neurons at DIV 5 (Wittenmayer et al., 2009) and extended

the observed exocytotic effect to more mature neurons. In addition, a specific block of the transsynaptic interaction between neuroligin-1 and β-neurexin (Fig. 3.17) confirmed the previously described retrograde modulation of presynaptic release by postsynaptic neuroligin-1 and verifies β-neurexin as a presynaptic mediator (Futai et al., 2007). The observed effect of N-cadherin on synaptic endocytosis strengthened previous studies that measured synaptic vesicle cycling with FM dyes (Bozdagi et al., 2004; Vitureira et al., 2011). Since FM stainings can only indirectly measure vesicle endocytosis, the SypHy data in this work directly show a major role of N-cadherin in synaptic vesicle endocytosis. Furthermore, the induction of vesicle endocytosis by N-cadherin was analyzed in terms of synaptic activity. Therefore, the endocytotic defect in N-cadherin knockout neurons was examined depending on the strength of preceding vesicle exocytosis. In a first experimental approach, vesicle exocytosis was induced in different $[Ca^{2+}]_{ex}$ with 200 to 800 stimuli (20 Hz) to get variation in vesicle exocytosis. Subsequently, vesicle cluster were grouped due to their synaptic activity (exocytosis) into weakly and strongly active puncta. Quantification of the effect of N-cadherin knockout revealed a stronger interference with compensatory vesicle endocytosis in highly active synapses as compared to less active vesicle cluster (Fig 3.18A,C,D). This indicated an important role of N-cadherin in the compensation of strong vesicle exocytosis by subsequent endocytosis. In a second, more elaborated experimental approach, the defect of compensatory endocytosis at high activity was examined individually for single vesicle cluster. Therefore, double-stimulation experiments were performed for the direct observation of endocytotic defects in highly active synapses, that were initially intact and showed normal endocytosis upon weak stimulation. Quantification of vesicle endocytosis revealed an activity-dependent effect of N-cadherin on vesicle endocytosis (Fig. 3.19). Double-stimulation experiments clearly showed a disrupted compensatory vesicle endocytosis in N-cadherin knockout neurons that was detectable upon strong stimulation (800 stimuli at 20 Hz), but was absent in the same synapses upon weak stimulation (200 stimuli at 20 Hz). Hence, a direct correlation between the endocytotic effect of N-cadherin and the activity level of the vesicle cluster was evident and this indicated an important function of N-cadherin adhesion for the coupling of vesicular exo- and endocytosis. This essential role of N-cadherin in the

maintenance of proper synaptic function in strongly active synapses has not been described before. Moreover, it particularly links the observation of a Ca^{2+}-dependent coupling of exo- and endocytosis (Hosoi et al., 2009) with the Ca^{2+}-dependent adhesion of N-cadherin.

4.6 Spatial relocalization of synaptic components upon strong synaptic activity

Based on the above described activity-dependent effect of N-cadherin on the coupling of vesicular exo- and endocytosis, further experiments were performed to examine structural changes of synaptic molecules upon intense vesicle exocytosis. Previous studies have shown a surface dispersion of N-cadherin upon strong synaptic stimulation followed by relocalization to synaptic sites during recovery (Tanaka et al., 2000; Yam et al., 2013). A similar experimental approach was performed to examine structural changes of N-cadherin, PSD95 and neuroligin-1 upon high $[K^+]$-treatment. Immunocytochemical stainings revealed a dispersion of N-cadherin upon intense synaptic exocytosis that was reversible 30 min after stimulation (Fig. 3.21A,B). Simultaneously, the spatial distribution of postsynaptic PSD95 was not altered upon stimulation. These data confirm the spreading of N-cadherin as well as the stable localization of postsynaptic PSD95 upon strong synaptic activity that was described by Tanaka et al. in 2000. Qualitatively, superresolution SIM images revealed the structural redistribution of N-cadherin from mainly round to oval shaped structures upon high $[K^+]$-treatment that recovered back to mainly round-shaped puncta (Fig. 3.22). In a next step, the experimental approach was adapted to analyze the distribution of neuroligin-1 upon intense synaptic activity. As it was shown that N-cadherin induces the clustering of neuroligin-1 (Fig. 3.11), a concurrent spatial redistribution (upon intense exocytosis) of neuroligin-1 together with N-cadherin seemed likely. Indeed, fluorescence microscopy of neuroligin-1-EGFP expression revealed the dispersion of neuroligin-1 from cluster to a more diffuse pattern upon intense synaptic activity that was not described before (Fig. 3.23). In line with these data, neuroligin-1 was described to be lost from synaptic sites upon neuronal activity (Peixoto et al., 2012). In this study, the authors described

the activity-dependent cleavage of neuroligin-1 upon long-term treatment with high [K^+] for 2 hours. The cleavage of neuroligin-1 in turn destabilizes β-neurexin which leads to a reduction of presynaptic release probability. Probably, the dispersion of neuroligin-1 along the dendrite upon short-term stimulation that was found in this work represents a pre-stage that might ultimately result into cleavage of neuroligin-1 upon prolonged stimulation. The coexpression of neuroligin-1-EGFP and DsRed2-PSD95 resulted in a stabilizing effect of PSD95 on the clustering of neuroligin-1 upon intense synaptic activity (Fig. 3.24), hence indicating a postsynaptic interaction of neuroligin-1 to be responsible for its delocalization upon stimulation. Next, SIM imaging was performed to get high resolution information about the distribution of synaptic molecules upon strong stimulation. Therefore cortical cultures (DIV10) were treated analogously to 3.3.1. Additionally, vesicle endocytosis was blocked with dynasore for a complete disruption of presynaptic coupling of vesicle exo- and endocytosis. Immunocytochemical stainings for MAP2, N-cadherin and VAMP2 were first checked with conventional deconvolution microscopy (Axiovert 200M). Fluorescence images qualitatively confirmed the dispersion of N-cadherin that was previously described. Additionally, immunocytochemical stainings for VAMP2 showed the inclusion of vesicle membrane within the presynaptic plasma membrane upon intense vesicle exocytosis leading to outspreading of VAMP2 fluorescence signal to non-synaptic areas (Fig. 3.25). Next, stainings were analyzed with SIM to circumvent technical limitations of conventional microscopy. Immunocytochemical stainings with antibodies against VAMP2, N-cadherin and PSD95 enabled a more detailed analysis of spatial organization of these molecules and of structural changes upon high [K^+]-treatment. Triple-stainings in non-stimulated control cells revealed a large variety of different formations of these pre- and postsynaptic molecules (Fig. 3.26). These findings are in line with a recent study showing a large spectrum of N-cadherin localization patterns with other synaptic molecules (Yam et al., 2013). Here, the authors generally found two different patterns of N-cadherin localization (perisynaptic puncta and synaptic cleft). The authors described a higher amount of rod-shaped N-cadherin in non-stimulated cells that was only rarely visible in this study. Intriguingly, it was shown that the distribution of different N-cadherin structures strongly depended on the maturity of the culture, indicating decreased amounts of rod-shaped

(synaptic cleft) N-cadherin in more mature neurons. Hence, slight variations in the maturation level of different cultures might result in significant changes of the spatial distribution of N-cadherin. Next, spatial changes of N-cadherin, VAMP2 and PSD95 upon high [K^+]-treatment and blocking of synaptic endocytosis were examined with SIM (Fig. 3.27). Non-stimulated control cells showed the typical alignment that was discussed above. Upon K^+-stimulation, presynaptic VAMP2 cluster spread out and showed a more diffuse distribution. This could be explained by the inclusion of vesicle membrane into the plasma membrane during exocytosis. The inhibition of endocytosis with dynasore on its part prohibited compensatory retrieval of presynaptic membrane thus amplifying the observed effect. These data support the activity-induced dispersion of the vesicle membrane associated molecule synaptophysin that was previously observed with conventional fluorescence microscopy (Tanaka et al., 2000). Furthermore, they confirm the dispersion and outspreading of synaptophysin and vGlut1 that was recently shown with SIM (Yam et al., 2013). Stimulation-induced dispersion of VAMP2 was accompanied by a spatial redistribution of N-cadherin. Round N-cadherin puncta spread out and neighboring cluster merged with each other and formed larger oval structures. These findings confirm the observation that N-cadherin moves away from the synaptic cleft upon the inclusion of new membrane lacking N-cadherin upon massive vesicle exocytosis (Yam et al., 2013). Accordingly, postsynaptic PSD95 showed no obvious changes upon stimulation, most likely due to the fact that the postsynaptic site was unaffected from vesicle membrane inclusion that occurred presynaptically.

4.7 Model of homeostatic coupling of synaptic exo- and endocytosis by N-cadherin

The above described results clearly demonstrate a functional cooperation of N-cadherin and neuroligin-1. FM4-64 experiments showed basic vesicle cycling inducing effects of N-cadherin and neuroligin-1 (Fig. 3.4 + Fig. 3.5). Additionally, FM4-64 destaining experiments in N-cadherin knockout neurons showed an influence of N-cadherin on exocytosis (Fig. 3.9). Furthermore, the examination of the cycling effect of neuroligin-1 in the absence of N-cadherin revealed a cooperation of

these cell adhesion molecules to control presynaptic vesicle cycling (Fig. 3.10). These observations confirm previous studies that showed this type of cooperation to be essential for presynaptic vesicle clustering in immature neurons (Stan et al., 2010; Aiga et al., 2011). Using FM stainings, this work demonstrated that the same interaction between N-cadherin and neuroligin-1 that was shown to affect synaptogenesis in immature neurons also controls the functionality of presynaptic vesicles in more mature neurons. Alteration of neuroligin-1 clustering at synaptic sites in the absence of N-cadherin further supports the idea of a functional cooperation of these cell adhesion molecules (Fig. 3.11). SypHy imaging experiments examined the above described cycling effects of N-cadherin and neuroligin-1 in more detail and revealed exocytotic effects of neuroligin-1 and N-cadherin expression and an endocytotic effect exclusively for N-cadherin expression (Fig. 3.16 + Fig. 3.20). Furthermore, SypHy experiments using function-blocking β-neurexin-Fcs (Fig. 3.17) confirmed electrophysiological data suggesting a crucial role of neuroligin-1/β-neurexin adhesion in the enhancement of presynaptic release probability (Futai et al., 2007). Additional SypHy imaging experiments in N-cadherin knockout neurons revealed that the endocytotic effect of N-cadherin depends on the activity level of the synapse. Proper N-cadherin adhesion is important for compensatory vesicle endocytosis; especially in highly active synapses (Fig. 3.18 + Fig. 3.19) indicating a crucial role of N-cadherin in the coupling of presynaptic vesicle exo- and endocytosis.

Potential effects of high synaptic activity levels on the spatial localization of synaptic molecules were examined by immunocytochemistry. Intense vesicle exocytosis (induced by high [K^+]-treatment for 5 min) appeared to be accompanied by uncoupling of vesicle exo- and endocytosis. In an additional experimental approach, blocking of endocytosis with dynasore further inhibited the exo-/ endocytotic coupling. Immunocytochemical stainings confirmed the dispersion of N-cadherin upon intense vesicle exocytosis (Fig. 3.21; see also Tanaka et al., 2000). Interestingly, fluorescence microscopy for neuroligin-1-EGFP indicated the same dispersion of clustered neuroligin-1 to a more diffuse distribution along the dendrite upon high [K^+]-treatment (Fig. 3.23). Together these data revealed the simultaneous dispersion of N-cadherin and neuroligin-1 in highly active synapses (with insufficient endocytotic

compensation). Finally, superresolution microscopy confirmed the delocalization of N-cadherin caused by massive inclusion of vesicle membrane into the presynaptic plasma membrane (Fig. 3.27; see also Yam et al. 2013).

In summary, the above described results support a model that suggests a control of the coupling of vesicle exo- and endocytosis by N-cadherin and neuroligin-1 that is particularly important during high synaptic activity (Fig. 4.1). The coupling of presynaptic vesicle exo- and endocytosis is crucial for the maintenance of synaptic activity (Haucke et al., 2011). Exocytosis of synaptic vesicles is accompanied by the inclusion of vesicle membrane within the presynaptic membrane and would lead to drastic morphological changes by swelling of the presynaptic terminal in case of altered compensatory endocytosis. Furthermore, intense vesicle exocytosis would bail out the limited number of release-competent vesicles. Consequences of altered compensatory endocytosis have been repeatedly observed, e.g. by the accumulation of endocytotic intermediates in dynamin I knockout mice (Ferguson et al., 2007) or by the strong phenotype observed in Drosophila shibire mutants (Koenig and Ikeda, 1989). The idea of exo- endocytotic coupling is supported by several studies that indicated molecules of the exocytotic machinery like VAMP2 or Synaptotagmin-1 to be also important to control vesicle endocytosis (Deák et al., 2004; Nicholson-Tomishima and Ryan, 2004; Poskanzer et al., 2003). The observation of a Ca^{2+}-dependent process that enables coupling of exo- and endocytosis further supports a direct link of Ca^{2+}-triggered exocytosis with compensatory endocytosis (Hosoi et al., 2009). Most of these studies investigated the role of presynaptic molecules of the CAZ in exo- endocytotic coupling most likely because of its direct involvement in vesicle turnover. Additionally, the observed effects of N-cadherin and neuroligin-1 on vesicle cycling in this work as well as in previous studies indicate a crucial role of these CAMs in the coupling of vesicle exo- and endocytosis. Thus, the following mechanism identifies N-cadherin and neuroligin-1 as mediators of presynaptic coupling to enable the maintenance of prolonged synaptic activity. At the resting state, N-cadherin and neuroligin-1 are arranged at and near the active zone of the synapse. The homophilic N-cadherin system is located at the pre- and postsynaptic site at the perisynaptic edge of the active zone and is connected to postsynaptic

neuroligin-1 via postsynaptic scaffolding molecules. Neuroligin-1 binds transsynaptically to β-neurexin enhancing release probability (Fig. 4.1A). Upon strong synaptic activity, vesicles fuse with the presynaptic membrane and cause the inclusion of vesicle membrane into the presynaptic membrane (Fig. 4.1B). The swelling of the presynaptic bouton causes lateral shifting of N-cadherin and neuroligin-1. Thereby, the transsynaptic interaction between neuroligin-1 and β-neurexin gets disrupted which leads to a decrease of presynaptic release probability. This in turn impedes further vesicle exocytosis thus preventing massive inflation of the presynaptic terminal (Fig. 4.1C). Most intriguingly, altered perisynaptic localization of N-cadherin leads to activation of compensatory endocytosis by N-cadherin. The constriction of the plasma membrane by compensatory endocytosis causes shrinking of the presynaptic bouton and the relocalization of N-cadherin and neuroligin-1 back to the active zone (Fig. 4.1D). Thereby, the synapse returns to the steady state thus maintaining proper synaptic function (Fig. 4.1A).

Summing up, this mechanism is based on activity-dependent spatial localization changes of N-cadherin and neuroligin1, which regulate the coupling of vesicle exo- and endocytosis that is essential for proper synaptic function, especially upon intense synaptic activity.

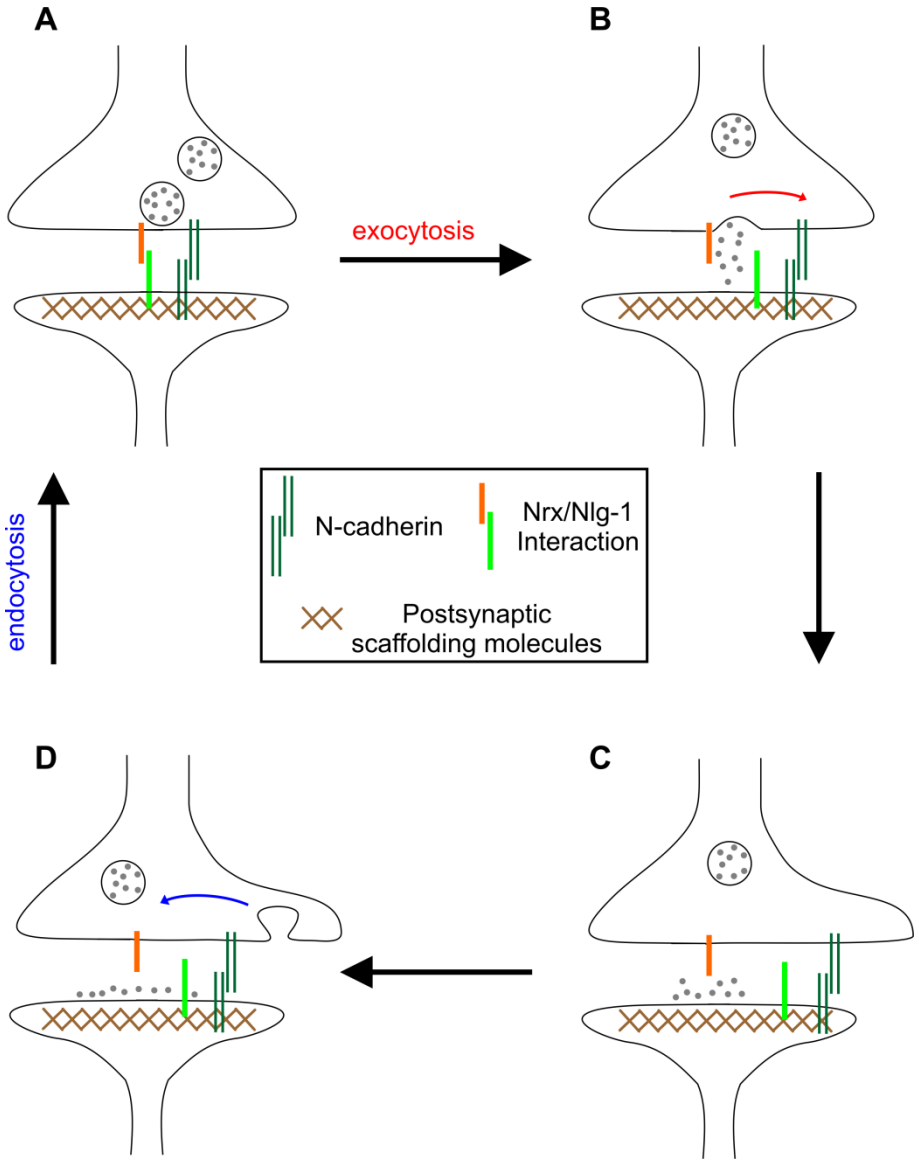

Figure 4.1 Coupling of vesicle exo- and endocytosis by N-cadherin and neuroligin-1
Schematic illustration of the roles of N-cadherin and neuroligin-1 in vesicle cycling. (**A**) At the resting state, the β-neurexin/neuroligin-1 adhesion system is localized centrally at the active zone. N-cadherin is localized at the periactive zone. Both cell adhesion systems are linked via postsynaptic scaffolding molecules. (**B**) Upon stimulation presynaptic vesicles fuse with the plasma membrane and release their neurotransmitter. N-cadherin is pushed away from the active zone by the inclusion of vesicle membrane. Postsynaptic neuroligin-1 delocalizes by linkage to N-cadherin and loses adhesion to presynaptic β-neurexin (**C**). (**D**) N-cadherin and neuroligin-1 relocalize more centrally to the active zone by vesicle endocytosis, induced by N-cadherin.

4.8 Effects of Aβ on vesicle cluster in human iPSC derived neurons

In addition to the regulation of vesicle cycling by CAMs, pathophysiological effects of oligomers of amyloid-β (Aβ) peptides on vesicle cluster were investigated in human iPSC derived neurons. The formation of Aβ peptides is thought to play a crucial role in the pathology of Alzheimer`s disease (Selkoe 2002; Haass and Selkoe 2007). A multitude of synaptotoxic effects of Aβ peptides has been reported, e.g. the loss of synapses in rodent neurons (Shankar et al., 2007; Lacor et al., 2007; Andreyeva et al., 2012) that further causes synapse degeneration (Wilcox et al., 2011; Wu et al., 2010). In this work, 8 days incubation of neuronal cultures derived from human iPS cells with Aβ-containing 7PA2-CM did not affect cell viability (Fig. 3.28). Hence, the short-term addition of 7PA2-CM to hiPSC derived neurons enables the examination of functional synaptic defects at an early stage of Alzheimer`s disease in which effects of Aβ oligomers on neuronal cell viability are largely absent. Furthermore, this model system enables the verification of Aβ-induced effects, which were initially shown in rodent model systems, in human neurons.

FM4-64 stainings revealed a clear defect in the density of axonal vesicle cluster that was induced by short-term application of Aβ peptides. In contrast, vesicle exocytosis (revealed by FM4-64 destainings) as well as vesicle endocytosis (revealed by FM4-64 puncta intensity) was unaffected in 7PA2-CM treated cells (Fig. 3.29). Furthermore, Aβ application for 8 days did not reduce the density of neuronal processes (Fig. 3.28). Together these results suggest an Aβ-induced defect in the axonal transport of vesicle cluster. Thus, these observations in human neurons confirm previous studies in rodent model systems that showed Aβ-induced defects in axonal transport in general (Hiruma et al., 2003; Stokin et al., 2005; Millecamps and Julien, 2013) and in particular in the transport of vesicles (Decker et al., 2010; Tang et al., 2012).

Unexpectedly, the cycling of presynaptic vesicle cluster at bona fide synapses was not affected by Aβ. FM4-64 stainings and destainings of presynaptic vesicle cluster that contacted postsynaptic dendrites revealed no significant alterations upon short-term incubation with 7PA2-CM (Fig. 3.30). Accordingly, Aβ appears not to affect synaptic vesicle exo- and endocytosis at early stages in human neurons, contrary to expectations based on studies in dissociated mouse neurons. In rodent neurons, FM

experiments had revealed functional defects of presynaptic vesicle exo- and endocytosis caused by Aβ (Ting et al., 2007; Parodi et al., 2010). Thus, human Alzheimer`s pathology might be characterized by an Aβ-induced defect in the axonal transport of vesicle cluster that might lead to downstream impairment of synaptic function and loss of synapses in the further course of the disease.

5 References

Aarts M, Liu Y, Liu L, Besshoh S, Arundine M, Gurd JW, Wang YT, Salter MW, Tymianski M (2002). Treatment of ischemic brain damage by perturbing NMDA receptor- PSD-95 protein interactions. Science. 298(5594):846-850.

Abe K, Chisaka O, Van Roy F, Takeichi M (2004). Stability of dendritic spines and synaptic contacts is controlled by alpha N-catenin. Nat Neurosci. 7(4):357-363.

Aiga M, Levinson JN, Bamji SX (2011). N-cadherin and neuroligins cooperate to regulate synapse formation in hippocampal cultures. J Biol Chem. 286(1):851-858.

Andreyeva A, Nieweg K, Horstmann K, Klapper S, Müller-Schiffmann A, Korth C, Gottmann K (2012). C-terminal fragment of N-cadherin accelerates synapse destabilization by amyloid-β. Brain. 135(Pt 7):2140-2154.

Aravanis AM, Pyle JL, Harata NC, Tsien RW (2003). Imaging single synaptic vesicles undergoing repeated fusion events: kissing, running, and kissing again. Neuropharmacology. 45(6):797-813.

Atluri PP, Ryan TA (2006). The kinetics of synaptic vesicle reacidification at hippocampal nerve terminals. J Neurosci. 26(8):2313-2320.

Augustine GJ, Betz H, Bommert K, Charlton MP, DeBello WM, Hans M, Swandulla D. (1994). Molecular pathways for presynaptic calcium signaling. Adv Second Messenger Phosphoprotein Res. 29:139-154.

Augustine GJ, Burns ME, DeBello WM, Hilfiker S, Morgan JR, Schweizer FE, Tokumaru H, Umayahara K (1999). Proteins involved in synaptic vesicle trafficking. J Physiol. 520 Pt 1:33-41.

Augustine GJ, Charlton MP, Smith SJ (1987). Calcium action in synaptic transmitter release. Annu Rev Neurosci. 10:633-693.

Banovic D, Khorramshahi O, Owald D, Wichmann C, Riedt T, Fouquet W, Tian R, Sigrist SJ, Aberle H (2010). Drosophila neuroligin 1 promotes growth and postsynaptic differentiation at glutamatergic neuromuscular junctions. Neuron. 66(5):724-738.

Bekkers JM (2003). Synaptic transmission: functional autapses in the cortex. Curr Biol. 13(11):R433-435.

Benson DL, Tanaka H (1998). N-cadherin redistribution during synaptogenesis in hippocampal neurons. J Neurosci. 18(17):6892-6904.

Betz A, Okamoto M, Benseler F, Brose N (1997). Direct interaction of the rat unc-13 homologue Munc13-1 with the N terminus of syntaxin. J Biol Chem. 272(4):2520-2526.

Blasi J, Chapman ER, Link E, Binz T, Yamasaki S, De Camilli P, Südhof TC, Niemann H, Jahn R (1993(a)). Botulinum neurotoxin A selectively cleaves the synaptic protein SNAP-25. Nature. 365(6442):160-163.

Blasi J, Chapman ER, Yamasaki S, Binz T, Niemann H, Jahn R (1993(b)). Botulinum neurotoxin C1 blocks neurotransmitter release by means of cleaving HPC-1/syntaxin. EMBO J. 12(12):4821-4828.

Bliss TV, Collingridge GL (2013). Expression of NMDA receptor-dependent LTP in the hippocampus: bridging the divide. Mol Brain. 6:5.

Bollmann JH, Sakmann B, Borst JG (2000). Calcium sensitivity of glutamate release in a calyx-type terminal. Science 289(5481):953-957.

Boucard AA, Chubykin AA, Comoletti D, Taylor P, Südhof TC (2005). A splice code for trans-synaptic cell adhesion mediated by binding of neuroligin 1 to alpha- and beta-neurexins. Neuron. 48(2):229-236.

Bowman EJ, Siebers A, Altendorf K (1988). Bafilomycins: a class of inhibitors of membrane ATPases from microorganisms, animal cells, and plant cells. Proc Natl Acad Sci U S A. 85(21):7972-7976.

Bozdagi O, Valcin M, Poskanzer K, Tanaka H, Benson DL (2004). Temporally distinct demands for classic cadherins in synapse formation and maturation. Mol Cell Neurosci. 27(4):509-521.

Bozdagi O, Wang XB, Nikitczuk JS, Anderson TR, Bloss EB, Radice GL, Zhou Q, Benson DL, Huntley GW (2010). Persistence of coordinated long-term potentiation and dendritic spine enlargement at mature hippocampal CA1 synapses requires N-cadherin. J Neurosci. 30(30):9984-9989.

Brasch J, Harrison OJ, Honig B, Shapiro L (2012). Thinking outside the cell: how cadherins drive adhesion. Trends Cell Biol. 22(6):299-310.

Brigidi GS, Bamji SX (2011). Cadherin-catenin adhesion complexes at the synapse. Curr Opin Neurobiol. 21(2):208-214.

Brose N, Hofmann K, Hata Y, Südhof TC (1995). Mammalian homologues of Caenorhabditis elegans unc-13 gene define novel family of C2-domain proteins. J Biol Chem. 270(42):25273-25280.

Brose N, Rosenmund C, Rettig J (2000). Regulation of transmitter release by Unc-13 and its homologues. Curr Opin Neurobiol. 10(3):303-311.

Brunger AT (2000). Structural insights into the molecular mechanism of Ca^{2+}-dependent exocytosis. Curr Opin Neurobiol. 10(3):293-302.

Budreck EC, Scheiffele P (2007). Neuroligin-3 is a neuronal adhesion protein at GABAergic and glutamatergic synapses. Eur J Neurosci. 26(7):1738-1748.

Burkhardt P, Hattendorf DA, Weis WI, Fasshauer D (2008). Munc18a controls SNARE assembly through its interaction with the syntaxin N-peptide. EMBO J. 27(7):923-933.

Burré J, Sharma M, Tsetsenis T, Buchman V, Etherton MR, Südhof TC (2010). Alpha-synuclein promotes SNARE-complex assembly in vivo and in vitro. Science. 329(5999):1663-1667.

Butz S, Okamoto M, Südhof TC (1998). A tripartite protein complex with the potential to couple synaptic vesicle exocytosis to cell adhesion in brain. Cell. 94(6):773-782.

Castillo PE, Schoch S, Schmitz F, Südhof TC, Malenka RC (2002). RIM1alpha is required for presynaptic long-term potentiation. Nature. 415(6869):327-330.

Chandra S, Gallardo G, Fernández-Chacón R, Schlüter OM, Südhof TC (2005). Alpha-synuclein cooperates with CSPalpha in preventing neurodegeneration. Cell. 123(3):383-396.

Chapman ER (2002). Synaptotagmin: a Ca^{2+} sensor that triggers exocytosis? Nat Rev Mol Cell Biol. 3(7):498-508.

Chen L, Chetkovich DM, Petralia RS, Sweeney NT, Kawasaki Y, Wenthold RJ, Bredt DS, Nicoll RA (2000). Stargazin regulates synaptic targeting of AMPA receptors by two distinct mechanisms. Nature. 408(6815):936-943.

Chen X, Nelson CD, Li X, Winters CA, Azzam R, Sousa AA, Leapman RD, Gainer H, Sheng M, Reese TS (2011). PSD-95 is required to sustain the molecular organization of the postsynaptic density. J Neurosci. 31(17):6329-6338.

Chi P, Greengard P, Ryan TA (2001). Synapsin dispersion and reclustering during synaptic activity. Nat Neurosci. 4(12):1187-1193.

Chih B, Engelman H, Scheiffele P (2005). Control of excitatory and inhibitory synapse formation by neuroligins. Science. 307(5713):1324-1328.

Clary DO, Griff IC, Rothman JE (1990). SNAPs, a family of NSF attachment proteins involved in intracellular membrane fusion in animals and yeast. Cell. 61(4):709-721.

Clayton EL, Evans GJ, Cousin MA (2008). Bulk synaptic vesicle endocytosis is rapidly triggered during strong stimulation. J Neurosci. 28(26):6627-6632.

Comoletti D, Grishaev A, Whitten AE, Taylor P, Trewhella J (2008). Characterization of the solution structure of a neuroligin/beta-neurexin complex. Chem Biol Interact. 175(1-3):150-155.

Comoletti D, Grishaev A, Whitten AE, Tsigelny I, Taylor P, Trewhella J (2007). Synaptic arrangement of the neuroligin/beta-neurexin complex revealed by X-ray and neutron scattering. Structure. 15(6):693-705.

Dai Y, Taru H, Deken SL, Grill B, Ackley B, Nonet ML, Jin Y (2006). SYD-2 Liprin-alpha organizes presynaptic active zone formation through ELKS. Nat Neurosci. 9(12):1479-1487.

Deák F, Schoch S, Liu X, Südhof TC, Kavalali ET (2004). Synaptobrevin is essential for fast synaptic-vesicle endocytosis. Nat Cell Biol. 6(11):1102-1108.

Deák F, Xu Y, Chang WP, Dulubova I, Khvotchev M, Liu X, Südhof TC, Rizo J (2009). Munc18-1 binding to the neuronal SNARE complex controls synaptic vesicle priming. J Cell Biol. 184(5):751-764.

Dean C, Scholl FG, Choih J, DeMaria S, Berger J, Isacoff E, Scheiffele P (2003). Neurexin mediates the assembly of presynaptic terminals. Nat Neurosci. 6(7):708-716.

Decker H, Lo KY, Unger SM, Ferreira ST, Silverman MA (2010). Amyloid-beta peptide oligomers disrupt axonal transport through an NMDA receptor-dependent mechanism that is mediated by glycogen synthase kinase 3beta in primary cultured hippocampal neurons. J Neurosci. 30(27):9166-9171.

Deng L, Kaeser PS, Xu W, Südhof TC (2011). RIM proteins activate vesicle priming by reversing autoinhibitory homodimerization of Munc13. Neuron. 69(2):317-331.

Dingledine R, Borges K, Bowie D, Traynelis SF(1999). The glutamate receptor ion channels. Pharmacol Rev. 51(1):7-61.

Diril MK, Wienisch M, Jung N, Klingauf J, Haucke V (2006). Stonin 2 is an AP-2-dependent endocytic sorting adaptor for synaptotagmin internalization and recycling. Dev Cell. 10(2):233-244.

El-Husseini AE, Schnell E, Chetkovich DM, Nicoll RA, Bredt DS (2000). PSD-95 involvement in maturation of excitatory synapses. Science. 290(5495):1364-1368.

Elste AM, Benson DL (2006). Structural basis for developmentally regulated changes in cadherin function at synapses. J Comp Neurol. 495(3):324-335.

Fei H, Grygoruk A, Brooks ES, Chen A, Krantz DE (2008). Trafficking of vesicular neurotransmitter transporters. Traffic. 9(9):1425-1436.

Ferguson SM, Brasnjo G, Hayashi M, Wölfel M, Collesi C, Giovedi S, Raimondi A, Gong LW, Ariel P, Paradise S, O'toole E, Flavell R, Cremona O, Miesenböck G, Ryan TA, De Camilli P (2007). A selective activity-dependent requirement for dynamin 1 in synaptic vesicle endocytosis. Science. 316(5824):570-574.

Ferguson SM, De Camilli P (2012). Dynamin, a membrane-remodelling GTPase. Nat Rev Mol Cell Biol. 13(2):75-88.

Flannery RJ, Brusés JL (2012). N-cadherin induces partial differentiation of cholinergic presynaptic terminals in heterologous cultures of brainstem neurons and CHO cells. Front Synaptic Neurosci. 4:6.

Fu Z, Washbourne P, Ortinski P, Vicini S (2003). Functional excitatory synapses in HEK293 cells expressing neuroligin and glutamate receptors. J Neurophysiol. 90(6):3950-3957.

Fujita Y, Sasaki T, Fukui K, Kotani H, Kimura T, Hata Y, Südhof TC, Scheller RH, Takai Y (1996). Phosphorylation of Munc-18/n-Sec1/rbSec1 by protein kinase C: its

implication in regulating the interaction of Munc-18/n-Sec1/rbSec1 with syntaxin. J Biol Chem. 271(13):7265-7268.

Funke L, Dakoji S, Bredt DS (2005). Membrane-associated guanylate kinases regulate adhesion and plasticity at cell junctions. Annu Rev Biochem. 74:219-245.

Futai K, Kim MJ, Hashikawa T, Scheiffele P, Sheng M, Hayashi Y (2007). Retrograde modulation of presynaptic release probability through signaling mediated by PSD-95-neuroligin. Nat Neurosci. 10(2):186-195.

Gad H, Löw P, Zotova E, Brodin L, Shupliakov O (1998). Dissociation between Ca^{2+}-triggered synaptic vesicle exocytosis and clathrin-mediated endocytosis at a central synapse. Neuron. 21(3):607-616.

Gandhi SP, Stevens CF (2003). Three modes of synaptic vesicular recycling revealed by single-vesicle imaging. Nature. 423(6940):607-613.

Geppert M, Goda Y, Hammer RE, Li C, Rosahl TW, Stevens CF, Südhof TC (1994). Synaptotagmin I: a major Ca^{2+} sensor for transmitter release at a central synapse. Cell. 79(4):717-727.

Graf ER, Kang Y, Hauner AM, Craig AM (2006). Structure function and splice site analysis of the synaptogenic activity of the neurexin-1 beta LNS domain. J Neurosci. 26(16):4256-4265.

Granseth B, Odermatt B, Royle SJ, Lagnado L (2006). Clathrin-mediated endocytosis is the dominant mechanism of vesicle retrieval at hippocampal synapses. Neuron. 51(6):773-786.

Gustafsson MG, Shao L, Carlton PM, Wang CJ, Golubovskaya IN, Cande WZ, Agard DA, Sedat JW (2008). Three-dimensional resolution doubling in wide-field fluorescence microscopy by structured illumination. Biophys J. 94(12):4957-4970.

Haass C, Selkoe DJ (2007). Soluble protein oligomers in neurodegeneration: lessons from the Alzheimer's amyloid beta-peptide. Nat Rev Mol Cell Biol. 8(2):101-112.

Han Y, Kaeser PS, Südhof TC, Schneggenburger R (2011). RIM determines Ca^{2+} channel density and vesicle docking at the presynaptic active zone. Neuron. 69(2):304-316.

Harata N, Pyle JL, Aravanis AM, Mozhayeva M, Kavalali ET, Tsien RW (2001). Limited numbers of recycling vesicles in small CNS nerve terminals: implications for neural signaling and vesicular cycling. Trends Neurosci. 24(11):637-643.

Harata NC, Choi S, Pyle JL, Aravanis AM, Tsien RW (2006). Frequency-dependent kinetics and prevalence of kiss-and-run and reuse at hippocampal synapses studied with novel quenching methods. Neuron. 49(2):243-256.

Haucke V, De Camilli P (1999). AP-2 recruitment to synaptotagmin stimulated by tyrosine-based endocytic motifs. Science. 285(5431):1268-1271.

Haucke V, Neher E, Sigrist SJ (2011). Protein scaffolds in the coupling of synaptic exocytosis and endocytosis. Nat Rev Neurosci. 12(3):127-138.

Hayashi Y, Shi SH, Esteban JA, Piccini A, Poncer JC, Malinow R (2000). Driving AMPA receptors into synapses by LTP and CaMKII: requirement for GluR1 and PDZ domain interaction. Science. 287(5461):2262-2267.

Heidelberger R, Heinemann C, Neher E, Matthews G (1994). Calcium dependence of the rate of exocytosis in a synaptic terminal. Nature. 371(6497):513-515.

Heuser JE, Reese TS, Dennis MJ, Jan Y, Jan L, Evans L (1979). Synaptic vesicle exocytosis captured by quick freezing and correlated with quantal transmitter release. J Cell Biol. 81(2):275-300.

Heuser JE, Reese TS, Landis DM (1974). Functional changes in frog neuromuscular junctions studied with freeze-fracture. J Neurocytol. 3(1):109-131.

Hinshaw JE, Schmid SL (1995). Dynamin self-assembles into rings suggesting a mechanism for coated vesicle budding. Nature. 374(6518):190-192.

Hiruma H, Katakura T, Takahashi S, Ichikawa T, Kawakami T (2003). Glutamate and amyloid beta-protein rapidly inhibit fast axonal transport in cultured rat hippocampal neurons by different mechanisms. J Neurosci. 23(26):8967-8977.

Hollmann M, Heinemann S (1994). Cloned glutamate receptors. Annu Rev Neurosci. 17:31-108.

Hollmann M, Maron C, Heinemann S (1994). N-glycosylation site tagging suggests a three transmembrane domain topology for the glutamate receptor GluR1. Neuron. 13(6):1331-1343.

Hoopmann P, Rizzoli SO, Betz WJ (2012). Imaging synaptic vesicle recycling by staining and destaining vesicles with FM dyes. Cold Spring Harb Protoc. (1):77-83.

Hosoi N, Holt M, Sakaba T (2009). Calcium dependence of exo- and endocytotic coupling at a glutamatergic synapse. Neuron. 63(2):216-229.

Hu SH, Christie MP, Saez NJ, Latham CF, Jarrott R, Lua LH, Collins BM, Martin JL (2011). Possible roles for Munc18-1 domain 3a and Syntaxin1 N-peptide and C-terminal anchor in SNARE complex formation. Proc Natl Acad Sci U S A. 108(3):1040-1045.

Hua Y, Woehler A, Kahms M, Haucke V, Neher E, Klingauf J (2013). Blocking endocytosis enhances short-term synaptic depression under conditions of normal availability of vesicles. Neuron. 80(2):343-349.

Ichtchenko K, Hata Y, Nguyen T, Ullrich B, Missler M, Moomaw C, Südhof TC (1995). Neuroligin 1: a splice site-specific ligand for beta-neurexins. Cell. 81(3):435-443.

Ichtchenko K, Nguyen T, Südhof TC (1996). Structures, alternative splicing, and neurexin binding of multiple neuroligins. J Biol Chem. 271(5):2676-2682.

Iida J, Hirabayashi S, Sato Y, Hata Y (2004). Synaptic scaffolding molecule is involved in the synaptic clustering of neuroligin. Mol Cell Neurosci. 27(4):497-508.

Inoue T, Wilkens S, Forgac M (2003). Subunit structure, function, and arrangement in the yeast and coated vesicle V-ATPases. J Bioenerg Biomembr. 35(4):291-299.

Irie M, Hata Y, Takeuchi M, Ichtchenko K, Toyoda A, Hirao K, Takai Y, Rosahl TW, Südhof TC (1997). Binding of neuroligins to PSD-95. Science. 277(5331):1511-1515.

Jahn R, Fasshauer D (2012). Molecular machines governing exocytosis of synaptic vesicles. Nature. 490(7419):201-207.

Jordan R, Lemke EA, Klingauf J (2005). Visualization of synaptic vesicle movement in intact synaptic boutons using fluorescence fluctuation spectroscopy. Biophys J. 89(3):2091-2102.

Jüngling K, Eulenburg V, Moore R, Kemler R, Lessmann V, Gottmann K (2006). N-cadherin transsynaptically regulates short-term plasticity at glutamatergic synapses in embryonic stem cell-derived neurons. J Neurosci. 26(26):6968-6978.

Kadowaki M, Nakamura S, Machon O, Krauss S, Radice GL, Takeichi M (2007). N-cadherin mediates cortical organization in the mouse brain. Dev Biol. 304(1):22-33.

Kaeser PS, Deng L, Fan M, Südhof TC (2012). RIM genes differentially contribute to organizing presynaptic release sites. Proc Natl Acad Sci U S A. 109(29):11830-11835.

Kasai H, Matsuzaki M, Noguchi J, Yasumatsu N, Nakahara H (2003). Structure-stability-function relationships of dendritic spines. Trends Neurosci. 26(7):360-368.

Kavalali ET, Jorgensen EM (2014). Visualizing presynaptic function. Nat Neurosci. 17(1):10-16.

Kerchner GA, Nicoll RA (2008). Silent synapses and the emergence of a postsynaptic mechanism for LTP. Nat Rev Neurosci. 9(11):813-825.

Kim E, Sheng M (2004). PDZ domain proteins of synapses. Nat Rev Neurosci. 5(10):771-781.

Kim MJ, Dunah AW, Wang YT, Sheng M (2005). Differential roles of NR2A- and NR2B-containing NMDA receptors in Ras-ERK signaling and AMPA receptor trafficking. Neuron. 46(5):745-760.

Koenig JH, Ikeda K (1989). Disappearance and reformation of synaptic vesicle membrane upon transmitter release observed under reversible blockage of membrane retrieval. J Neurosci. 9(11):3844-3860.

Koo SJ, Markovic S, Puchkov D, Mahrenholz CC, Beceren-Braun F, Maritzen T, Dernedde J, Volkmer R, Oschkinat H, Haucke V (2011). SNARE motif-mediated sorting of synaptobrevin by the endocytic adaptors clathrin assembly lymphoid myeloid leukemia (CALM) and AP180 at synapses. Proc Natl Acad Sci U S A. 108(33):13540-13545.

Kornau HC, Schenker LT, Kennedy MB, Seeburg PH (1995). Domain interaction between NMDA receptor subunits and the postsynaptic density protein PSD-95. Science. 269(5231):1737-1740.

Kostetskii I, Li J, Xiong Y, Zhou R, Ferrari VA, Patel VV, Molkentin JD, Radice GL (2005). Induced deletion of the N-cadherin gene in the heart leads to dissolution of the intercalated disc structure. Circ Res. 96(3):346-354.

Koushika SP, Richmond JE, Hadwiger G, Weimer RM, Jorgensen EM, Nonet ML (2001). A post-docking role for active zone protein Rim. Nat Neurosci. 4(10):997-1005.

Krueger DD, Tuffy LP, Papadopoulos T, Brose N (2012). The role of neurexins and neuroligins in the formation, maturation, and function of vertebrate synapses. Curr Opin Neurobiol. 22(3):412-422.

Lacor PN, Buniel MC, Furlow PW, Clemente AS, Velasco PT, Wood M, Viola KL, Klein WL (2007). Abeta oligomer-induced aberrations in synapse composition, shape, and density provide a molecular basis for loss of connectivity in Alzheimer's disease. J Neurosci. 27(4):796-807.

Lai AL, Huang H, Herrick DZ, Epp N, Cafiso DS (2011). Synaptotagmin 1 and SNAREs form a complex that is structurally heterogeneous. J Mol Biol. 405(3):696-706.

Levinson JN, El-Husseini A (2005). Building excitatory and inhibitory synapses: balancing neuroligin partnerships. Neuron. 48(2):171-174.

Li Y, Zhou Z, Zhang X, Tong H, Li P, Zhang ZC, Jia Z, Xie W, Han J (2013). Drosophila neuroligin 4 regulates sleep through modulating GABA transmission. J Neurosci. 33(39):15545-15554.

Link E, Edelmann L, Chou JH, Binz T, Yamasaki S, Eisel U, Baumert M, Südhof TC, Niemann H, Jahn R (1992). Tetanus toxin action: inhibition of neurotransmitter release linked to synaptobrevin proteolysis. Biochem Biophys Res Commun. 189(2):1017-1023.

Lisman JE, Raghavachari S, Tsien RW (2007). The sequence of events that underlie quantal transmission at central glutamatergic synapses. Nat Rev Neurosci. 8(8):597-609.

Llinás R, Gruner JA, Sugimori M, McGuinness TL, Greengard P (1991). Regulation by synapsin I and Ca^{2+}-calmodulin-dependent protein kinase II of the transmitter release in squid giant synapse. J Physiol. 436:257-282.

Llinás R, Sugimori M, Simon SM (1982). Transmission by presynaptic spike-like depolarization in the squid giant synapse. Proc Natl Acad Sci U S A. 79(7):2415-2419.

Macia E, Ehrlich M, Massol R, Boucrot E, Brunner C, Kirchhausen T (2006). Dynasore, a cell-permeable inhibitor of dynamin. Dev Cell. 10(6):839-850.

Marambaud P, Wen PH, Dutt A, Shioi J, Takashima A, Siman R, Robakis NK (2003). A CBP binding transcriptional repressor produced by the PS1/epsilon-cleavage of N-cadherin is inhibited by PS1 FAD mutations. Cell. 114(5):635-645.

Mayer ML (2011). Emerging models of glutamate receptor ion channel structure and function. Structure. 19(10):1370-1380.

McMahon HT, Missler M, Li C, Südhof TC (1995). Complexins: cytosolic proteins that regulate SNAP receptor function. Cell. 83(1):111-119.

Mendez P, De Roo M, Poglia L, Klauser P, Muller D (2010). N-cadherin mediates plasticity-induced long-term spine stabilization. J Cell Biol. 189(3):589-600.

Miesenböck G, De Angelis DA, Rothman JE (1998). Visualizing secretion and synaptic transmission with pH-sensitive green fluorescent proteins. Nature. 394(6689):192-195.

Millecamps S, Julien JP (2013). Axonal transport deficits and neurodegenerative diseases. Nat Rev Neurosci. 14(3):161-176.

Missler M, Südhof TC (1998). Neurexins: three genes and 1001 products. Trends Genet. 14(1):20-26.

Mochida S (2000). Protein-protein interactions in neurotransmitter release. Neurosci Res. 36(3):175-182.

Mukherjee K, Yang X, Gerber SH, Kwon HB, Ho A, Castillo PE, Liu X, Südhof TC (2010). Piccolo and bassoon maintain synaptic vesicle clustering without directly participating in vesicle exocytosis. Proc Natl Acad Sci U S A. 107(14):6504-6509.

Nakanishi S (1994). Metabotropic glutamate receptors: synaptic transmission, modulation, and plasticity. Neuron. 13(5):1031-1037.

Newton J, Murthy V (2006). Measuring exocytosis in neurons using FM labeling. J Vis Exp. (1):117.

Nguyen T, Südhof TC (1997). Binding properties of neuroligin 1 and neurexin 1beta reveal function as heterophilic cell adhesion molecules. J Biol Chem. 272(41):26032-26039.

Nicholson-Tomishima K, Ryan TA (2004). Kinetic efficiency of endocytosis at mammalian CNS synapses requires synaptotagmin I. Proc Natl Acad Sci U S A. 101(47):16648-16652.

Niethammer M, Kim E, Sheng M (1996). Interaction between the C terminus of NMDA receptor subunits and multiple members of the PSD-95 family of membrane-associated guanylate kinases. J Neurosci. 16(7):2157-2163.

Nishimura W, Yao I, Iida J, Tanaka N, Hata Y (2002). Interaction of synaptic scaffolding molecule and Beta -catenin. J Neurosci. 22(3):757-765.

Obst-Pernberg K, Medina L, Redies C (2001). Expression of R-cadherin and N-cadherin by cell groups and fiber tracts in the developing mouse forebrain: relation to the formation of functional circuits. Neuroscience. 106(3):505-533.

Owald D, Khorramshahi O, Gupta VK, Banovic D, Depner H, Fouquet W, Wichmann C, Mertel S, Eimer S, Reynolds E, Holt M, Aberle H, Sigrist SJ (2012). Cooperation of Syd-1 with Neurexin synchronizes pre- with postsynaptic assembly. Nat Neurosci. 15(9):1219-1226.

Pang ZP, Südhof TC (2010). Cell biology of Ca^{2+}-triggered exocytosis. Curr Opin Cell Biol. 22(4):496-505.

Parodi J, Sepúlveda FJ, Roa J, Opazo C, Inestrosa NC, Aguayo LG (2010). Beta-amyloid causes depletion of synaptic vesicles leading to neurotransmission failure. J Biol Chem. 285(4):2506-2514.

Peixoto RT, Kunz PA, Kwon H, Mabb AM, Sabatini BL, Philpot BD, Ehlers MD (2012). Transsynaptic signaling by activity-dependent cleavage of neuroligin-1. Neuron. 76(2):396-409.

Peng J, Kim MJ, Cheng D, Duong DM, Gygi SP, Sheng M (2004). Semiquantitative proteomic analysis of rat forebrain postsynaptic density fractions by mass spectrometry. J Biol Chem. 279(20):21003-21011.

Pielarski KN, van Stegen B, Andreyeva A, Nieweg K, Jüngling K, Redies C, Gottmann K (2013). Asymmetric N-cadherin expression results in synapse dysfunction, synapse elimination, and axon retraction in cultured mouse neurons. PLoS One. 8(1):e54105.

Plank C, Schillinger U, Scherer F, Bergemann C, Rémy JS, Krötz F, Anton M, Lausier J, Rosenecker J (2003). The magnetofection method: using magnetic force to enhance gene delivery. Biol Chem. 384(5):737-747.

Poirier MA, Xiao W, Macosko JC, Chan C, Shin YK, Bennett MK (1998). The synaptic SNARE complex is a parallel four-stranded helical bundle. Nat Struct Biol. 5(9):765-769.

Pokutta S, Weis WI (2007). Structure and mechanism of cadherins and catenins in cell-cell contacts. Annu Rev Cell Dev Biol. 23:237-261.

Poskanzer KE, Marek KW, Sweeney ST, Davis GW (2003). Synaptotagmin I is necessary for compensatory synaptic vesicle endocytosis in vivo. Nature. 426(6966):559-563.

Prange O, Wong TP, Gerrow K, Wang YT, El-Husseini A (2004). A balance between excitatory and inhibitory synapses is controlled by PSD-95 and neuroligin. Proc Natl Acad Sci U S A. 101(38):13915-13920.

Prybylowski K, Chang K, Sans N, Kan L, Vicini S, Wenthold RJ (2005). The synaptic localization of NR2B-containing NMDA receptors is controlled by interactions with PDZ proteins and AP-2. Neuron. 47(6):845-857.

Radice GL, Rayburn H, Matsunami H, Knudsen KA, Takeichi M, Hynes RO (1997). Developmental defects in mouse embryos lacking N-cadherin. Dev Biol. 181(1):64-78.

Raimondi A, Ferguson SM, Lou X, Armbruster M, Paradise S, Giovedi S, Messa M, Kono N, Takasaki J, Cappello V, O'Toole E, Ryan TA, De Camilli P (2011). Overlapping role of dynamin isoforms in synaptic vesicle endocytosis. Neuron. 70(6):1100-1114.

Redies C, Engelhart K, Takeichi M (1993). Differential expression of N- and R-cadherin in functional neuronal systems and other structures of the developing chicken brain. J Comp Neurol. 333(3):398-416.

Rizo J, Südhof TC (2002). Snares and Munc18 in synaptic vesicle fusion. Nat Rev Neurosci. 3(8):641-653.

Rizo J, Rosenmund C (2008). Synaptic vesicle fusion. Nat Struct Mol Biol. 15(7):665-674.

Rizzoli SO, Betz WJ (2005). Synaptic vesicle pools. Nat Rev Neurosci. 6(1):57-69.

Rizzoli SO, Jahn R (2007). Kiss-and-run, collapse and 'readily retrievable' vesicles. Traffic. 8(9):1137-1144.

Royle SJ, Granseth B, Odermatt B, Derevier A, Lagnado L (2008). Imaging phluorin-based probes at hippocampal synapses. Methods Mol Biol. 457:293-303.

Ryan TA, Smith SJ, Reuter H (1996). The timing of synaptic vesicle endocytosis. Proc Natl Acad Sci U S A. 93(11):5567-5571.

Saglietti L, Dequidt C, Kamieniarz K, Rousset MC, Valnegri P, Thoumine O, Beretta F, Fagni L, Choquet D, Sala C, Sheng M, Passafaro M (2007). Extracellular interactions between GluR2 and N-cadherin in spine regulation. Neuron. 54(3):461-477.

Saheki Y, De Camilli P (2012). Synaptic vesicle endocytosis. Cold Spring Harb Perspect Biol. 4(9): a005645.

Sankaranarayanan S, De Angelis D, Rothman JE, Ryan TA (2000). The use of pHluorins for optical measurements of presynaptic activity. Biophys J. 79(4):2199-2208.

Sankaranarayanan S, Ryan TA (2001). Calcium accelerates endocytosis of vSNAREs at hippocampal synapses. Nat Neurosci. 4(2):129-136.

Sara Y, Biederer T, Atasoy D, Chubykin A, Mozhayeva MG, Südhof TC, Kavalali ET (2005). Selective capability of SynCAM and neuroligin for functional synapse assembly. J Neurosci. 25(1):260-270.

Scheiffele P, Fan J, Choih J, Fetter R, Serafini T (2000). Neuroligin expressed in nonneuronal cells triggers presynaptic development in contacting axons. Cell. 101(6):657-669.

Schermelleh L, Carlton PM, Haase S, Shao L, Winoto L, Kner P, Burke B, Cardoso MC, Agard DA, Gustafsson MG, Leonhardt H, Sedat JW (2008). Subdiffraction multicolor imaging of the nuclear periphery with 3D structured illumination microscopy. Science. 320(5881):1332-1336.

Schermelleh L, Heintzmann R, Leonhardt H (2010). A guide to super-resolution fluorescence microscopy. J Cell Biol. 190(2):165-175.

Schiavo G, Benfenati F, Poulain B, Rossetto O, Polverino de Laureto P, DasGupta BR, Montecucco C (1992). Tetanus and botulinum-B neurotoxins block neurotransmitter release by proteolytic cleavage of synaptobrevin. Nature. 359(6398):832-835.

Schikorski T, Stevens CF (1997). Quantitative ultrastructural analysis of hippocampal excitatory synapses. J Neurosci. 17(15):5858-5867.

Schneggenburger R, Neher E (2000). Intracellular calcium dependence of transmitter release rates at a fast central synapse. Nature 406(6798):889-893.

Schoch S, Castillo PE, Jo T, Mukherjee K, Geppert M, Wang Y, Schmitz F, Malenka RC, Südhof TC (2002). RIM1alpha forms a protein scaffold for regulating neurotransmitter release at the active zone. Nature. 415(6869):321-326.

Selkoe DJ (2002). Alzheimer's disease is a synaptic failure. Science. 298(5594):789-791.

Shankar GM, Bloodgood BL, Townsend M, Walsh DM, Selkoe DJ, Sabatini BL (2007). Natural oligomers of the Alzheimer amyloid-beta protein induce reversible synapse loss by modulating an NMDA-type glutamate receptor-dependent signaling pathway. J Neurosci. 27(11):2866-2875.

Shapiro L, Fannon AM, Kwong PD, Thompson A, Lehmann MS, Grübel G, Legrand JF, Als-Nielsen J, Colman DR, Hendrickson WA (1995). Structural basis of cell-cell adhesion by cadherins. Nature. 374(6520):327-337.

Sharma M, Burré J, Bronk P, Zhang Y, Xu W, Südhof TC (2012). CSPα knockout causes neurodegeneration by impairing SNAP-25 function. EMBO J. 31(4):829-841.

Sheng M, Kim E (2011). The postsynaptic organization of synapses. Cold Spring Harb Perspect Biol. 3(12): a005678.

Shtrahman M, Yeung C, Nauen DW, Bi GQ, Wu XL (2005). Probing vesicle dynamics in single hippocampal synapses. Biophys J. 89(5):3615-3627.

Siddiqui TJ, Craig AM (2011). Synaptic organizing complexes. Curr Opin Neurobiol. 21(1):132-143.

Siekevitz P (1985). The postsynaptic density: a possible role in long-lasting effects in the central nervous system. Proc Natl Acad Sci U S A. 82(10):3494-3498.

Söllner T, Whiteheart SW, Brunner M, Erdjument-Bromage H, Geromanos S, Tempst P, Rothman JE (1993). SNAP receptors implicated in vesicle targeting and fusion. Nature. 362(6418):318-324.

Song JY, Ichtchenko K, Südhof TC, Brose N (1999). Neuroligin 1 is a postsynaptic cell-adhesion molecule of excitatory synapses. Proc Natl Acad Sci U S A. 96(3):1100-1105.

Sprengel R, Suchanek B, Amico C, Brusa R, Burnashev N, Rozov A, Hvalby O, Jensen V, Paulsen O, Andersen P, Kim JJ, Thompson RF, Sun W, Webster LC, Grant SG, Eilers J, Konnerth A, Li J, McNamara JO, Seeburg PH (1998). Importance of the intracellular domain of NR2 subunits for NMDA receptor function in vivo. Cell. 92(2):279-289.

Stan A, Pielarski KN, Brigadski T, Wittenmayer N, Fedorchenko O, Gohla A, Lessmann V, Dresbach T, Gottmann K (2010). Essential cooperation of N-cadherin and neuroligin-1 in the transsynaptic control of vesicle accumulation. Proc Natl Acad Sci U S A. 107(24):11116-11121.

Stevens CF, Williams JH (2000). "Kiss and run" exocytosis at hippocampal synapses. Proc Natl Acad Sci U S A. 97(23):12828-12833.

Stokin GB, Lillo C, Falzone TL, Brusch RG, Rockenstein E, Mount SL, Raman R, Davies P, Masliah E, Williams DS, Goldstein LS (2005). Axonopathy and transport deficits early in the pathogenesis of Alzheimer's disease. Science. 307(5713):1282-1288.

Südhof TC (2004). The synaptic vesicle cycle. Annu Rev Neurosci. 27:509-547.

Südhof TC (2008). Neuroligins and neurexins link synaptic function to cognitive disease. Nature. 455(7215):903-911.

Südhof TC (2012). The presynaptic active zone. Neuron. 75(1):11-25.

Südhof TC (2013). Neurotransmitter release: the last millisecond in the life of a synaptic vesicle. Neuron. 80(3):675-690.

Südhof TC, Rothman JE (2009). Membrane fusion: grappling with SNARE and SM proteins. Science. 323(5913):474-477.

Sun M, Xing G, Yuan L, Gan G, Knight D, With SI, He C, Han J, Zeng X, Fang M, Boulianne GL, Xie W (2011). Neuroligin 2 is required for synapse development and function at the Drosophila neuromuscular junction. J Neurosci. 31(2):687-699.

Sutton RB, Fasshauer D, Jahn R, Brunger AT (1998). Crystal structure of a SNARE complex involved in synaptic exocytosis at 2.4 A resolution. Nature. 395(6700):347-353.

Tai CY, Mysore SP, Chiu C, Schuman EM (2007). Activity-regulated N-cadherin endocytosis. Neuron. 54(5):771-785.

Takei K, Mundigl O, Daniell L, De Camilli P (1996). The synaptic vesicle cycle: a single vesicle budding step involving clathrin and dynamin. J Cell Biol. 133(6):1237-1250.

Tanaka H, Shan W, Phillips GR, Arndt K, Bozdagi O, Shapiro L, Huntley GW, Benson DL, Colman DR (2000). Molecular modification of N-cadherin in response to synaptic activity. Neuron. 25(1):93-107.

Tang Y, Scott DA, Das U, Edland SD, Radomski K, Koo EH, Roy S (2012). Early and selective impairments in axonal transport kinetics of synaptic cargoes induced by soluble amyloid β-protein oligomers. Traffic. 13(5):681-693.

Thompson HM, McNiven MA (2006). Discovery of a new 'dynasore'. Nat Chem Biol. 2(7):355-356.

Ting JT, Kelley BG, Lambert TJ, Cook DG, Sullivan JM (2007). Amyloid precursor protein overexpression depresses excitatory transmission through both presynaptic and postsynaptic mechanisms. Proc Natl Acad Sci U S A. 104(1):353-358.

Tobaben S, Thakur P, Fernández-Chacón R, Südhof TC, Rettig J, Stahl B (2001). A trimeric protein complex functions as a synaptic chaperone machine. Neuron. 31(6):987-999.

Togashi H, Abe K, Mizoguchi A, Takaoka K, Chisaka O, Takeichi M (2002). Cadherin regulates dendritic spine morphogenesis. Neuron. 35(1):77-89.

Traynelis SF, Wollmuth LP, McBain CJ, Menniti FS, Vance KM, Ogden KK, Hansen KB, Yuan H, Myers SJ, Dingledine R (2010). Glutamate receptor ion channels: structure, regulation, and function. Pharmacol Rev. 62(3):405-496.

Ubach J, Zhang X, Shao X, Südhof TC, Rizo J (1998). Ca^{2+} binding to synaptotagmin: how many Ca^{2+} ions bind to the tip of a C2-domain? EMBO J. 17(14):3921-3930.

Uriu Y, Kiyonaka S, Miki T, Yagi M, Akiyama S, Mori E, Nakao A, Beedle AM, Campbell KP, Wakamori M, Mori Y (2010). Rab3-interacting molecule gamma isoforms lacking the Rab3-binding domain induce long lasting currents but block neurotransmitter vesicle anchoring in voltage-dependent P/Q-type Ca^{2+} channels. J Biol Chem. 285(28):21750-21767.

Ushkaryov YA, Petrenko AG, Geppert M, Südhof TC (1992). Neurexins: synaptic cell surface proteins related to the alpha-latrotoxin receptor and laminin. Science. 257(5066):50-56.

Varoqueaux F, Aramuni G, Rawson RL, Mohrmann R, Missler M, Gottmann K, Zhang W, Südhof TC, Brose N (2006). Neuroligins determine synapse maturation and function. Neuron. 51(6):741-754.

Varoqueaux F, Jamain S, Brose N (2004). Neuroligin 2 is exclusively localized to inhibitory synapses. Eur J Cell Biol. 83(9):449-456.

Varoqueaux F, Sigler A, Rhee JS, Brose N, Enk C, Reim K, Rosenmund C (2002). Total arrest of spontaneous and evoked synaptic transmission but normal synaptogenesis in the absence of Munc13-mediated vesicle priming. Proc Natl Acad Sci U S A. 99(13):9037-9042.

Verhage M, Maia AS, Plomp JJ, Brussaard AB, Heeroma JH, Vermeer H, Toonen RF, Hammer RE, van den Berg TK, Missler M, Geuze HJ, Südhof TC (2000). Synaptic assembly of the brain in the absence of neurotransmitter secretion. Science. 287(5454):864-869.

Vitureira N, Letellier M, White IJ, Goda Y (2011). Differential control of presynaptic efficacy by postsynaptic N-cadherin and β-catenin. Nat Neurosci. 15(1):81-89.

Wakeham DE, Ybe JA, Brodsky FM, Hwang PK (2000). Molecular structures of proteins involved in vesicle coat formation. Traffic. 1(5):393-398.

Whiteheart SW, Rossnagel K, Buhrow SA, Brunner M, Jaenicke R, Rothman JE (1994). N-ethylmaleimide-sensitive fusion protein: a trimeric ATPase whose hydrolysis of ATP is required for membrane fusion. J Cell Biol. 126(4):945-954.

Wilcox KC, Lacor PN, Pitt J, Klein WL (2011). Aβ oligomer-induced synapse degeneration in Alzheimer's disease. Cell Mol Neurobiol. 31(6):939-948.

Williams E, Williams G, Gour BJ, Blaschuk OW, Doherty P (2000). A novel family of cyclic peptide antagonists suggests that N-cadherin specificity is determined by amino acids that flank the HAV motif. J Biol Chem. 275(6):4007-4012.

Wittenmayer N, Körber C, Liu H, Kremer T, Varoqueaux F, Chapman ER, Brose N, Kuner T, Dresbach T (2009). Postsynaptic Neuroligin1 regulates presynaptic maturation. Proc Natl Acad Sci U S A. 106(32):13564-13569.

Wu HY, Hudry E, Hashimoto T, Kuchibhotla K, Rozkalne A, Fan Z, Spires-Jones T, Xie H, Arbel-Ornath M, Grosskreutz CL, Bacskai BJ, Hyman BT (2010). Amyloid beta induces the morphological neurodegenerative triad of spine loss, dendritic simplification, and neuritic dystrophies through calcineurin activation. J Neurosci. 30(7):2636-2649.

Xing G, Gan G, Chen D, Sun M, Yi J, Lv H, Han J, Xie W (2014). Drosophila neuroligin3 regulates neuromuscular junction development and synaptic differentiation. J Biol Chem. 289(46):31867-31877.

Yam PT, Pincus Z, Gupta GD, Bashkurov M, Charron F, Pelletier L, Colman DR (2013). N-cadherin relocalizes from the periphery to the center of the synapse after transient synaptic stimulation in hippocampal neurons. PLoS One. 8(11):e79679.

Yamada S, Pokutta S, Drees F, Weis WI, Nelson WJ (2005). Deconstructing the cadherin-catenin-actin complex. Cell. 123(5):889-901.

Yamagata M, Sanes JR, Weiner JA (2003). Synaptic adhesion molecules. Curr Opin Cell Biol. 15(5):621-632.

Yap AS, Brieher WM, Gumbiner BM (1997). Molecular and functional analysis of cadherin-based adherens junctions. Annu Rev Cell Dev Biol. 13:119-146.

6 Appendix

6.1 Abbreviations

AD	Alzheimer`s disease
AMPA	α-amino-3-hydroxy-5-methylisoxazol-4-propionacid
APP	Amyloid precursor protein
ARA-C	Cytosine β-D-arabinofuranoside-hydrochloride
ATP	Adenosine triphosphate
ATPase	Adenosine triphosphatase
Aβ	Amyloid-β
BME	Basal medium eagle
BSA	Bovine serum albumine
$[Ca^{2+}]_{ex}$	extracellular calcium concentration
$[Ca^{2+}]_{i}$	intracellular calcium concentration
CaMKII	Calcium-calmodulin-dependent proteinkinase II
CAMs	cell adhesion molecules
CASK	Calcium-calmodulin-dependent serine proteinkinase
CAZ	Cytoplasmic matrix of the active zones
CHO	Chinese hamster ovary
CME	Clathrin-mediated endocytosis
CNR	Cadherin-related neuronal receptors
CNS	Central nervous system
CSPα	Cysteine string protein α
DIV	Days in vitro
DL-AP5	DL-2-Amino-5-phosphonopentanoic acid
DNA	Deoxyribonucleic acid
DNQX	6,7-dinitroquinoxalin-2,3-dion
ECD	Extracellular domain
EGFP	Enhanced green fluorescent protein
EPSP	Excitatory postsynaptic potential
ES	Embryonic stem
FBS	Fetal bovine serum
FM4-64	*N*-(3-triethylammoniumpropyl)-4-(6-(4-(diethylamino)phenyl)hexatrienyl)pyridinium dibromide
GABA	γ-aminobutanoic acid
GTP	Guanosine triphosphate
GTPase	Guanosine triphosphatase
HEPES	N-2-hydroxyethylpiperazin-N`-2-ethansulfonacid
hiPSC	Human induced pluripotent stem cell

HSC70	Heat shock cognate 70 kDa protein
Hz	Hertz
ICC	Immunocytochemistry
IPSP	Inhibitory postsynaptic current
LNS domain	Laminin-neurexin–sex hormone–binding domain
LTD	Long-term depression
LTP	Long-term potentiation
MAGUK	Membrane-associated guanylate kinase
mEPSC	Miniature excitatory postsynaptic current
mGluRs	metabotropic glutamate receptors
mIPSC	Miniature inhibitory postsynaptic current
Munc-18	Mammalian uncoordinated-18
Munc-13	Mammalian uncoordinated-13
NB-media	Neurobasal medium
$Ncad^{flox}$	homozygous floxed N-cadherin mice
NMDA	N-methyl D-aspartate
NMJ	Neuromuscular junction
NSF	Soluble N-ethylmaleimide-sensitive-factor
PBS	Phosphate buffered saline
PDZ domain	PSD-95-Drosophila discs large tumor suppressor-zona occludens-1 protein domain
PFA	Paraformaldehyde
PKC	Protein kinase C
PO	Poly-L-Ornithine
P_r	Release probability
PSD	Postsynaptic density
PSD95	Postsynaptic density protein of 95 kDa
RIM	Rab3 interacting molecule
RIM-BP	RIM-binding protein
ROI	Region of interest
RRP	Readily releasable pool
SH3 domain	SRC homology 3 domain
SIM	Stimulated illumination microscopy
SM	Sec1/Munc-18-like
SNAP-25	Soluble N-ethylmaleimide-sensitive-factor-attachment-protein 25
SNARE	Soluble N-ethylmaleimide-sensitive-factor-attachment-protein-receptor complex
S-SCAM	Synaptic scaffolding molecule
SynGAP	Synaptic GTPase activating protein
SypHy	Synaptophysin-pHluorin
VAMP2	Vesicle-associated membrane protein 2
VDCC	Voltage-dependent calcium channel

vGLUT1	Vesicular glutamate transporter 1
α-SNAP	α-soluble N-ethylmaleimide-sensitive-factor-attachment-protein

6.2 List of illustrations

6.2.1 Figures

6.2.2 Tables

6.3 Curriculum vitae

Name	Bernd van Stegen
Date of birth	28.08.1982
Place of birth	Wesel, Germany
Marital status	married, with two children

2009-2015	PhD at the Institute of Neuro- and Sensory Physiology, University of Düsseldorf, Germany
09.2009	Graduation “Diplom-Biologe”
2008-2009	Diploma thesis at the Institute of Neuro- and Sensory Physiology, University of Düsseldorf, Germany
2003-2008	Studies of Biology at the University of Düsseldorf, Germany
2002-2003	Civilian service: Deutsches Rotes Kreuz
1993-2002	St. Georg Gymnasium Bocholt, Germany
1989-1993	Ludgerus Grundschule Dingden, Germany

6.4 Publications and conferences

6.4.1 Publications

Pielarski KN, **van Stegen B**, Andreyeva A, Nieweg K, Jüngling K, Redies C, Gottmann K (2013). Asymmetric N-cadherin expression results in synapse dysfunction, synapse elimination, and axon retraction in cultured mouse neurons. PLoS One. 8(1):e54105.

Nieweg K, Andreyeva A, **van Stegen B**, Tanriöver G, Gottmann K. Alzheimer`s disease related amyloid-β induces synaptotoxicity in human iPS cell derived neurons. Cell Death Dis., in revision.

van Stegen B, Ochs R, Aberle H, Gottmann K. Coupling of release-dependent control of endocytosis and neuroligin-1-dependent control of exocytosis by N-cadherin (article in preparation).

6.4.2 Conferences

2013	SfN Neuroscience Meeting, San Diego, USA. Poster presentation: “Transsynaptic modulation of the synaptic vesicle cycle by synaptic adhesion molecules”.
2012	8th FENS Forum of Neuroscience, Barcelona, Spain. Poster presentation: “Conditional knock-out of N-cadherin in individual neurons results in inhibition of dendrite growth and in axon retraction”.
2011	9th Meeting of the German Neuroscience Society, Göttingen, Germany. Poster presentation: “Essential cooperation of N-cadherin and neuroligin 1 at glutamatergic synapses”.
2010	7th FENS Forum of Neuroscience, Amsterdam, Netherlands.
2009	International Symposium “Structure and function of synapses”, Freiburg, Germany.

<u>Annual Meeting of the GRK 1033</u>

2011	7th Annual Meeting, Herinich-Heine-Saal, Düsseldorf, Germany. Oral presentation: “Modulation of synaptic endocytosis by cell adhesion molecules”.
2010	6thAnnual Meeting, Kardinal Schulte Haus, Bergisch Gladbach, Germany. Oral presentation: “Modulation of synaptic endocytosis by cell adhesion molecules”.
2009	5th Annual Meeting, Kardinal Schulte Haus, Bergisch Gladbach, Germany. Oral presentation: “Modulation of synaptic endocytosis by cell adhesion molecules”.

7 Danksagung

An dieser Stelle möchte ich all denen einen herzlichen Dank aussprechen, die zum Gelingen dieser Doktorarbeit beigetragen haben.

Ganz besonders danken möchte ich Prof. Dr. Kurt Gottmann, der mir die Möglichkeit gegeben hat, diese Doktorarbeit anzufertigen, sowie für seine uneingeschränkte Diskussionsbereitschaft und sein Interesse an meiner Arbeit.

Des Weiteren danke ich Prof. Dr. Hermann Aberle für die Betreuung der Doktorarbeit und die Diskussion meiner Ergebnisse.

Besonders danken möchte ich außerdem allen Mitgliedern der Arbeitsgruppe von Herrn Prof. Dr. Kurt Gottmann für das entspannte Arbeitsklima und die anregenden Diskussionen. Zudem danke ich dem Graduiertenkolleg GRK 1033 für die finanzielle Unterstützung.

Mein größter Dank gilt meiner Familie und meinen Freunden.
Ich danke meinen Eltern und Großeltern sowie meinen Geschwistern für die langjährige, uneingeschränkte Unterstützung und ihr Vertrauen.
Besonders bedanken möchte ich mich bei meiner Frau Julia für ihre Zuneigung und Geduld während der letzten fünf Jahre. Ohne deine Unterstützung wäre der Abschluss meiner Doktorarbeit undenkbar gewesen.
Danke Hannes und Bo für euer Lachen, welches mir täglich neue Energie und Freude gibt.

Erklärung

Ich versichere an Eides Statt, dass die Dissertation von mir selbständig und ohne unzulässige fremde Hilfe unter Beachtung der „Grundsätze zur Sicherung guter wissenschaftlicher Praxis an der Heinrich-Heine-Universität Düsseldorf“ erstellt worden ist. Diese Dissertation wurde keiner anderen Fakultät vorgelegt und es gab bisher keine erfolglosen Promotionsversuche.

Düsseldorf, den 10. Februar 2015

Bernd van Stegen